


Summer 2024

# Mathematical Modeling of Coupled Heat and Mass Transfer in Metal-Hydride Hydrogen Storage Systems

Muhammad Hasnain

Follow this and additional works at: <https://digitalcommons.georgiasouthern.edu/etd>

 Part of the [Energy Systems Commons](#), [Heat Transfer, Combustion Commons](#), [Numerical Analysis and Computation Commons](#), [Other Mechanical Engineering Commons](#), [Partial Differential Equations Commons](#), [Thermodynamics Commons](#), and the [Transport Phenomena Commons](#)

---

## Recommended Citation

Hasnain, Muhammad, "Mathematical Modeling of Coupled Heat and Mass Transfer in Metal-Hydride Hydrogen Storage Systems" (2024). *Electronic Theses and Dissertations*. 2802.

<https://digitalcommons.georgiasouthern.edu/etd/2802>

This thesis (open access) is brought to you for free and open access by the Jack N. Averitt College of Graduate Studies at Georgia Southern Commons. It has been accepted for inclusion in Electronic Theses and Dissertations by an authorized administrator of Georgia Southern Commons. For more information, please contact [digitalcommons@georgiasouthern.edu](mailto:digitalcommons@georgiasouthern.edu).

# MATHEMATICAL MODELING OF COUPLED HEAT AND MASS TRANSFER IN METAL-HYDRIDE HYDROGEN STORAGE SYSTEMS

MUHAMMAD HASNAIN

(Under the Direction of Hayri Sezer)

## ABSTRACT

As a promising clean energy carrier hydrogen has recently gained significant interest, but its efficient and safe storage is a major challenge. Compared to the gaseous state and liquid state, metal hydrides (MH) offer a potentially more effective storage approach for hydrogen. However, the main challenge in this approach is the low thermal conductivity of the MH bed that leads to low heat transfer and ultimately to higher charging and discharging times. The purpose of this work is to develop an in-house comprehensive heat and mass transfer model for hydrogen sorption in MH reactors to simulate the dynamic behavior of hydrogen storage. A 2D axis-symmetrical mathematical model for hydrogen absorption and desorption is presented for a cylindrical  $\text{LaNi}_5$  reactor. The model is validated using experimental temperature and reaction kinetics data while the relation for the equilibrium pressure is derived from PCT parameters, plateau flatness, and hysteresis factors making it a function of both temperature and hydrogen to metal atomic ratio  $[\text{H}/\text{M}]$ . A comparative examination of two models, one incorporating Darcy's velocity due to pressure gradients and the other neglecting it, demonstrates that while Darcy's law introduces numerical instability in the model, its overall effect on model outcomes can be neglected for the analyzed reactors. The developed model is then used to conduct different parametric studies to investigate the effect of discharging pressure, heating fluid temperature, porosity, and reactor size on the time histories of temperature and reacted fraction profiles. The effect of changing the non-homogeneous Neumann to Dirichlet boundary condition is also demonstrated to anticipate the utilization of phase change materials (PCM) instead of the cooling fluid. The research findings reveal the influence of charging/discharging pressure on the maximum/minimum temperatures attained and reaction kinetics, while highlighting the

predominant impact of fluid temperature on sorption kinetics. The model can be conveniently adapted for other metal hydrides and system configurations, including MH reactors with heat transfer fluid or finned heat exchangers or both. This work contributes to the development of more efficient hydrogen storage technologies, bringing us closer to realizing the potential of hydrogen as a clean and sustainable energy carrier.

INDEX WORDS: Hydrogen storage, Metal hydrides, Heat and mass transfer, Mathematical modeling, 2D transient model, Darcy's velocity, Reactive porous media, Finite volume method, Hydrogen absorption and desorption

MATHEMATICAL MODELING OF COUPLED HEAT AND MASS TRANSFER IN METAL-  
HYDRIDE HYDROGEN STORAGE SYSTEMS

by

MUHAMMAD HASNAIN

B.S., Ghulam Ishaq Khan Institute of Engineering Sciences and Technology, Pakistan 2021

M.S., Georgia Southern University, 2024

A Thesis Submitted to the Graduate Faculty of Georgia Southern University

in Partial Fulfillment of the Requirements for the Degree

MASTER OF SCIENCE IN MECHANICAL ENGINEERING

STATESBORO, GEORGIA



© 2024

MUHAMMAD HASNAIN

All Rights Reserved

MATHEMATICAL MODELING OF COUPLED HEAT AND MASS TRANSFER IN METAL-  
HYDRIDE HYDROGEN STORAGE SYSTEMS

by

MUHAMMAD HASNAIN

Major Professor:

Hayri Sezer

Committee:

David Calamas

Hossain Ahmed

Jerry Hunter Mason

Electronic Version Approved:

July 2024

## DEDICATION

In the name of Allah, the Most Gracious, the Most Merciful.

This thesis is dedicated to my beloved parents, Muhammad Riaz and Musarat Bibi. Despite living in a remote area in Northern Pakistan, far away from the academic world, their silent prayers and support have been my guiding light. Though they may never fully comprehend what a thesis is or the significance it holds for me, their hard work, countless sacrifices, and sleepless nights have made this achievement possible. Coming from an underprivileged background, I owe every bit of my success to their endless love and dedication. This is for you, with all my heart.

بسم الله الرحمن الرحيم

یہ تھیسس میرے پیارے والدین، محمد ریاض اور مسرت بی بی کے نام ہے۔ شمالی پاکستان کے دور دراز علاقے میں رہتے ہوئے، تعلیمی دنیا سے دور، ان کی خاموش دعائیں میری رہنمائی کرتی رہی ہے۔ اگرچہ وہ کبھی بھی مکمل طور پر یہ نہیں سمجھ پائیں گے کہ تھیسس کیا ہوتا ہے یا اس کی میرے لیے کیا اہمیت ہے، ان کی محنت، بے شمار قربانیاں، اور بے خواب راتیں اس کامیابی کو ممکن بنانے والی ہیں۔ معاشی طور پر محروم پس منظر سے آتے ہوئے، میں اپنی کامیابی کے ہر پہلو کا مقروض ان کی بے پناہ محبت کا ہوں۔ یہ سب آپ کے نام، دل کی گہرائیوں سے۔

## ACKNOWLEDGMENTS

First and foremost, I express my deepest gratitude to Allah, who bestowed upon me the capabilities and strength to complete this work.

I extend my heartfelt thanks to my research advisor, Dr. Hayri Sezer, who trusted me, trained me, and supported me in every possible way. This work would not have been possible without his exceptional support and mentorship. Dr. Sezer's guidance and encouragement have been pivotal in shaping my research endeavors.

I would also like to acknowledge the partial financial support from National Institute of Justice (NIJ), Office of Justice Programs, U.S. Department of Justice (Award Nos. 15PNIJ-23-GG-04204-RESS and 2020-R2-CX-0050). Although this work is not directly related to our projects with NIJ, I conducted research on the three-dimensional mathematical modeling of heat and mass transfer in gypsum board exposed to fire with applications in forensics fire investigations.

Special thanks go to my colleagues Shehzad Khan, and Muhammad Usman Khan, other members of our research group, 'Fire and Energy Lab (FireGY)', and all those who, directly or indirectly, contributed to this thesis. Your support has made a significant difference in my academic and personal growth.

# TABLE OF CONTENTS

	Page
ACKNOWLEDGMENTS .....	3
TABLE OF CONTENTS.....	4
LIST OF TABLES .....	6
LIST OF FIGURES .....	7
NOMENCLATURE .....	10
CHAPTER 1 .....	12
INTRODUCTION .....	12
1.1. Background and Motivation .....	12
1.2. How this Study is Novel.....	14
CHAPTER 2 .....	16
LITERATURE REVIEW .....	16
2.1. Hydrogen: A Clean and Green Energy Source.....	16
2.2. Hydrogen Production and Applications .....	18
2.3. Storage of Hydrogen.....	20
2.4. Selection of Optimum Metal Hydride .....	22
2.5. Heat Transfer Enhancements in MH Systems .....	24
2.6. Mathematical Modeling of MH Reactors .....	28
CHAPTER 3 .....	31
MATHEMATICAL MODEL .....	31
3.1. System Description and Schematic .....	31
3.2. Effective Medium Theory: From Microscopic to Macroscopic Scale .....	32
3.3. Partial Differential Equations (PDEs) Model Formulation .....	33
3.3.1. Conservation of Mass: .....	34
3.3.2. Reaction Kinetics:.....	35
3.3.3. Conservation of Energy: .....	38
3.4. Computational Domain.....	44
3.5. Initial and Boundary Conditions.....	45
3.5.1. Initial conditions: .....	45
3.5.2. Boundary conditions: .....	45
3.6. Numerical Approach: Finite Volume Method (FVM).....	46
CHAPTER 4 .....	48

RESULTS AND DISCUSSION .....	48
4.1.    Results for Hydrogen Absorption Process in MH Reactors .....	48
4.1.1.    Equilibrium Pressure as a Function of Temperature and H/M Atomic Ratio .....	48
4.1.2.    Effect of Pressure Gradients on the Reacted Fraction Profile .....	48
4.1.3.    Temperature Profile Validation .....	50
4.1.4.    Temperature and Reacted Fraction Contours at Different Times .....	51
4.1.5.    Shape Consideration for Reactor 2 .....	55
4.1.6.    Reactor Size Impact on Charging and Temperature Profiles.....	56
4.1.7.    Pressure, Cooling Fluid Temperature and Boundary Conditions Analysis .....	57
4.2.    Results for Hydrogen Desorption Process in MH Reactors .....	60
4.2.1.    Validation of the Developed Numerical Model for Desorption.....	60
4.2.2.    Parametric Analysis of Pressure, Heating Fluid Temperature, and Porosity for Reactor 2	63
4.2.3.    Reactor Size Impact on Discharging Profile and Temperature Histories .....	67
CHAPTER 5 .....	69
CONCLUSION AND FUTURE SCOPE .....	69
5.1.    Conclusion.....	69
5.2.    Future Scope .....	71
RESULTING PUBLICATIONS AND AWARDS.....	72
REFERENCES .....	73

## LIST OF TABLES

	Page #
Table 2.1: Gravimetric energy densities of H <sub>2</sub> and several other fuels (Qazi 2022) .....	#17
Table 2.2: Comparison of the volumetric capacities of hydrogen in different states (Züttel et al. 2010; “Hydrogen Tools   CMB.TECH,” n.d.; “Hydrogen Calculators - Stargate Hydrogen,” n.d.).....	#20
Table 3.1: Thermo-physical properties and operating conditions (Yang et al. 2010; Elkhatab and Louahlia 2023; Nam, Ko, and Ju 2012; Hasnain, Khan, et al. 2024).....	#39
Table 3.2: Reactions kinetics and P-C-T parameters in eq. (8) to eq. (11) (Yang et al. 2010; Nam, Ko, and Ju 2012; Elkhatab and Louahlia 2023; Yuqi Wang et al. 2010).....	#42

## LIST OF FIGURES

	Page #
Figure 1.1: Increasing trends of atmospheric CO <sub>2</sub> and global temperature since 1880 (“Global Warming Update,” n.d.).....	#13
Figure 2.1: The different colors of hydrogen depending on production method (Shafiee 2021).....	#18
Figure 2.2: A schematic for solar energy system coupled with water electrolyzer and fuel cell (Zeng and Zhang 2010).....	#19
Figure 2.3: Schematic for simplified configuration of the metal hydride tank with heat transfer fluid (1: HTF pathway, 2: MH bed, 3: Hydrogen pathway) (Manai et al. 2019; Satheesh, Muthukumar, and Dewan 2009).....	#22
Figure 2.4: Volumetric and gravimetric hydrogen density of few selected hydrides (Modi and Aguey-Zinsou 2021).....	#23
Figure 2.5: The schematic of MH tank design with concentric tubes for fluid flow and transverse annular fins (Nyamsi, Yang, and Zhang 2012).....	#27
Figure 2.6: (a) The MH Hydrogen Storage Tank Only with Heat Transfer Fluid (NO PCM) (b) Modified Tank with PCM (Ye et al. 2022).....	#27
Figure 3.1: Cross sectional schematic for (a) MH reactor 1 (A. Jemni and Nasrallah 1995b; Hasnain, Khan, et al. 2024) (b) MH reactor 2 (Satheesh, Muthukumar, and Dewan 2009).....	#32
Figure 3.2: Averaging volume for porous MH bed with solid and gas phases.....	#33
Figure 3.3: 2D axis-symmetrical computational domain (a) For reactor 1 (b) For reactor 2.....	#44
Figure 3.4: Control volume for two-dimensional model (In 2D, each cell has four faces labeled with east (E), west (W), north (N), and south (S)).....	#47
Figure 4.1: Equilibrium pressure as a function of the H/M atomic ratio and temperature for hydrogen absorption (experimental data source: Dhaou et al. (Dhaou et al. 2007)).....	#48



Figure 4.2: Validation of reacted fraction profiles (a) For reactor 1 with experimental data (Yang et al. 2010), (b) Comparison between simplified model (no pressure gradients) and Nam et al. model (considering darcy's law) for reactor 2 (Nam, Ko, and Ju 2012) .....	#50
Figure 4.3: Validation of the temperature profile at (1.5 cm, 4.5 cm) for reactor 2 with (a) Experimental data (Abdelmajid Jemni, Nasrallah, and Lamloumi 1999; Elkhatib and Louahlia 2023) , (b) Comparison with Nam et al. model (Nam, Ko, and Ju 2012) .....	#51
Figure 4.4: Comparison of reacted fraction contours for reactor 1 at (a) Time = 10 seconds (11% charged system: start of the absorption process) (b) Time = 100 seconds (63% charged system: middle of the absorption) (c) Time = 600 seconds (99.3% charged system: end of the absorption) .....	#52
Figure 4.5: Comparison of temperature contours for reactor 1 at <b>(a)</b> Time = 10 seconds (11% charged system: start of the absorption process) <b>(b)</b> Time = 100 seconds (63% charged system: middle of the absorption) <b>(c)</b> Time = 600 seconds (99.3% charged system: end of the absorption) .....	#53
Figure 4.6: Comparison of reacted fraction contours for reactor 2 at (a) Time = 100 seconds (3.3% of the Charging Duration) (b) Time = 1000 seconds (33.3% of the Charging Duration) (c) Time = 2000 seconds (66.7% of the Charging Duration) .....	#54
Figure 4.7: Comparison of temperature contours [in Kelvin] for reactor 2 at (a) Time = 100 seconds (3.3% of the Charging Duration) (b) Time = 1000 seconds (33.3% of the Charging Duration) (c) Time = 2000 seconds (66.7% of the Charging Duration).....	#55
Figure 4.8: Comparison of (a) Reacted fraction and (b) Temperature evolution profiles.....	#56
Figure 4.9: The effect of reactor size on (a) Mean reacted fraction profile and (b) Temperature evolution profile.....	#57
Figure 4.10: Correlation of charging duration with (a) Length of the reactor, (b) Cross-sectional area of the reactor .....	#58
Figure 4.11: Comparison of the mean reacted fraction profiles for different charging pressures .....	#58
Figure 4.12: Comparison of the temperature profiles for different charging pressures (a) At (15, 45) mm, (b) Mean temperature.....	#59

Figure 4.13: Comparison of mean reacted fraction profiles for different (a) Cooling fluid temperatures, (b) Boundary conditions .....	#60
Figure 4.14: Equilibrium pressure as a function of H/M atomic ratio and temperature for hydrogen desorption (experimental data source: (Kyoung et al. 2015)).....	#61
Figure 4.15: Experimental validation and verification of reacted fraction profile with Yang et al. (yang et al. 2010) for reactor 1.....	#62
Figure 4.16: Experimental validation and verification of the temperature profiles with Kyoung et al. model (Kyoung et al. 2015) for reactor 2 (a) At point A, (b) At point B (c) locations of point A and point B in the reactor 2.....	#63
Figure 4.17: Comparison of the (a) Mean reacted fraction profiles (b) Time histories of mean temperature, at different discharging pressures .....	#64
Figure 4.18: Comparison of the (a) Mean reacted fraction profiles (b) Time histories of mean temperature, at different heating fluid temperatures .....	#66
Figure 4.19: Comparison of the (a) Mean reacted fraction profiles (b) Time histories of mean temperature, at different porosities of the MH bed .....	#67
Figure 4.20: Effect of reactor size on the (a) Reacted fraction profiles (b) Time histories of mean temperatures.....	#68

## NOMENCLATURE

A	parameter in P-C-T equation
B	parameter in P-C-T equation [K]
$C_p$	specific heat capacity [J/kg K]
E	activation energy [J/mol]
h	convective heat transfer coefficient [ $\text{W/m}^2 \text{ K}$ ]
$\Delta H$	reaction enthalpy [J/mol $\text{H}_2$ ]
[H/M]	hydrogen to metal ratio
k	reaction rate constant [ $\text{s}^{-1}$ ]
K	permeability [ $\text{m}^2$ ]
$\dot{m}$	mass source term of reaction [ $\text{kg/m}^3 \text{ s}$ ]
P	pressure [Pa]
P-C-T	pressure-composition-temperature
q	mass flow rate [kg/s]
r	r-coordinate [m]
$R_g$	general gas constant [J/mol K]
t	time [s]
T	temperature [K]
U	gas velocity [m/s]
W	mass [kg]
X	reacted fraction of hydrogen
z	z-coordinate [m]

## GREEK SYMBOLS

$\beta$	hysteresis factor in P-C-T equation
$\varepsilon$	porosity

$\lambda$	thermal conductivity [W/m K]
$\mu$	dynamic viscosity [Pa.s]
$\rho$	density [kg/m <sup>3</sup> ]
$\phi$	plateau flatness factor in P-C-T equation
$\phi_0$	plateau flatness factor in P-C-T equation

### **SUBSCRIPTS**

a	absorption
b	bulk
d	desorption
e	equilibrium
eff	effective
ex	exerted
f	heat transfer fluid
g	hydrogen gas
MH	metal hydride
sat	saturated

## CHAPTER 1

### 1. INTRODUCTION

#### 1.1. Background and Motivation

In light of rapidly increasing global energy demands and growing concerns regarding the environmental impacts of non-renewable energy sources, there is an escalating need for reliable and sustainable alternatives. In this context, fig. (1.1) illustrates the trajectory of global temperature anomaly and atmospheric CO<sub>2</sub> concentrations since the 1880s, providing a visual depiction of the evolving climate landscape (“Global Warming Update,” n.d.). Renewable energy technologies, exemplified by solar and wind power, play pivotal roles in mitigating greenhouse gas emissions and meeting energy demands. However, due to dependence on many natural factors (such as wind speed, sunlight intensity, daylight duration, weather etc.), their availability at a given location and time cannot be predetermined (Modi and Aguey-Zinsou 2021). Resultantly, it can lead to an imbalance between energy demand and supply. Addressing this challenge necessitates effective energy storage solutions. While batteries are commonly employed for energy storage, their utility is limited by factors such as high cost, uncertain lifespan, low energy density, self-discharge, safety concerns, thermal runaway, and rapid degradation, rendering them unsuitable for long-term or high-capacity applications (Y. Zhang et al. 2017; S. Khan, Hasnain, and Casa 2024; S. Khan et al. 2022; 2024).

In this context, hydrogen (H<sub>2</sub>) emerges as a promising candidate for energy storage that can be utilized as a fuel as well (Jang, Cho, and Kang 2021; Hasnain, Khan, et al. 2024). Hydrogen has long been recognized as a viable, carbon-free alternative to hydrocarbon fuels and has a high gravimetric energy density, surpassing that of gasoline and diesel by up to three times (Kharel and Shabani 2018; Jang, Cho, and Kang 2021). It can react with oxygen to generate water, heat, and electricity in fuel cells (Modi and Aguey-Zinsou 2021; Nguyen and Shabani 2021) with no emissions. Nevertheless, challenges persist in efficiently producing, ensuring environmental friendliness, and safely storing hydrogen. Of the challenges encountered, storage remains a critical issue, prompting

exploration of various hydrogen storage techniques (Jain, Jain, and Jain 2010; Shabani, Andrews, and Badwal 2010). These techniques can be broadly categorized into three main approaches: 1) high-pressure gaseous-state hydrogen storage, 2) liquefaction of hydrogen gas for liquid-phase storage, and 3) solid-state reversible hydrogen storage employing carbon materials or metallic hydrides (Shabani and Andrews 2015; Hasnain, Khan, et al. 2024).

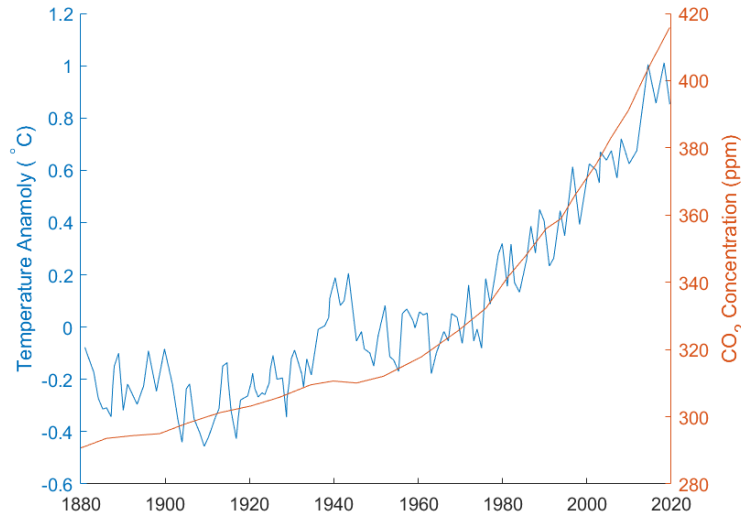


Figure 1.1: Increasing trends of atmospheric CO<sub>2</sub> and global temperature since 1880 (“Global Warming Update,” n.d.)

Solid-state hydrogen storage method utilizing metal hydrides has gained significant attention due to its relatively higher volumetric storage density, enhanced safety, and lower cost (Niaz, Manzoor, and Pandith 2015; Lototsky et al. 2017). A primary concern for metal hydride hydrogen storage systems is achieving rapid hydrogen charging/discharging rates under appropriate operating conditions. As depicted in eq. (1), hydrogen absorption and desorption with metals are exothermic and endothermic processes, respectively, with the reaction enthalpy varying depending on the metal hydride materials used (Hasnain, Khan, et al. 2024).



The heat released and absorbed during the absorption and desorption processes respectively raise and lower the temperature of the MH bed, resulting in a decrease in the corresponding reaction

rates (Nguyen and Shabani 2021). To accelerate these reactions, substantial heat uptake and release are necessary during the absorption and desorption of hydrogen. However, the inadequate thermal conductivity of the metal hydride bed hampers heat conduction within the bed, leading to prolonged charging and discharging durations. Therefore, when designing MH reactors, different thermal enhancements including the use of fins, heating fluid, or phase change materials (PCM) are considered (Afzal, Mane, and Sharma 2017). Moreover, to operate at room temperature, several critical physical parameters and operating conditions like the porosity of the bed, effective thermal conductivity, bed material, system pressure, fluid temperature, reactor size as well as other characteristics must be considered during designing these systems (Modi and Aguey-Zinsou 2021; Singh, Maiya, and Murthy 2015; Manai et al. 2019).

The objective of this work is to model the coupled heat and mass transfers during sorption processes and utilize it to examine the effect of various critical parameters, including charging pressure, cooling fluid temperature, reactor geometry and size, and different boundary conditions on the thermal performance and reaction kinetics of the system. The conservative nature of finite volume method ensures the conservation of parameters in each control volume and in the whole computational domain, making this model more efficient over its counterparts such as finite element method. This modeling work can be utilized to optimize the process parameters for specific applications that can lead to higher hydrogen storage efficiency and rapid system charging and discharging (Hasnain, Khan, et al. 2024). This study advances our comprehension of solid-state hydrogen storage and contributes to the development of efficient and dependable hydrogen storage technologies. Ultimately, this work plays a key role in advancing hydrogen as a green and sustainable future energy carrier.

## **1.2. How this Study is Novel**

The novelties listed below establish the originality of this work.

- i. The developed model can be effectively utilized to examine the performance of a broad range of metal hydrides and perform different parametric studies under varying thermophysical properties and environmental conditions.
- ii. In contrast to the studies in literature that primarily use commercial software, the model developed in this work is based on an open-source package based on finite volume method (FVM) available in MATLAB, Python, and Julia (Eftekhari and Schüller 2015). FVM inherently satisfies energy, mass, and momentum conservations; hence it is the fast and convenient discretization approach for the numerical solution of the partial differential equations governing the heat and mass transfer mechanisms in hydrogen absorption and desorption processes in metal hydrides.
- iii. This study pioneers a comparative examination into the impact of incorporating Darcy's velocity arising from pressure gradients into the model, an analysis that has not been done before.
- iv. This study conducts a comprehensive parametric analysis with respect to different thermophysical parameters, as well as the dimensions and configurations of the reactor, an area that is yet unexplored in the existing literature.



## CHAPTER 2

### 2. LITERATURE REVIEW

#### 2.1. Hydrogen: A Clean and Green Energy Source

The increasing global energy demand, growing concern about greenhouse gas emissions leading towards air pollution and global warming, and the reducing cost of renewable energy is driving the development of sustainable energy systems (Hasnain, Khan, et al. 2024). However, the energy obtained from renewable sources depends on and varies with many environmental conditions that cannot be predicted at a certain point in time and space (Modi and Aguey-Zinsou 2021; Beaudin et al. 2010). These variations cause fluctuations in the rate of power generation and therefore, the energy might not always be available when needed (Ibrahim, Ilinca, and Perron 2008). In order to avoid fluctuations, new solutions have been developed including storing the electricity for some time with rechargeable batteries (S. Khan et al. 2024; 2022; S. Khan, Hasnain, and Casa 2024).

In this context, batteries have gained interest as a potential energy storage solution, but the amount of possible stored energy is rather limited by current battery chemistries (S. Khan et al. 2024; S. Khan, Hasnain, and Casa 2024). In comparison, hydrogen ( $H_2$ ) can be used as an alternative environmentally friendly fuel because of its natural abundance, and high gravimetric energy density per unit mass (approximately 142 MJ /kg) (Mohammadshahi, Gray, and Webb 2016a; Hasnain, Khan, et al. 2024). Hydrogen also provides a green and clean secondary energy storage solution to the inconsistent availability of renewable energy sources (Mazloomi and Gomes 2012). High heating value (HHV) hydrogen has a gravimetric energy density that is up to three times greater than hydrocarbons present in traditional fuels like diesel, gasoline, and liquefied petroleum gas (Mazloomi and Gomes 2012) as shown in table 2.1. Besides,  $H_2$  is a clean fuel that produces only water as a biproduct with the generation of heat and electric power when consumed in a fuel cell (Hasnain, Khan, et al. 2024). Fuel cells are preferable to hydrogen combustion for energy generation due to their significantly higher energy conversion efficiency, with the theoretical maximum

exceeding 90% energy conversion efficiency for fuel cells (Haseli 2018). In contrast, hydrogen-based internal combustion engines have maximum conversion efficiency of around 45% (Onorati et al. 2022).

Hydrogen is considered a promising candidate for green energy storage mainly because of its superior efficiency in terms of its comparatively high energy content than traditional fuels as shown in table 2.1, overall storage capacity, renewability, versatility, and its lack of harmful emissions (Jang, Cho, and Kang 2021; Javaid 2021; Sánchez, Barreiro, and Maroño 2014; Pereira et al. 2017). Furthermore, hydrogen can be easily converted into heat or electric power by using internal combustion engines (ICEs) or fuel cells (FCs), respectively (Eriksson and Gray 2017; Verhelst 2014). Because of these features, hydrogen is a more cost-effective energy carrier for a wide range of large-scale and long-term applications, including the transportation and power generating industries (Maniatopoulos, Andrews, and Shabani 2015; Shin, Hwang, and Choi 2019), and stationary applications (Nguyen and Shabani 2021; Kharel and Shabani 2018).

Table 2.1: Gravimetric energy densities of H<sub>2</sub> and several other fuels (Qazi 2022)

Fuel	Fuel Energy Content (MJ /kg)
Hydrogen (H <sub>2</sub> )	142
Liquefied natural gas (LNG)	54.4
Propane	49.6
Aviation gasoline	46.8
Automotive gasoline	46.4
Automotive diesel	45.6
Ethanol	29.6
Methanol	19.7
Coke	27

Dry Wood	16.2
----------	------

## 2.2. Hydrogen Production and Applications

Apart from being the most abundant element in the universe, hydrogen does not exist in the gas form in sufficient quantities to generate power and must therefore be harvested from other organic substances and water (Dincer and Acar 2014; Momirlan and Veziroglu 2002). Hydrogen production process requires energy as an input. The energy used to extract hydrogen from organic substances releases carbon to the environment. Based on the amount of the carbon released to the atmosphere, the generated hydrogen is classified into colors as shown in fig. (2.1) (Shafiee 2021). Grey hydrogen is generated from natural sources that produces carbon waste to the environment. Blue hydrogen is relatively a cleaner approach in which the air pollutants are filtered, stored, or reused for different industrial applications. The production of green hydrogen is not associated with any emissions directly and can be ideally referred to as zero emissions process (Momirlan and Veziroglu 2002).

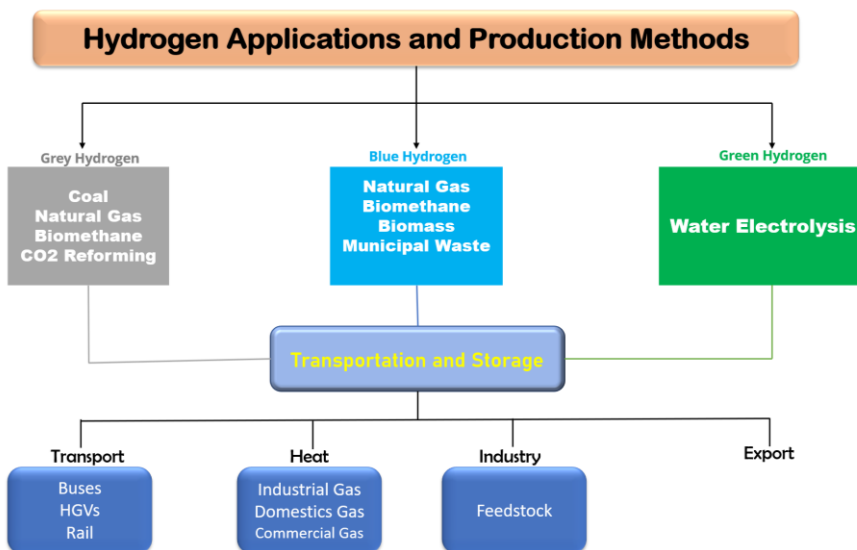


Figure 2.1: The different colors of hydrogen depending on production method (Shafiee 2021)

For utilizing renewable energy sources, water electrolysis is the simplest and most sustainable way to produce green hydrogen (Zeng and Zhang 2010; Dunn 2002). This method plays

a critical role in the coupling of solar or wind power systems with fuel cells. The excess electrical energy obtained from wind or solar energy can be utilized in the electrolyzers for breaking water ( $H_2O$ ) molecules to produce hydrogen gas that can be used as a promising candidate for energy storage and transportation for small-scale applications (Zeng and Zhang 2010). The generated hydrogen can be input to the fuel cells to generate electrical power and heat energy (Granovskii, Dincer, and Rosen 2006; Young, Mill, and Wall 2007). The conceptualized schematic of such a renewable energy generation, and conversion system coupled with a fuel cell is shown in fig. (2.2) (Zeng and Zhang 2010). The commercial production of green hydrogen is much more expensive and inefficient at this time, inhibiting its viability compared to other methods of production (Nikolaidis and Poullikkas 2017). Alternative approaches for grey or blue hydrogen production include steam methane reforming (SMR) (Sharma and Ghoshal 2015), gasification of coal and other hydrocarbons including biomass and municipal wastes and refining of petroleum (Trommer et al. 2005; Rosen and Scott 1998; Zeng and Zhang 2010).

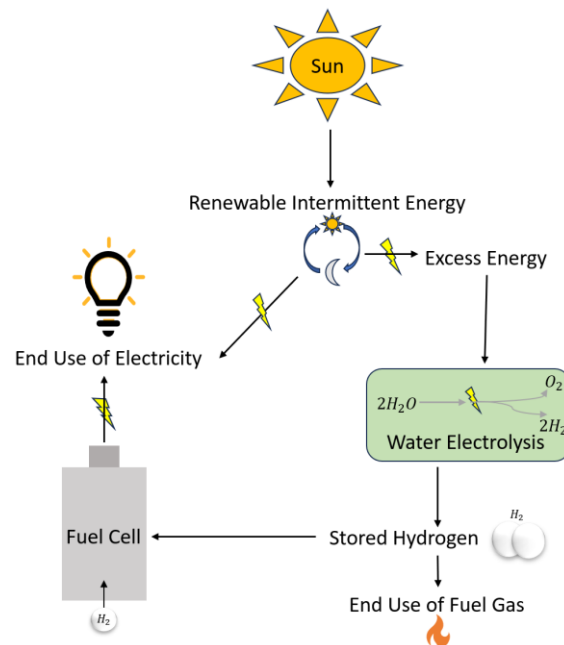


Figure 2.2: A schematic for solar energy system coupled with water electrolyzer and fuel cell

(Zeng and Zhang 2010)

Hydrogen can be used in fuel cells to generate electricity or directly used as a fuel for powering combustion engines. In industrial applications, hydrogen is used for large scale production of ammonia (Ramachandran and Menon 1998), refining of petroleum (Barreto, Makihiro, and Riahi 2003) and many metallic elements such as nickel, copper, zinc and tungsten (Eliaz, Eliezer, and Olson 2000; Eliezer et al. 2000). Utilizing water electrolysis to create hydrogen can help remote places with excess solar or wind energy sources fulfill their domestic energy needs for things like lighting and heating, and many industrial and telecommunication facilities (Hollmuller et al. 2000; Varkaraki, Lymberopoulos, and Zachariou 2003; Zeng and Zhang 2010).

### 2.3. Storage of Hydrogen

Integrated hydrogen systems (consisting of fuel cells or combustion engines, electrolyzers, and energy generation system) need technology to store and transport  $H_2$  for many applications (Jain, Jain, and Jain 2010; Shabani, Andrews, and Badwal 2010). Hydrogen can be kept either in gaseous state under high pressure or as a liquid, depending on the application where weight is an influential constraint.

In its gaseous state, hydrogen exhibits a low volumetric energy density, approximately 27 kg  $H_2/m^3$  as shown in table 2.2 (Züttel et al. 2010; “Hydrogen Tools | CMB.TECH,” n.d.; “Hydrogen Calculators - Stargate Hydrogen,” n.d.). Consequently, a substantially larger storage area is required relative to alternative energy storing solutions, posing technical challenges in storage, transportation, and portable applications (Andrews and Shabani 2012; Nguyen and Shabani 2021). To address this issue, two primary approaches have been explored: high-pressure gas compression at around 700 bars and liquefaction achieved by maintaining cryogenic temperatures near 20 K. However, both methods require additional costs associated with maintaining extreme temperature and pressure conditions (J. Zhang et al. 2005; Azzaro-Pantel 2018; Rowsell and Yaghi 2005).

Table 2.2: Comparison of the volumetric capacities of hydrogen in different states (Züttel et al.

2010; “Hydrogen Tools | CMB.TECH,” n.d.)

Hydrogen storage forms and conditions	Volumetric capacity (kg H <sub>2</sub> /m <sup>3</sup> system)	Theoretical limit (kg H <sub>2</sub> /m <sup>3</sup> system)
Gaseous state (25°C and 50 MPa)	27	30.81
Liquefied hydrogen (−253°C and 0.1 MPa)	40	71
Metal hydride (25°C and 3 MPa)	50	110

\* "Theoretical limit" is the storage density of the pure material under ideal conditions, and the "Volumetric hydrogen density" includes the reduction due to storage vessel and other practical limitations. The theoretical limit for compressed hydrogen is calculated by using online available tools like Stargate Hydrogen ("Hydrogen Calculators - Stargate Hydrogen," n.d.) and CMB Hydrogen Tools ("Hydrogen Tools | CMB.TECH," n.d.) since hydrogen does not behave as an ideal gas under 50 MPa.

The former is the most popular commercial way for storing and transporting hydrogen to demand locations due to its simplicity and maturity (Jang, Cho, and Kang 2021). The latter approach consumes—up to 30%— of available energy during the liquefaction process, thus, making it energy inefficient (Modi and Aguey-Zinsou 2021; von Helmholt and Eberle 2007). For large-scale applications, however, both of these technologies have significant obstacles, including energy efficiency and safety due to low volumetric density and high pressure respectively (Abdalla et al. 2018).

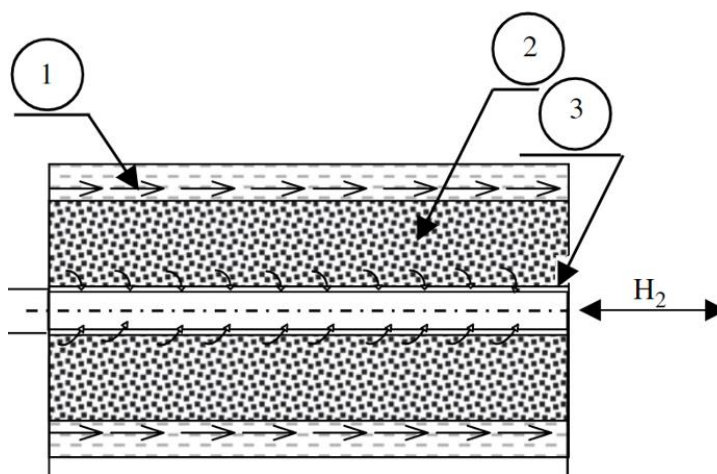


Figure 2.3: Schematic for simplified configuration of the metal hydride tank with heat transfer fluid (1: HTF pathway, 2: MH bed, 3: Hydrogen pathway) (Manai et al. 2019; Satheesh, Muthukumar, and Dewan 2009)

In comparison to the gaseous and liquified hydrogen storage methods, using solid state MH as hydrogen storage materials has the competitive potential to provide high volumetric energy density, high storage capacity as well as minimizing the safety risk associated with high pressure (Niaz, Manzoor, and Pandith 2015). The volumetric storage densities of hydrogen in each of its three states are shown in table 2.2. The popularity of MH based hydrogen storage systems, both in research and industry, is mainly attributed to its safety and lack of high pressure or low temperature requirements (Hasnain, Khan, et al. 2024). Unlike the former approaches, this method involves the absorption of hydrogen as atoms rather than gas phase molecules to the metal hydride material. However, due to the involvement of external metal hydride material (MH) as the storage medium, this method for hydrogen storage is intrinsically heavy, and is therefore best suited for stationary applications where bulk is not a major concern (Shabani and Andrews 2015). Other compelling advantages of using this technology include its relatively high volumetric storage density, safety, and reversibility, all of which enhance the viability of this solution (Lototskyy et al. 2017). The simplified configuration of the metal hydride tank with a heat transfer fluid is shown in the schematic shown in fig. (2.3) (Manai et al. 2019; Satheesh, Muthukumar, and Dewan 2009).

#### **2.4. Selection of Optimum Metal Hydride**

Metal hydrides are formed as the output of the reversible reactions between metal alloys and hydrogen at specific temperatures and pressures with a significant change in enthalpy (Nguyen and Shabani 2021). They are capable of safely and reliably storing substantial quantities of hydrogen in a solid phase. Since the 1970s, there has been a large amount of research and development on metal hydride adaption for hydrogen storage (Buschow, van Mal, and Miedema 1975; Vucht et al. 1970). Despite studying this group of materials for five decades, no consensus is yet established on the optimum MH due to wide range of stationary applications with varying storage parameters such as

sorption rates, operating temperatures, and tank pressures (Muthukumar and Groll 2010a). For example, the requirement of power-to-power systems is fast absorption/desorption kinetics while that of the seasonal storage systems are low-cost material and high volumetric storage density of the system for bulk hydrogen storage (Modi and Aguey-Zinsou 2021).

The selection of suitable hydride material requires the consideration of several critical factors. These include but are not limited to the reaction kinetics, the heat of formation of hydride, the system cyclic stability and life, safety in hydride production, sensitivity to gaseous impurities and particulates, process operation and handling, as well as the  $H_2$  hysteresis effects (Sandrock 1999; Lototsky et al. 2017).

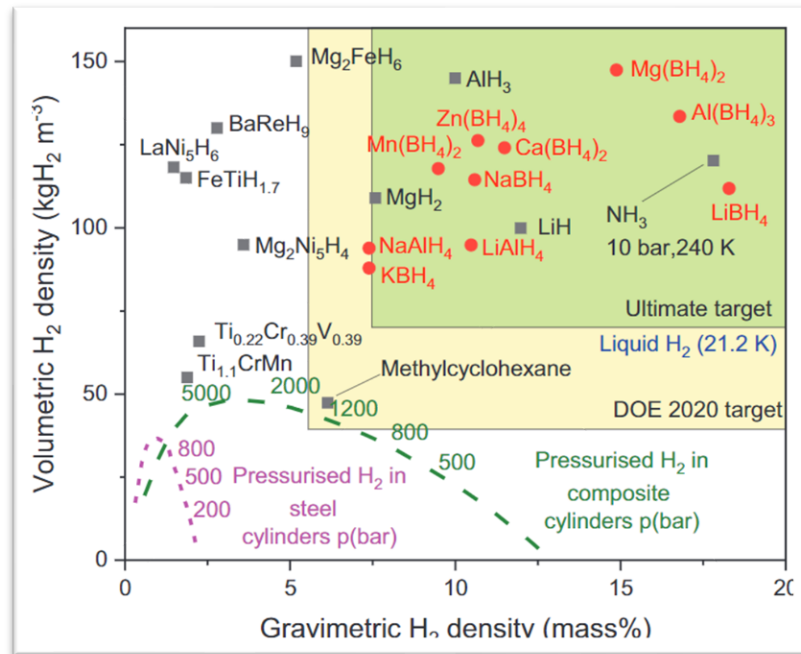


Figure 2.4: Volumetric and gravimetric hydrogen density of few selected hydrides (Modi and Aguey-Zinsou 2021; Lai et al. 2018)

Individual elements are typically not viable as practical hydrogen storage materials because of their low storage capacities and the requirement of extreme pressure and temperature conditions for absorption and desorption of hydrogen (Modi and Aguey-Zinsou 2021). For example, titanium (Ti) can absorb hydrogen to make titanium hydride (TiH<sub>2</sub>), however, it will need temperatures up to



800°C to fully release hydrogen during the discharge process (Suwarno et al. 2012). A material with high hydrogen storage capacity and reversible hydrogen uptake/release at ambient temperature and pressure would be an ideal choice for storing hydrogen. Complex metallic hydrides have high gravimetric and volumetric densities, but they are irreversible and therefore, are not practicable. As can be seen from fig. (2.4), the complex hydrides like  $\text{Mg}(\text{BH}_4)_2$ ,  $\text{Al}(\text{BH}_4)_3$  and  $\text{LiBH}_4$  have the capability to meet the higher gravimetric and volumetric hydrogen densities but their application is limited by their irreversible nature (Lai et al. 2018). An alternative choice would be to use intermetallic compounds or metal alloys since they can be operated at ambient settings (Sandrock 1999; Broom 2011). For instance,  $\text{LaNi}_5\text{H}_6$  is mostly suggested as the preferred metal hydride in the literature due to its high volumetric density and its reversibility at low temperature and pressure (Modi and Aguey-Zinsou 2021). To operate the MH-based hydrogen storage systems at room temperature, the design optimization of the MH tanks is a key challenge (Hasnain, Khan, et al. 2024). This needs the consideration of many important physical parameters like the overall porosity of the hydride bed, the packing density, effective thermal conductivity, the material of the cylinder, and the compactness of bed (Modi and Aguey-Zinsou 2021; Singh, Maiya, and Murthy 2015; Manai et al. 2019).

## 2.5. Heat Transfer Enhancements in MH Systems

The amount of heat absorbed or released during the reversible sorption processes accounts for around 10 – 20% of the high heating value (HHV) of hydrogen depending on the nature of MH and the pressure and temperature conditions (Lototskyy et al. 2017; Nguyen and Shabani 2020). To keep the operation temperature at the desired range, the extra heat generated from the exothermic absorption process needs to be removed from the MH bed (Nguyen and Shabani 2021). This is necessary to maintain the rate of absorption (also called charging rate) and maximize the utilization of available storage capacity of the MH and hence, the efficiency of the system. On the contrary, the thermal energy or heat required for the endothermic desorption (discharging) process must be continuously provided to the bed to maintain the desorption or discharge rate of hydrogen to meet

the energy demand from the fuel cell (Lototskyy et al. 2017; Nguyen and Shabani 2021). Due to the significant influence of heat on the rates of sorption reactions, the thermal management techniques should be taken into consideration while designing MH-based hydrogen storage systems (Moradi and Groth 2019; Ye et al. 2022).

As cooling during absorption and heating during desorption significantly influence the equilibrium pressure, leading to faster hydrogen charging and discharging, managing temperature is crucial in MH reactors. Currently, there are many thermal management approaches employed and modeled for MH-based hydrogen storage tanks (Afzal, Mane, and Sharma 2017).

- i. The first one involves the utilization of a heat transfer fluid (HTF). In the hydrogen absorption process, discharged heat is absorbed by the HTF, while during desorption, the fluid is externally heated to supply the additional heat required for hydrogen release (Chung et al. 2013; Bao, Yang, Wu, Cao, et al. 2013a; Hasnain, Khan, et al. 2024).
- ii. The second approach to heat transfer management involves integrating phase change materials (PCM) with hydrogen storage tanks (Ye et al. 2022). PCM has the capability to store waste heat generated during hydrogen absorption and release it when required for hydrogen desorption, eliminating the need for heat exchangers. This method enables the practical recycling of waste heat, thereby enhancing the overall efficiency of the system (Shamberger and Bruno 2020).
- iii. The third approach to thermal management, that in fact is a complement to the first two approaches, involves the use of fins to maximize the surface area of the bed with the heat transfer fluid (HTF) or phase change material (PCM), ultimately resulting in an increased heat transfer rate (Satya Sekhar et al. 2015).

Many attempts have been made to optimize the hydrogen storage process in MH storage systems by incorporating different heat exchangers inside hydrogen storage tanks. The major heat exchanger designs considered in the literature are axial heat exchanger tubes, coiled heat exchanger

tubes, and transversal heat distribution fins (Satya Sekhar et al. 2015). (Chaise et al. 2010) experimentally investigated a metal hydride tank incorporating a central tube heat exchanger and developed a two-dimensional numerical heat transfer model. (Bao, Yang, Wu, Cao, et al. 2013b) implemented a one-dimensional heat and mass transfer model to examine the temperature, pressure, and density distributions inside the magnesium hydride reactors.

The optimization study on different configurations of multi-tube heat exchange was done by (Bao, Wu, et al. 2013). (Ma et al. 2014) studied the performance of multi-tubular finned heat exchangers in MH tanks and optimized the heat transfer through fins. The heat exchanger designs are considered under four varying heat transfer configurations including natural convection, finned surfaces, internal circulation of fluid, and with the concentric fins inside the hydride tank (Modi and Aguey-Zinsou 2021). The most efficient design in terms of charging/discharging time found this study was the design with a concentric tube for fluid flow with transverse fins attached to the tube (Mohammadshahi, Gray, and Webb 2016a; Askri, ben Salah, et al. 2009). The schematic showing the design of such tank and fin configuration is shown in fig. (2.5). These studies show that the improvement is as a result of increased heat transfer areas. However, the complexity of the heat exchangers to further enhance the heat transfer limits the applicability of this approach. Furthermore, the requirement of an external heating source during the hydrogen desorption process is another factor lowering the efficiency further (Ye et al. 2022).

Numerous studies have investigated the performance of hydrogen storage tanks with and without the involvement of PCM. (Ye et al. 2022) develops a two-dimensional numerical model to provide a comparative analysis of the heat transfer mechanisms in the MH-tanks before and after the incorporation of PCM (as shown in fig. (2.6)). An experimental study was done by (Garrier et al. 2013) on magnesium hydride ( $\text{MgH}_2$ ) tanks using  $\text{Mg}_{69}\text{Zn}_{28}\text{Al}_3$  as the phase change material. However, the overall gravimetric storage density of the storage system was reduced (to about 0.315 wt%) due to the involvement of the dense PCM alloy. (Marty et al. 2013) developed a computational



Many numerical studies have been conducted to evaluate the influence of the physical properties of various choices of PCMs on absorption and desorption of hydrogen (Hatem ben Mâad et al. 2018) and (H. ben Mâad, Askri, and ben Nasrallah 2016). It was found out that the optimal selection of PCM, along with many other design and operation variables, depends on the MH material used for storage.  $\text{Mg}_{69}\text{Zn}_{28}\text{Al}_3$  was devised to be the suitable PCM for  $\text{Mg}_2\text{Ni}$  hydrogen storage material. While selecting a PCM many different parameters including but not limited to the nature of the MH material, its enthalpy of hydrogenation/dehydrogenation, operating temperature and pressure ranges, and the weight as well as the latent heat of the PCM are considered. (Yao et al. 2020a) performed a numerical study to optimize the storage performance in  $\text{LaNi}_5$  MH tanks with  $\text{Na}_2\text{HPO}_3 \cdot 7\text{H}_2\text{O}$  as the PCM. This study investigated various important parameters like the physical properties of PCM and absorption pressure of hydrogen to utilize the maximum storage capacity. Due to the lack of heat exchangers in hydrogen storage tanks with PCM, a huge amount of PCM must be provided to fully absorb the generated heat during absorption and maintain the reaction rate. Resultantly, this highly increases the weight of the tank and significantly reduces the gravimetric hydrogen storage density. Combining these two approaches, a more efficient storage can be designed with both heat exchangers and PCM used in parallel (Ye et al. 2022).

## 2.6. Mathematical Modeling of MH Reactors

The Numerical models for metal hydride hydrogen storage systems have been developed and reviewed in existing literature (A. Jemni and Nasrallah 1995a; Ben Nasrallah and Jemni 1997; Gopal and Murthy 1995; Gambini, Manno, and Vellini 2008; Brown et al. 2008; Nam, Ko, and Ju 2012; Mohammadshahi, Gray, and Webb 2016b; MacDonald and Rowe 2006; Hasnain, Khan, et al. 2024). These computational models are utilized to analyze one-dimensional (El Oseriy 1983; Lucas and Richards 1984; Ram Gopal and Srinivasa Murthy 1992; Mayer, Groll, and Supper 1987), two-dimensional (Muthukumar, Singhal, and Bansal 2012; Akanji and Kolesnikov 2012; Demircan et al. 2005; Muthukumar, Madhavakrishna, and Dewan 2007; Askri, Ben Salah, et al. 2009; A. Jemni and Nasrallah 1995b; Hasnain, Khan, et al. 2024), and three-dimensional (Aldas, Mat, and Kaplan 2002;

Hardy and Anton 2009a; Bao, Yang, Wu, Nyallang Nyamsi, et al. 2013; Hardy and Anton 2009b; Yun Wang et al. 2009) systems. These models traditionally incorporate heat and mass balance equations alongside empirically derived reaction kinetics, and serve to analyze the transport properties, equilibrium conditions, and reaction kinetics of MH systems. Notably, the three-dimensional model, while providing more comprehensive insights, demands significantly more time and computing capacity for execution. As a result, it is often selectively employed to investigate effects that two-dimensional models may not fully capture (Hardy and Anton 2009b).

In 1995, Jemni and Nasrallah (A. Jemni and Nasrallah 1995b) investigated the key parameters for a two-dimensional metal hydride reactor during hydrogen absorption. Their study challenged the local thermal equilibrium assumption between solid phase porous medium and gaseous phase hydrogen. However, in a later work in 1997, Nasrallah and Jemni (Ben Nasrallah and Jemni 1997) presented contradictory findings on this assumption and concluded that neglecting the temperature difference between the two phases has a minimal effect on the mass evolution profile during both hydrogen absorption and desorption processes. Following their work, almost all the subsequent studies simplified their models by assuming local thermal equilibrium, with the aim of minimizing computational complexity (Muthukumar and Groll 2010b; Mohammadshahi, Gray, and Webb 2016b; Nguyen and Shabani 2021; Chibani, Bougriou, and Merouani 2018). Several studies overlooked the impact of pressure drop and advection heat transport, due to the low hydrogen velocity in porous metal hydride bed (Elkhatib and Louahlia 2023; Ben Nasrallah and Jemni 1997; A. Jemni and Nasrallah 1995a; Mohammadshahi, Gray, and Webb 2016b; Hasnain, Sezer, and Mason 2024). Moreover, certain models assumed that equilibrium pressure was exclusively a function of temperature, neglecting its dependence on the hydrogen-to-metal atomic ratio (H/M) (Freni, Cipiti, and Cacciola 2009; Aldas, Mat, and Kaplan 2002; MacDonald and Rowe 2006; Kumar Phate, Prakash Maiya, and Murthy 2007; Chung and Ho 2009; Mohan, Prakash Maiya, and Srinivasa Murthy 2007).

Despite these modeling efforts, there is a pressing need for a comprehensive investigation into factors such as considering the influence of Darcy's velocity due to pressure gradients (Darcy's law), cooling strategy variations, reactor size impact on charging time, and a parametric analysis that is crucial for both enhancing fundamental understanding and optimizing the metal hydride hydrogen storage systems (Hasnain, Khan, et al. 2024; Hasnain, Sezer, and Mason 2024).

The objective of this work is to develop a numerical model to reveal the physics behind the hydrogen absorption and desorption, analyze the dynamic behavior of reaction kinetics, and optimize the processes in MH reactors. This purpose is achieved using a finite volume (FV) based discretization approach involving implicit Euler's time integration scheme (Eftekhari and Schüller 2015; S. Khan et al. 2022; Hasnain, Khan, et al. 2024; S. Khan et al. 2024; Hasnain et al., n.d.). The resulting linear system of equations is solved using a sparse matrix solver available in MATLAB (S. Khan, Hasnain, and Sezer 2024; S. Khan, Hasnain, and Casa 2024; M. U. Khan, Hasnain, and Khan 2024; Hasnain, Paye, et al. 2024; Hasnain, Khan, et al. 2024; S. Khan et al. 2024). The results obtained from the 2D axis-symmetrical model are found to be in good agreement with experimental data reported in the literature. Then the model is used to examine the effect of various pivotal parameters, including charging pressure, cooling fluid temperature, reactor geometry and size, and different boundary conditions on the thermal performance and reaction kinetics of the system. The influence of H/M atomic ratio on equilibrium pressure is also examined and validated with experimental data for varying temperatures (Hasnain, Sezer, and Mason 2024). This framework allows us to systematically evaluate the sensitivity of these parameters by analyzing temperature and reaction fraction profiles aimed at optimizing the storage efficiency. Furthermore, a comparative analysis is conducted between two models: one incorporating Darcy's velocity and the other without, while maintaining constant pressure within the metal hydride bed. Interestingly, incorporating Darcy's law introduces increased system complexity and numerical instability in the coupled equations, but it has minimal effect on the overall model outcomes (Hasnain, Sezer, and Mason 2024).

## CHAPTER 3

### 3. MATHEMATICAL MODEL

#### 3.1. System Description and Schematic

The schematic of a MH based hydrogen storage reactor is given in fig. (3.1). The reactor tank is divided into three sections as shown in the schematic. Section 1 represents the pathway for the heat transfer that is mostly considered to be water. Section 2 is the porous MH bed where the hydrogen absorption and desorption processes take place. Section 3 is the region where hydrogen is given into or taken out of the bed.

In the current work, two distinct MH reactors are examined, each characterized by unique cooling fluid configuration and size. Experimental data for both reactors are available in the literature (Yang et al. 2010; Elkhatab and Louahlia 2023; Ben Nasrallah and Jemni 1997), allowing for the validation of our model for each reactor configuration and comparison with other models. In this context, the MH tank shown in fig. (3.1a) is referred to as 'Reactor 1,' while the MH tank depicted in fig. (3.1b) is denoted as 'Reactor 2'. The dimensions of both reactors and corresponding computational domains are shown in fig. (3.3a) and (3.3b) respectively. Reactor 1 transfers heat only through its lateral side to the cooling fluid, whereas reactor 2 accomplishes this through both its lateral and base areas. Water is considered as the cooling fluid in this work.

In the cross-sectional view of the system, as depicted in fig. (3.1), the blue region at the base and lateral sides denotes the pathway for water flowing at a steady speed. The light blue color region represents the metal hydride (MH) powder bed, where the hydrogen absorption/desorption occurs. During absorption, the hydrogen diffuses from the pressurized region, reacts and gets stored in the interstitial sites of the crystal structure and vice versa. A thin stainless-steel (Yang et al. 2010) or brass (A. Jemni and Nasrallah 1995b) wall serves as a barrier, separating the heat transfer fluid from the MH bed. In this study,  $\text{LaNi}_5$  is utilized as the metal for hydrogen capture/release, which undergoes a transformation to  $\text{LaNi}_5\text{H}_6$  when it is fully saturated with hydrogen. The maximum mass of hydrogen that can be stored in reactor 1 and reactor 2 are, respectively, 0.2171 and 10.5975 grams.



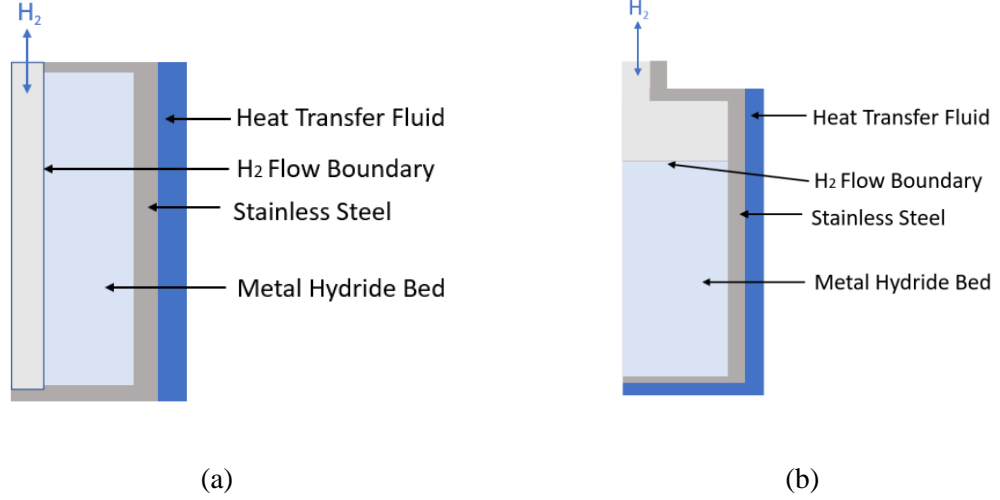


Figure 3.1: Cross sectional schematic for (a) MH reactor 1 (A. Jemni and Nasrallah 1995b; Hasnain, Khan, et al. 2024) (b) MH reactor 2 (Satheesh, Muthukumar, and Dewan 2009)

### 3.2. Effective Medium Theory: From Microscopic to Macroscopic Scale

The metal hydride bed is a discontinuous two-phase medium consisting of solid MH particles and hydrogen in the gaseous phase. The principles of conservation for energy, mass, and momentum that govern the heat, mass, and momentum transfer, respectively, in a reactive porous medium are derived by transitioning from a microscopic to a macroscopic scale based on the effective medium theory (Choy 2016). While shifting from a microscopic standpoint, where the average volume ( $\omega$ ) is significantly smaller than the pores volumes, to a macroscopic scale where the pores volume is almost negligible compared to averaging volume. This change of scale allows for the substitution the actual medium that is inherently discontinuous with a hypothetical continuous medium (A. Jemni and Nasrallah 1995a; Choy 2016). Each term in the macroscopic-scale continuum equation can be formulated by averaging its corresponding term in the microscopic equation. The averaging volume for a porous material with solid and gaseous phases is demonstrated by fig. (3.2). For a specific microscopic function ( $\bar{\phi}$ ), the average is given by eq. (2a). Similarly, eq. (2b) shows its intrinsic average over a phase  $i$  in the multi-phase porous medium.

$$\bar{\Phi} = 1/\omega \int_{\omega} \Phi \, d\omega \quad (2a)$$

$$\bar{\Phi}_i = 1/\omega_i \int_{\omega_i} \Phi_i \, d\omega \quad (2b)$$

where  $\omega_i$  represents the volume of phase i in the total averaging volume  $\omega$ .

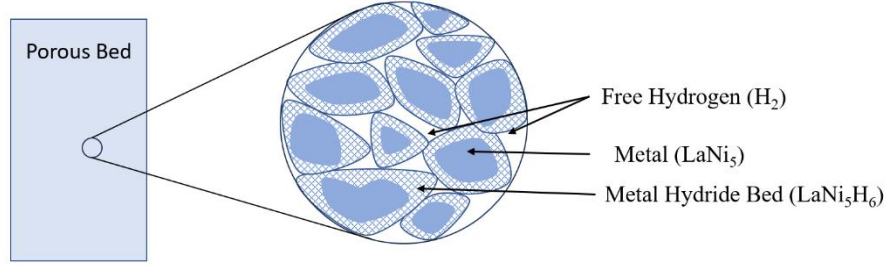


Figure 3.2: Averaging volume for porous MH bed with solid and gas phases

### 3.3. Partial Differential Equations (PDEs) Model Formulation

The macroscopic PDE model for the hypothetical continuous medium is derived by applying an averaging process to the corresponding microscopic equations and incorporating closure assumptions across the averaging volume  $\omega$ . The microscopic equations are based on the mass, energy, and momentum balance equations for each phase. The mathematical formulation for modeling the multi physics sorption phenomena in an MH reactor can be established based on the following simplifying assumptions:

- i. There is local thermal equilibrium between hydrogen gas and MH bed boundary. In other words, there is a common temperature on the interface between solid and gas phases and no temperature slip is involved.
- ii. Since the operating conditions are close to ambient temperature, and pressure, the gaseous phase within the metal hydride (MH) bed is considered to be an ideal gas. This allows for the utilization of the ideal gas equation for relating pressure and density of hydrogen in the bed.

- iii. The radiation heat transfer mechanism is neglected because the system is operated in a moderate temperature range.
- iv. The volumetric expansion/compression, viscous dissipation, and porosity variation of MH during the absorption/desorption process are considered negligible (Busqué et al. 2017).

### 3.3.1. Conservation of Mass:

The mathematical model for heat and mass transport in the MH bed integrates the principles of mass, energy, and momentum conservations within the reactive porous medium. These governing principles are coupled to formulate the modeling equations for MH-based hydrogen storage reactors (Satheesh, Muthukumar, and Dewan 2009; Yang et al. 2010; Elkhatib and Louahlia 2023). The conservation of mass for the gas phase is given by eq. (3) (Yang et al. 2010; Nam, Ko, and Ju 2012; Muhammad Hasnain et al. 2023).

$$\frac{\partial \varepsilon_g \rho_g}{\partial t} + \nabla(\rho_g \vec{U}) = -\dot{m} \quad (3)$$

Assuming hydrogen behaves as an ideal gas (as per eq. (4)) and incorporating Darcy's law given by eq. (5), the mass conservation equation for hydrogen can also be expressed as shown in eq. (6).

$$\rho_g = \frac{M_g P_g}{R T_g} \quad (4)$$

$$\vec{U} = -\frac{K}{\mu} \nabla P_g \quad (5)$$

$$\frac{\varepsilon M_g}{R_g} \frac{1}{T_g} \frac{\partial(P_g)}{\partial t} + \frac{\varepsilon M_g P_g}{R_g} \frac{\partial}{\partial t} \left( \frac{1}{T_g} \right) - \frac{k}{v_g} \frac{1}{r} \frac{\partial}{\partial r} \left( r \frac{\partial(P_g)}{\partial r} \right) - \frac{k}{v_g} \frac{\partial^2(P_g)}{\partial z^2} = -\dot{m} \quad (6)$$

In many studies the pressure gradients in the porous MH bed are considered negligible, due to the low hydrogen velocity (Elkhatib and Louahlia 2023; Ben Nasrallah and Jemni 1997; A. Jemni and Nasrallah 1995a; Mohammadshahi, Gray, and Webb 2016b; Hatem Ben Mâad et al. 2016; Chaise

et al. 2009). Under the assumption of uniform pressure, the mass transfer equations for gaseous and solid phase are given by eq. (7a) and (7b) respectively (Yao et al. 2020b):

$$\frac{\partial \varepsilon_{MH} \rho_g}{\partial t} = -\dot{m} \quad (7a)$$

$$\frac{\partial (1-\varepsilon_{MH}) \rho_s}{\partial t} = \dot{m} \quad (7b)$$

Where  $\varepsilon_{MH}$  and  $\rho_g$  represent the bed porosity and hydrogen density respectively, while  $\vec{U}$  stands for Darcy's velocity of hydrogen inside the bed given by eq. (5) where the parameters  $K$ , and  $\mu$  represent the bed permeability and dynamic viscosity of hydrogen respectively, while  $\nabla P_g$  denotes the pressure gradient in the computational domain.

### 3.3.2. Reaction Kinetics:

The source term in mass conservation equation ( $\dot{m}$ ) is obtained from the reaction kinetics and represents the absorption/desorption reaction rate of hydrogen per unit volume at a specific operating pressure given by eq. (8) and eq. (9) (Hattem Ben Mâad et al. 2016; A. Jemni and Nasrallah 1995c; Tao and He 2015; Gkanas et al. 2018; Nam, Ko, and Ju 2012). In other words, it relates the hydrogen uptake/release rate with the species concentrations (Mohammadshahi, Gray, and Webb 2016b). To establish a relationship for an MH reactor, Supper et al. (Supper, Groll, and Mayer 1984) and Suda et al. (Suda, Kobayashi, and Yoshida 1980) conducted experiments for the hydrogenation of metals like  $\text{LaNi}_5$  and  $\text{MmNi}_5$ . The reaction kinetics relations for the heat and mass transfer in  $\text{AB}_5$  types of MH systems presented by Mayer et al. (Mayer, Groll, and Supper 1987) have served as a foundation for subsequent researchers in modeling MH reactors (Akanji and Kolesnikov 2012; Ben Nasrallah and Jemni 1997; A. Jemni and Nasrallah 1995b; Askri, Ben Salah, et al. 2009).

$$\dot{m}_a = k_a \cdot e^{\left(-\frac{E_a}{RT_b}\right)} \cdot \ln\left(\frac{P_g}{P_{eq,a}}\right) \cdot (\rho_{sat} - \rho_s) \quad (8)$$

$$\dot{m}_d = k_d \cdot e^{\left(-\frac{E_d}{RT_b}\right)} \cdot \left(\frac{P_g - P_{eq,d}}{P_{eq,d}}\right) \quad (9)$$

In eq. (8) and eq. (9),  $\rho_{\text{sat}}$  and  $\rho_{\text{emp}}$  represent the saturation density of the bed, and hydrogen-free metal hydride density respectively.  $k_a$  and  $k_d$  are the rate constants, while  $E_a$  and  $E_d$  represent the activation energy for hydrogen absorption and desorption respectively.

The equilibrium pressures,  $P_{\text{eq},a}$  and  $P_{\text{eq},d}$  in eq. (8) and eq. (9) play a significant role in controlling the rates of both absorption and desorption reactions, as evident from eq. (3) and (4). The difference between the equilibrium pressure and the hydrogen pressure in the domain serves as the driving force for sorption processes. This implies that lower equilibrium pressure, given the same hydrogen pressure, leads to faster hydrogen absorption, while a higher equilibrium pressure enhances desorption (Mohammadshahi, Gray, and Webb 2016b).

The van 't Hoff equation, shown by eq. (10a), has been used in the literature to relate the equilibrium pressure ( $P_{\text{eq}}$ ) to the absolute bed temperature ( $T_b$ ), the change in enthalpy ( $\Delta H$ ) and entropy ( $\Delta S$ ) at a specific reacted fraction ( $X$ ) (Mellouli et al. 2010; Nam, Ko, and Ju 2012). For a specific metal hydride, the constant value of the change in enthalpy and entropy at a particular reaction fraction implies that the equilibrium pressure is not solely a function of bed temperature but also depends on the reacted fraction (H/M atomic ratio) (Nyamsi, Yang, and Zhang 2012; Walker and Institute of Materials 2008). The correlation of the equilibrium pressure with H/M atomic ratio and bed temperature, derived through van 't Hoff equation, is given by eq. (10b).

$$P_{\text{eq}} = \exp \left( \frac{\Delta H}{R T_b} - \frac{\Delta S}{R_g} \right) \quad (10a)$$

$$P_{\text{eq}} = f\left(\frac{H}{M}\right) \cdot \exp \left( \frac{\Delta H}{R} \left( \frac{1}{T_b} - \frac{1}{T_{\text{ref}}} \right) \right) \quad (10b)$$

Many other studies in the literature use an alternative approach based on the reacted fraction to solve the rate of absorption/desorption per unit volume (Nyamsi, Yang, and Zhang 2012; Yang et al. 2010; Ye et al. 2022; Bao, Yang, Wu, Cao, et al. 2013a). The formulation for that approach is presented in eq. (11)-eq. (13). The reacted fraction of hydrogen ( $X$ ) is the parameter (Yang et al. 2010; Chibani, Merouani, and Bougriou 2022; Nyamsi, Yang, and Zhang 2012) that quantifies the

H/M atomic ratio on a scale of 0 to 1. Following a linear interpolation and taking  $\rho_s = \rho_{\text{sat}}$  when  $X = 1$ , and  $\rho_s = \rho_{\text{emp}}$  when  $X = 0$ , the equation representing the reacted fraction  $X$  is shown by eq. (11).

$$X = \frac{\rho_{\text{sat}} - \rho_{\text{emp}}}{\rho_{\text{sat}} - \rho_{\text{emp}}} \quad (11)$$

$$\dot{m} = \frac{(1 - \varepsilon_{\text{MH}})\rho_{\text{MH}}}{M_{\text{MH}}} \left[ \frac{H}{M} \right]_{\text{max}} \frac{dX}{dt} \quad (12)$$

$$\frac{dX}{dt} = k_a \cdot e^{\left(-\frac{E_a}{RT_b}\right)} \cdot \ln\left(\frac{P_g}{P_{\text{eq},a}}\right) (1 - X) \quad (13a)$$

$$\frac{dX}{dt} = k_d \cdot e^{\left(-\frac{E_d}{RT_b}\right)} \cdot \left(\frac{P_g - P_{\text{eq},d}}{P_{\text{eq},d}}\right) (X) \quad (13b)$$

Achieving the most appropriate equilibrium pressure ( $P_{\text{eq}}$ ) is crucial for efficient MH tank design, emphasizing the need for accurate expressions for  $P_{\text{eq}}$  (Wijayanta et al. 2011; Mat and Kaplan 2001). While a temperature dependent van 't Hoff relation is widely used by the researchers to determine the equilibrium pressures, there are many studies utilizing the PCT and reaction kinetics parameters for determining the equilibrium pressures (Nishizaki, Miyamoto, and Yoshida 1983; Yang et al. 2010). Eq. (14a) and (14b) show the relations for absorption and desorption equilibrium pressures, respectively. These equations consider the effects of hysteresis and plateau slope (Nishizaki, Miyamoto, and Yoshida 1983) and exhibit a strong dependency on both the bed temperature and the reacted fraction. The values for the PCT parameters for absorption and desorption changes slightly in different studies as can be noticed from the studies done by (Yang et al. 2010; Muhammad Hasnain et al. 2023).

$$P_{\text{eq},a} = \exp\left(\frac{\Delta S}{R} - \frac{\Delta H}{RT_b} + (\phi + \phi_0) \cdot \tan\left(\pi\left(X - \frac{1}{2}\right)\right) + \frac{\beta}{2}\right) \quad (14a)$$

$$P_{\text{eq},d} = \exp\left(\frac{\Delta S}{R} - \frac{\Delta H}{RT_b} + (\phi - \phi_0) \cdot \tan\left(\pi\left(X - \frac{1}{2}\right)\right) - \frac{\beta}{2}\right) \quad (14b)$$

Yao et al. (Yao et al. 2020b), Elkhatib et al. (Elkhatib and Louahlia 2023) and many other researchers (Kyoung et al. 2015; Chung and Ho 2009; Elkhatib and Louahlia 2023; Mohan, Prakash Maiya, and Srinivasa Murthy 2007; Kumar Phate, Prakash Maiya, and Murthy 2007; MacDonald and Rowe 2006) used a different approach by assigning  $\frac{\Delta S}{R} - \ln(10) = A$  and  $\frac{\Delta H}{R} = B$  and considered the simplified version of the equilibrium pressure equation, obtained from Van't Hoff equation, that is only a function of temperature as listed in eq. (15).

$$\ln \left( \frac{P_{eq}}{P_{ref}} \right) = A - \frac{B}{T_b} \quad (15)$$

Where  $P_{ref} = 10$  bars.

In eq. (15) the values of A and B were considered to be 10.7 and 3704.6, respectively, and the reference pressure  $P_{ref}$  was taken as 10 bars. Elkhatib et al. (Elkhatib and Louahlia 2023) utilized the same relation for the equilibrium pressure, but they considered  $A = 14.045$  and  $B = 3719$  based on the experimental data, following by the regression analysis.

### 3.3.3. Conservation of Energy:

Considering local thermal non-equilibrium within the metal hydride (MH) bed, the energy balance equations can be formulated independently for the gas and solid phases within the porous MH bed. In 1995, Jemni and Nasrallah introduced their two-dimensional heat and mass transfer models for absorption and desorption in MH beds (A. Jemni and Nasrallah 1995b; 1995c), suggesting the following local thermal non-equilibrium equations for each phase.

$$(1 - \varepsilon) \rho_s^s C_{ps} \frac{\partial T_s}{\partial t} = (1 - \varepsilon) \lambda_s \nabla^2 T_s - H_{gs} (T_g - T_s) A_c + \dot{m} (\Delta H + C_{ps} T_s - C_{pg} T_g) \quad (16)$$

$$\varepsilon \rho_g^g C_{pg} \frac{\partial T_g}{\partial t} = \varepsilon \lambda_g \nabla^2 T_g - \rho_g^g C_{pg} \vec{v} \cdot \nabla T_g + H_{gs} (T_g - T_s) A_c + \dot{m} C_{pg} (T_g - T_s) \quad (17)$$

In eq. (16), and (17) "s" and "g" stand for the solid and gas phases,  $A_c$  represents the solid-gas contact area, and  $\lambda$  is the thermal conductivity.  $\dot{m}$  is the rate of reacted mass of hydrogen per unit

time per unit volume during absorption (Hattem Ben Mâad et al. 2016; Tao and He 2015; Gkanas et al. 2018) and  $H_{gs}$  stands for the heat transfer coefficient between the gas and solid phases in the bed.

The heat transfer equations for both phases include heat conduction ( $\lambda \nabla^2 T$ ), inter-phase natural convection ( $H_{gs}(T_g^g - T_s^s)S$ ), and changes in molecular energy due to sorption of hydrogen ( $\dot{m}C_{pg}(T_g^g - T_s^s)$ ). Eq. (17) also considers heat transfer due to gas movement ( $\rho_g^g C_{pg} \vec{U} \cdot \nabla T_g^g$ ), and the enthalpy changes of the hydriding and dehydriding reactions ( $\dot{m} \Delta H$ ) which are not needed for the solid phase equation.

Table 3.1: Thermo-physical properties and operating conditions (Yang et al. 2010; Elkhatib and Louahlia 2023; Nam, Ko, and Ju 2012; Hasnain, Khan, et al. 2024)

Parameters	Value	Unit
Initial temperature, $T_0$	293	[K]
Cooling fluid temperature, $T_f$	293	[K]
Exerted hydrogen pressure, $P_{ex}$	6 and 8	[bars]
Specific heat of hydrogen, $C_{p,g}$	14890	[J/(kg. K)]
Specific heat of the metal, $C_{p,s}$	419	[J/(kg. K)]
Thermal conductivity of hydrogen, $k_g$	0.167	[W/(m. K)]
Thermal conductivity of the metal, $k_s$	3.18	[W/(m. K)]
Porosity of the metal, $\epsilon_{MH}$	0.5	---
Permeability of the metal, $K$	$1.11 \times 10^{-11}$	[m <sup>2</sup> ]
Convective heat transfer coefficient, $h$	1500	[W/(m <sup>2</sup> . K)]



Dynamic viscosity of hydrogen, $\mu$	$8.9 \times 10^{-6}$	[Pa . s]
Molar mass of hydrogen, $M_g$	$2.0158 \times 10^{-3}$	[kg/mol]

To obtain the combined heat transfer equation based on local thermal equilibrium assumption, equations (16) and (17) are added:

$$\begin{aligned}
& \left[ (1 - \varepsilon) \rho_s^s C_{ps} \frac{\partial T_s}{\partial t} \right] + \left[ \varepsilon \rho_g^g C_{pg} \frac{\partial T_g}{\partial t} \right] \\
& = \left[ (1 - \varepsilon) \lambda_s \nabla^2 T_s - H_{gs} (T_g - T_s) A \right. \\
& \quad \left. + \dot{m} (\Delta H + C_{ps} T_s - C_{pg} T_g) \right] \\
& \quad + \left[ \varepsilon \lambda_g \nabla^2 T_g - \rho_g^g C_{pg} \vec{U} \cdot \nabla T_g + H_{gs} (T_g - T_s) A \right. \\
& \quad \left. + \dot{m} C_{pg} (T_g - T_s) \right]
\end{aligned} \tag{18}$$

Adding the corresponding terms in eq. (18) and expanding the terms  $\dot{m} (\Delta H^\circ + C_{ps} T_s - C_{pg} T_g)$  and  $\dot{m} C_{pg} (T_g - T_s)$  based on distributive property of multiplication over addition will yield eq. (19) below:

$$\begin{aligned}
& \left[ (1 - \varepsilon) \rho_s^s C_{ps} \frac{\partial T_s}{\partial t} + \varepsilon \rho_g^g C_{pg} \frac{\partial T_g}{\partial t} \right] \\
& = \left[ (1 - \varepsilon) \lambda_s \nabla^2 T_s + \varepsilon \lambda_g \nabla^2 T_g - H_{gs} (T_g - T_s) A \right. \\
& \quad \left. + H_{gs} (T_g - T_s) A - \rho_g^g C_{pg} \vec{U} \cdot \nabla T_g + \dot{m} \Delta H \right. \\
& \quad \left. + \dot{m} C_{ps} T_s - \dot{m} C_{pg} T_g + \dot{m} C_{pg} T_g - \dot{m} C_{pg} T_s \right]
\end{aligned} \tag{19}$$

Cancel out the inverse terms  $-H_{gs} (T_g - T_s) A$  and  $H_{gs} (T_g - T_s) A$  as well as  $-\dot{m} C_{pg} T_g$  and  $\dot{m} C_{pg} T_g$ , the equation can be rewritten as:

$$\begin{aligned}
& \left[ (1 - \varepsilon) \rho_s^s C_{ps} \frac{\partial T_s}{\partial t} + \varepsilon \rho_g^g C_{pg} \frac{\partial T_g}{\partial t} \right] \\
& = \left[ (1 - \varepsilon) \lambda_s \nabla^2 T_s + \varepsilon \lambda_g \nabla^2 T_g - \rho_g^g C_{pg} \vec{U} \cdot \nabla T_g \right. \\
& \quad \left. + \dot{m} \Delta H + \dot{m} C_{ps} T_s - \dot{m} C_{pg} T_s \right]
\end{aligned} \tag{20}$$

Now substitute  $T_g = T_b$  and  $T_s = T_b$  based on local thermal equilibrium assumption to get eq. (21).

$$\begin{aligned}
& \left[ (1 - \varepsilon) \rho_s^s C_{ps} \frac{\partial T_b}{\partial t} + \varepsilon \rho_g^g C_{pg} \frac{\partial T_b}{\partial t} \right] \\
& = \left[ (1 - \varepsilon) \lambda_s \nabla^2 T_b + \varepsilon \lambda_g \nabla^2 T_b - \rho_g^g C_{pg} \vec{U} \cdot \nabla T_b + \dot{m} \Delta H + \dot{m} C_{ps} T_s \right. \\
& \quad \left. - \dot{m} C_{pg} T_s \right]
\end{aligned} \tag{21}$$

Taking common factors outside of all the corresponding terms:

$$\begin{aligned}
& \left[ (1 - \varepsilon) \rho_s^s C_{ps} + \varepsilon \rho_g^g C_{pg} \right] \frac{\partial T_b}{\partial t} \\
& = \left[ \left( (1 - \varepsilon) \lambda_s + \varepsilon \lambda_g \right) \nabla^2 T_b - \rho_g^g C_{pg} \vec{U} \cdot \nabla T_b + \dot{m} (\Delta H + T_b (C_{pg} - C_{ps})) \right]
\end{aligned} \tag{22}$$

Substitute  $[(1 - \varepsilon) \rho_s^s C_{ps} + \varepsilon \rho_g^g C_{pg}] = (\rho_b C_{p,b})_{\text{eff}}$  and  $(1 - \varepsilon) \lambda_s + \varepsilon \lambda_g = \lambda_{\text{eff}}$  in eq. (22) to get the final heat transfer equation for the effective medium (MH bed).

$$\left[ (\rho_b C_{p,b})_{\text{eff}} \right] \frac{\partial T_b}{\partial t} = \left[ (\lambda_{\text{eff}} \nabla^2 T_b - \rho_g^g C_{pg} \vec{U} \cdot \nabla T_b + \dot{m} (\Delta H + T_b (C_{pg} - C_{ps}))) \right] \tag{23}$$

Different studies in literature have considered the heat transfer equation differently based on various assumptions and these are presented in eq. (24) through (26). Eq. (24) accounts for the impact of Darcy's velocity due to pressure gradients but neglects the linear source term responsible for the change in molecular energy (Yang et al. 2010; Nam, Ko, and Ju 2012; Mohammadshahi, Gray, and Webb 2016b), while eq. (25) neglects the pressure gradients and Darcy's velocity as well as the linear source term (D. Wang et al. 2019; Chibani, Bougriou, and Merouani 2018). Similarly, eq. (26) only neglects the convection heat transfer between the two phases due to Darcy's velocity (Abdelmajid Jemni, Nasrallah, and Lamloumi 1999; Elkhatib and Louahlia 2023; Chaise et al. 2009).

$$\frac{\partial(\rho_b C_{p,b})_{\text{eff}} T_b}{\partial t} + \nabla \cdot (\rho_g C_{p,g} \vec{U} T_b) = \nabla(\lambda_{\text{eff}} \nabla T_b) + \dot{m} \cdot \Delta H \quad (24)$$

$$\frac{\partial(\rho_b C_{p,b})_{\text{eff}} T_b}{\partial t} = \nabla(\lambda_{\text{eff}} \nabla T_b) + \dot{m} \cdot \Delta H \quad (25)$$

$$\frac{\partial(\rho_b C_{p,b})_{\text{eff}} T_b}{\partial t} = \nabla(\lambda_{\text{eff}} \nabla T_b) + \dot{m} \cdot \Delta H + \dot{m} \cdot T_b (C_{p,g} - C_{p,s}) \quad (26)$$

The coefficients of the transient term, representing the effective heat capacity, and that of the diffusion term  $\lambda_{\text{eff}}$ , representing the effective thermal conductivity, are given by eq. (27) and eq. (28) respectively.

$$(\rho_b C_{p,b})_{\text{eff}} = \varepsilon_{\text{MH}} \rho_g C_{p,g} + (1 - \varepsilon_{\text{MH}}) \rho_s C_{p,s} \quad (27)$$

$$\lambda_{\text{eff}} = [\varepsilon_{\text{MH}} \lambda_g + (1 - \varepsilon_{\text{MH}}) \lambda_{\text{MH}}] \quad (28)$$

The coefficient of the transient term in the energy equation, representing the bulk heat capacity of the bed, is determined by the product of the MH bed density and specific heat. This value accounts for the sum of all constituent phases present in the system (Yang et al. 2010).

$$\rho_b C_{p,b} = \sum_{i=1} \varepsilon_i \rho_i C_{p,i} \quad (29)$$

The physical parameters like porosity, permeability, initial densities, and other pertinent values, considered in this work, are shown in table 3.1. The constant reaction kinetic parameters are shown in table 3.2.

Table 3.2: Reactions kinetics and P-C-T parameters in eq. (8) to eq. (11) (Yang et al. 2010; Nam, Ko, and Ju 2012; Elkhatib and Louahlia 2023; Yuqi Wang et al. 2010)

Parameters	Absorption	Desorption	Unit	References
Rate constant, $k_{a,d}$	59.187	9.57	$[s^{-1}]$	(Elkhatib and Louahlia 2023; Yang et al. 2010; Mohammadshahi, Gray, and Webb 2016b)

Activation energy, $E_{a,d}$	21179 16473	[J/mol H <sub>2</sub> ]	(Elkhatib and Louahlia 2023; Yang et al. 2010; Mohammadshahi, Gray, and Webb 2016b)
P-C-T parameter, A	13.1	---	(Elkhatib and Louahlia 2023; Yang et al. 2010)
P-C-T parameter, B	3700	[K]	(Yang et al. 2010)
Plateau flatness factor, $\phi$	0.038	---	(Yang et al. 2010)
Plateau flatness factor, $\phi_0$	0	---	(Yang et al. 2010)
Hysteresis factor, $\beta$	0.137	---	(Elkhatib and Louahlia 2023; Yang et al. 2010)
Reaction enthalpy, $\Delta H$	30100 - 30800	[J/mol]	(D. Wang et al. 2019; MacDonald and Rowe 2006) -(Elkhatib and Louahlia 2023; Yang et al. 2010)
Saturation density, $\rho_{sat}$	6520 - 8527	[kg/m <sup>3</sup> ]	(Elkhatib and Louahlia 2023)- (Kyoung et al. 2015; Bao, Yang, Wu, Nyallang Nyamsi, et al. 2013)

Hydrogen-free metal	6430 -	[kg/m <sup>3</sup> ]	(Elkhatib and Louahlia 2023)
density, $\rho_{\text{emp}}$	8400		

### 3.4. Computational Domain

The system can be modeled as an axis symmetrical two-dimensional domain in cylindrical coordinates. The dimensions of the MH tank cross section are shown in fig. (3.3a) and fig. (3.3b) for reactor 1 and reactor 2 respectively (Hasnain, Sezer, and Mason 2024). These dimensions are considered for initial analysis and can be customized to optimize the performance of the system. It is assumed that the heat exchange between MH bed and heat transfer fluid takes place instantly and hence the tank material (stainless steel/brass) is not considered in the simplified model.

#### Reactor 1:

Axial coordinates:  $z = 0$  to 25.4 mm

Radial coordinates:  $r = r_i = 6.35/2$  mm to  $r_o = 6.35$  mm

#### Reactor 2:

Axial coordinates:  $z = 0$  to 60 mm

Radial coordinates:  $r = r_i = 0$  to  $r_o = 25$  mm

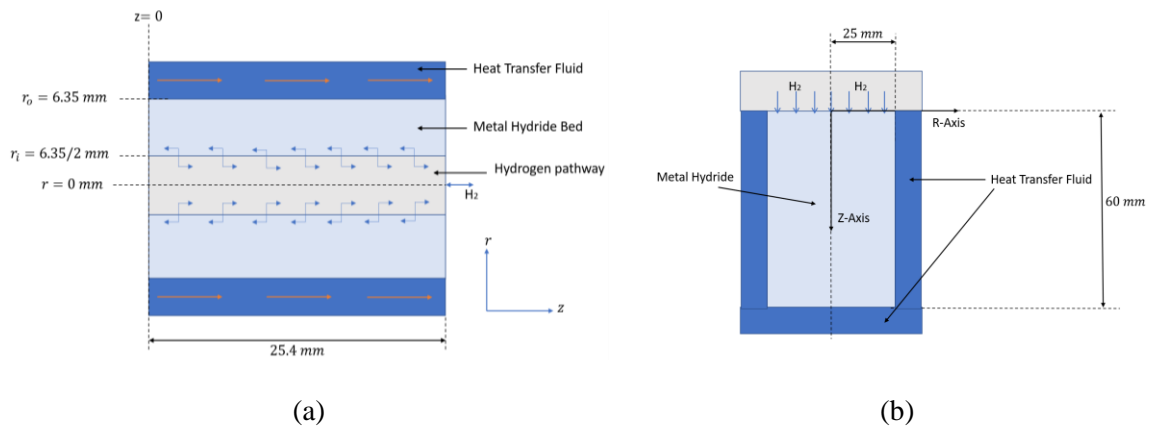


Figure 3.3: 2D axis-symmetrical computational domain (a) For reactor 1 (b) For reactor 2

### 3.5. Initial and Boundary Conditions

#### 3.5.1. Initial conditions:

It is assumed that the system is in equilibrium thermodynamically. This implies that the temperature of the hydride bed and hydrogen gas is the same. Initially, the bed is considered at room temperature.

$$T(r, z, t = 0) = T_{\text{initial}} = 298 \text{ K} \quad (30)$$

#### 3.5.2. Boundary conditions:

The insulated tank walls, in the case of reactor 1, are subject to homogeneous Neumann's boundary conditions due to zero slip velocity (impermeable wall or no flow condition) and no-flux. Likewise, because of the symmetry, the same boundary conditions are applied at the axis of reactor 2.

$$\nabla T_b = 0, \quad \nabla P_g = 0 \quad (31)$$

The boundary conditions for the interfaces where the bed exchanges heat with the cooling fluid (heat transfer walls) are given by eq. (32) and (33), where  $T_f$  is the temperature of the fluid.

$$-\lambda_{\text{eff}} \nabla T_b = h(T_b - T_f) \quad (32)$$

$$\nabla P_g = 0 \quad (33)$$

At the mass transfer interface where hydrogen is absorbed into the bed (mass exchange boundary), a Danckwerts' boundary condition (Siyakatshana, Kudrna, and Machoň 2005) is considered as shown by eq. (34a) to ensure the continuous flow rate of hydrogen across the wall for the model that considers pressure gradients. In eq. (34a),  $T_{\text{in}}$  represents the temperature of the wall in contact with the fluid and is obtained from the energy conservation equation. However, for the simplified model with  $\nabla P = 0$ , this boundary is treated under no flux condition given by eq. (34b).

$$-\lambda_{\text{eff}} \nabla T_b = \rho_{g, \text{in}} \vec{U} C_{p,g} (T_{\text{in}} - T_b) \quad (34a)$$

$$\nabla T_b = 0 \quad (34b)$$

For the model considering Darcy's velocity, the gas pressure at the mass transfer boundary is assumed to be equal to the tank's internal pressure. The mass conservation equation for the gaseous phase, along with the ideal gas law, is utilized to determine the density and pressure within the bed. Conversely, for the model neglecting pressure gradients, a uniform pressure is assumed throughout the entire domain.

$$P_g|_{\text{@ mass transfer interface}} = P_{\text{ex}} \quad (\text{For model considering } \vec{U}) \quad (35a)$$

$$P_g = P_{\text{ex}} \quad (\text{For model neglecting } \vec{U}) \quad (35b)$$

### 3.6. Numerical Approach: Finite Volume Method (FVM)

The finite volume method is a discretization approach used to solve complex differential equations by integrating the equations of mass, energy, and momentum conservation (S. Khan, Hasnain, and Sezer 2024; Hasnain, Khan, et al. 2024). This technique divides the domain into a finite number of adjacent control volumes, referred to as cells. Within each cell, the values of the variable parameters relevant to the differential equations are calculated at the cell's centroid. Surface values within the control volume are determined using mathematical interpolation methods, such as arithmetic or harmonic means, to accurately represent the distribution of variables. Fig. (3.4) illustrates a typical control volume for a two-dimensional model, with each cell having four faces labeled as East (E), West (W), North (N), and South (S) (S. Khan et al. 2022; Hasnain, Khan, et al. 2024).

The finite volume method (FVM) utilizes control volumes rather than grid intersection points for discretization, which makes it highly adaptable and suitable for various grid types. In this study, an open-source finite volume toolbox called Simulkade (Eftekhari and Schüller 2015; S. Khan, Hasnain, and Sezer 2024; Hasnain, Paye, et al. 2024; S. Khan et al. 2022; Hasnain, Khan, et

al. 2024; Hasnain et al., n.d.) is employed to solve the partial differential equations (PDEs) resulting from the coupling of conservation equations and Darcy's law. To ensure the reliability of our numerical simulations, a mesh and time step independence study was conducted as can be found in the supplementary section of our published work (Hasnain, Sezer, and Mason 2024). The results of this study confirmed convergence, indicating that the chosen mesh resolution adequately captured the physics of the system. Specifically, simulations were performed using a mesh consisting of 15 cells in the axial direction and 10 cells in the radial direction with a time step of 0.5 seconds.

This toolbox allows for flexible and customized simulations to accurately model the system. FVM inherently satisfies the conservation equations for mass, heat, and momentum transfers across the cell boundaries. Therefore, along with more customization, this approach will be fast and will yield more accurate results (S. Khan et al. 2022; S. Khan, Hasnain, and Sezer 2024; S. Khan, Hasnain, and Casa 2024; M. U. Khan, Hasnain, and Khan 2024; Hasnain, Paye, et al. 2024; Hasnain, Khan, et al. 2024; S. Khan et al. 2024; Hasnain et al., n.d.; 2022).

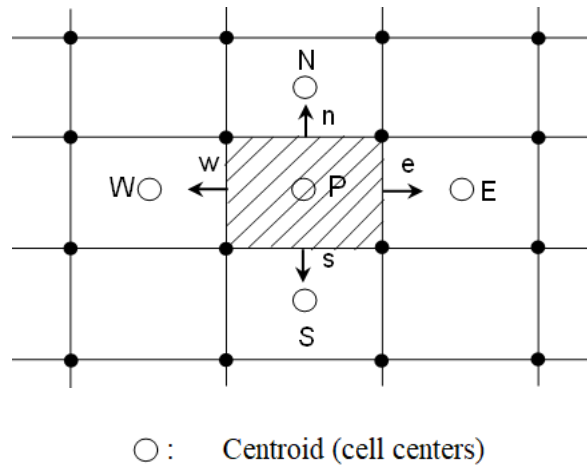


Figure 3.4: Control volume for two-dimensional model (In 2D, each cell has four faces labeled with east (E), west (W), north (N), and south (S))



## CHAPTER 4

### 4. RESULTS AND DISCUSSION

#### 4.1. Results for Hydrogen Absorption Process in MH Reactors

##### 4.1.1. Equilibrium Pressure as a Function of Temperature and H/M Atomic Ratio

To validate our hydrogen absorption model against experimental data, initial numerical simulations were performed. Fig. (4.1) provides a comprehensive comparison of experimental and theoretical equilibrium pressure profiles at various temperatures, for  $\text{LaNi}_5$  alloy as the hydrogen absorption material. The equilibrium pressure ( $P_{eq}$ ) is plotted against temperature and the hydrogen-to-metal atomic ratio (H/M) since it is not a function of the reactor size or computational domain. The H/M atomic ratio is derived by multiplying the reacted fraction 'X' in the model by 6, as it takes 6 hydrogen atoms to fully saturate  $\text{LaNi}_5$  and transform it into  $\text{LaNi}_5\text{H}_6$ . The model's predictions exhibit strong agreement with the experimental equilibrium pressure data (Dhaou et al. 2007), confirming its accuracy.

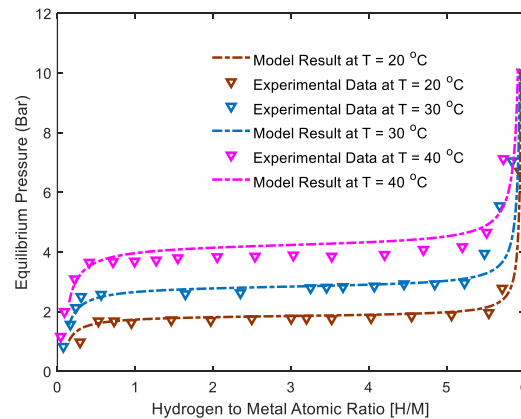


Figure 4.1: Equilibrium pressure as a function of the H/M atomic ratio and temperature for hydrogen absorption (experimental data source: Dhaou et al. (Dhaou et al. 2007))

##### 4.1.2. Effect of Pressure Gradients on the Reacted Fraction Profile

Fig. (4.2a) presents the reacted fraction profile for reactor 1, where both models, one incorporating Darcy's law and the other without, closely match experimental data from Yang et al.

(Yang et al. 2010). The model neglecting Darcy's velocity assumes uniform pressure, implying instantaneous and uniform hydrogen availability at a constant pressure across the entire domain. Although it slightly overestimates the charging rate compared to experimental data, the overall agreement remains acceptable. In contrast, including pressure gradients improves results but introduces significant numerical instability and stiffness. Given that the simplified model without pressure gradients aligns well with experimental data and requires less computational time, it is selected for further analysis.

During the initial absorption stages (first 50 seconds), both models produce similar results because pressurized hydrogen is readily available throughout the system. However, as the process continues, the model results diverge due to increasing pressure gradients, resulting from a concentration of hydrogen exceeding the advection supply. Near the end of the absorption process, the profiles reunite as the reaction rate slows down, and advection-driven hydrogen supply becomes sufficient to overcome the pressure gradients.

Different studies have reported varying values for PCT parameters A and B, with A ranging from 10.7 (Nam, Ko, and Ju 2012) to 14.045 (Yang et al. 2010; Elkhatib and Louahlia 2023), and B ranging from 3704.6 (Nam, Ko, and Ju 2012; Elkhatib and Louahlia 2023) to 3780 (Yang et al. 2010). To validate the results of the developed simplified model without considering pressure gradients against the model considering them,  $A = 13.1$  and  $B = 3719.59$  were used based on the model developed by Nam et al. (Nam, Ko, and Ju 2012). Fig. (4.2b) illustrates a good agreement in the mean reacted fraction profiles for reactor 2 between both models.

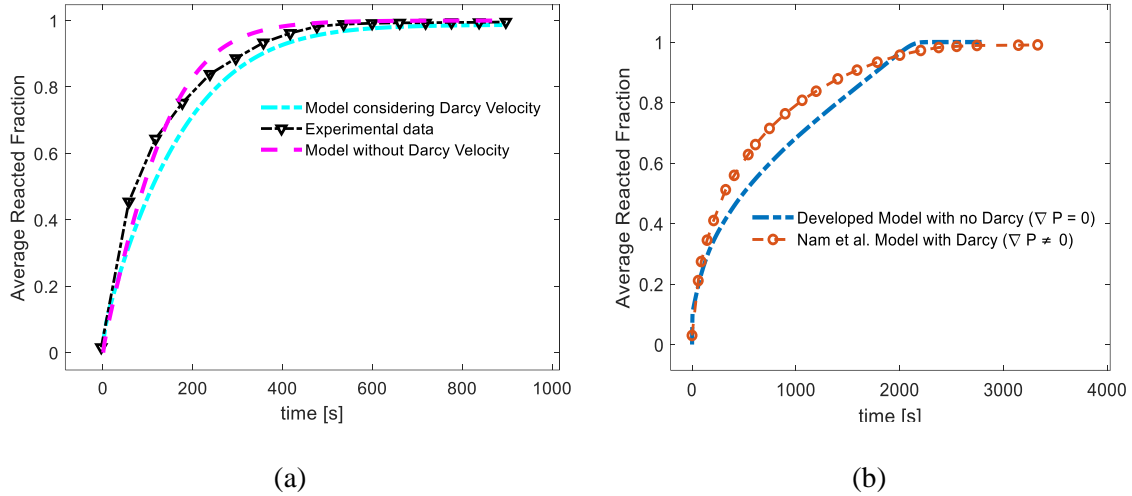


Figure 4.2: Validation of reacted fraction profiles (a) For reactor 1 with experimental data (Yang et al. 2010), (b) Comparison between simplified model (no pressure gradients) and Nam et al. model (considering Darcy's law) for reactor 2 (Nam, Ko, and Ju 2012)

#### 4.1.3. Temperature Profile Validation

Fig. (4.3a) provides a comparison of temperature evolution profile for reactor 2, as predicted by the developed numerical model, and measurements conducted by Jemni and Nasrallah (A. Jemni and Nasrallah 1995b; Abdelmajid Jemni, Nasrallah, and Lamloumi 1999) inside the MH bed at  $r = 1.5$  cm and  $z = 4.5$  cm. Our numerical model demonstrates a strong agreement with experimental data, affirming the model's accuracy. Both simulations and experiments exhibit an initial rapid temperature increase, reflecting fast hydrogen absorption kinetics during the initial stage, followed by a gradual decline in temperature due to cooling fluid influence and diminishing absorption rates caused by an increase in equilibrium pressure.

In fig. (4.3b), temperature profiles are compared at the point indicated in fig. (6a) (with PCT parameters  $A = 13.1$  and  $B = 3719.59$ ) between Nam et al.'s model (Nam, Ko, and Ju 2012), which accounts for Darcy velocity due to pressure gradients, and the developed model with a constant input pressure throughout the domain. The comparison reveals that the inclusion of Darcy effects has a negligible impact on the temperature variation at the selected point within the domain.

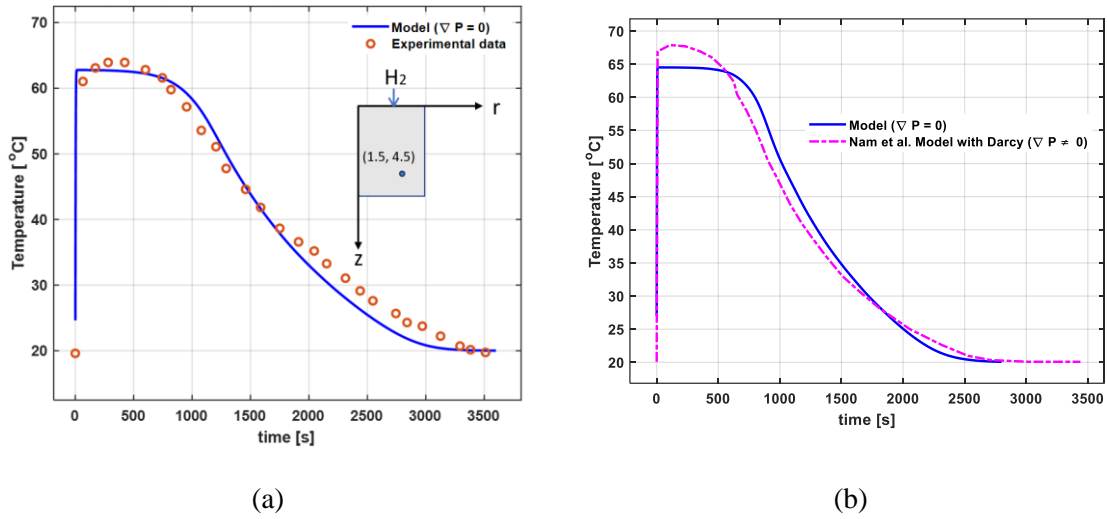


Figure 4.3: Validation of the temperature profile at (1.5 cm, 4.5 cm) for reactor 2 with (a) Experimental data (Abdelmajid Jemni, Nasrallah, and Lamloumi 1999; Elkhatib and Louahlia 2023) , (b) Comparison with Nam et al. model (Nam, Ko, and Ju 2012)

#### 4.1.4. Temperature and Reacted Fraction Contours at Different Times

##### 4.1.4.1. Contours for Reactor 1

The distribution of the reacted fraction of hydrogen in the metal hydride (MH) bed and temperature in the domain during the absorption process at three different times were analyzed. The three different times considered for retrieving the results are 10, 100 and 600 seconds, corresponding to the start, middle, and end of the absorption process, respectively (Hasnain, Khan, et al. 2024).

The results showed that at 10 seconds, the reacted fraction of hydrogen in the domain varied from 9.5% at the heat transfer boundary (outer boundary) to 12.5% at the mass transfer boundary (inner boundary) as shown in fig. (4.4a). This indicates that the absorption rate was higher at the inner boundary due to direct contact with hydrogen. Additionally, the temperature distribution at the beginning of the absorption process (as shown in fig. (4.5a)) revealed a maximum temperature

of approximately 301 K at the inner boundary and a minimum temperature of about 295 K at the outer boundary, where it was in contact with the low-temperature cooling fluid.

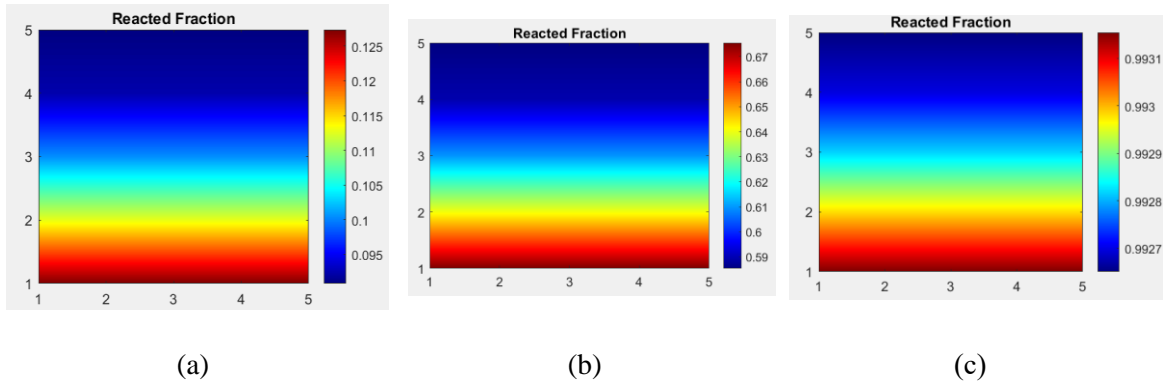


Figure 4.4: Comparison of reacted fraction contours for reactor 1 at (a) Time = 10 seconds (11% charged system: start of the absorption process) (b) Time = 100 seconds (63% charged system: middle of the absorption) (c) Time = 600 seconds (99.3% charged system: end of the absorption) (Hasnain, Khan, et al. 2024)

\* Notice that the contours look the same at all the 3 times, but the coloring scale keeps changing. The purpose of showing these contours was to show how the reacted fraction distribution is changing in the computational domain. By using the same scale, it would not be possible to observe the variations. Therefore, the same scale is not used.

As the absorption process progressed, the reacted fraction of hydrogen in the MH bed increased and spread towards the outer boundary. At 100 seconds, as can be noticed from fig. (4.4b), the reacted fraction ranged from 59% at the outer boundary to 67% at the inner boundary, indicating that the system was charged to more than 50% of its full capacity within the first 100 seconds. The high rate of absorption was facilitated by the significant temperature difference between the cooling fluid and the MH bed. Interestingly, the temperature distribution revealed a reduction in temperature in the MH bed, despite the exothermic nature of the absorption process, as the cooling fluid absorbed the heat from the computational domain. The temperature profile in fig. (4.5b) indicated that the temperature of the MH bed decreased from 298 K to 285 K at the heat transfer boundary and to 288 K at the mass transfer boundary, suggesting that the rate of heat release

due to absorption was less than the rate of heat absorption by the cooling fluid (Hasnain, Khan, et al. 2024).

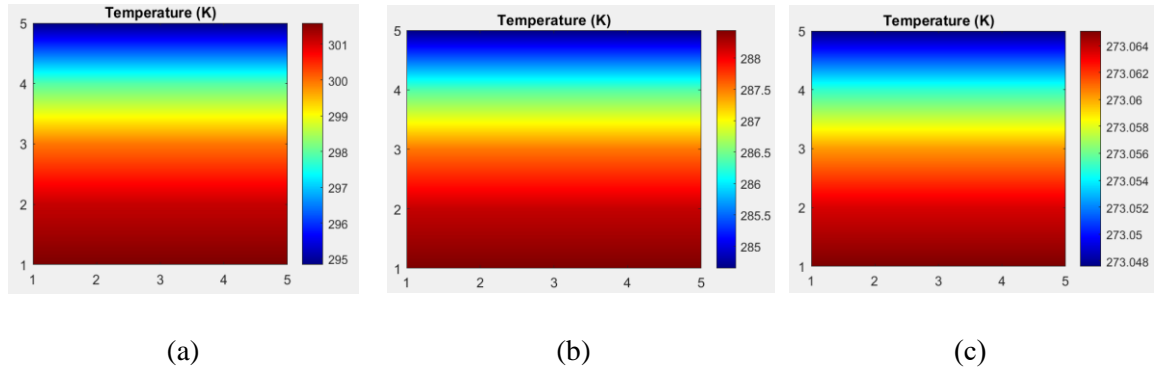


Figure 4.5: Comparison of temperature contours for reactor 1 at **(a)** Time = 10 seconds (11% charged system: start of the absorption process) **(b)** Time = 100 seconds (63% charged system: middle of the absorption) **(c)** Time = 600 seconds (99.3% charged system: end of the absorption) (Hasnain, Khan, et al. 2024)

\* Notice that the contours look the same at all the 3 times, but the coloring scale keeps changing. The purpose of showing these contours was to show how the temperature distribution changes in the computational domain. By using the same scale, it would not be possible to observe the variations. Therefore, the same scale is not used.

The final stage of the absorption process was analyzed by studying the distribution of the reacted fraction of hydrogen in the MH bed at 600 seconds. The results from fig. (4.4c) indicate that the reacted fraction increased to a maximum of 99.31% at the inner boundary and 99.27% at the outer boundary. This suggests that most of the metal molecules  $\text{LaNi}_5$  are now attached with hydrogen and are present as  $\text{LaNi}_5\text{H}_6$ , indicating that the absorption process has almost reached the saturation point (Hasnain, Khan, et al. 2024).

As the absorption progresses to saturation, its rate becomes negligible, and the rate of heat production also decreases. Therefore, the cooling fluid absorbs heat from the MH bed, and it can be observed from fig. (4.5c) that the whole domain is almost at the same temperature as the initial temperature of the cooling fluid.

#### 4.1.4.2. Contours for Reactor 2

Fig. (4.6) presents contours showing the mean reacted fraction within reactor 2 at three different times. Considering the total absorption duration as 3000 seconds, as indicated in fig. (4.8), the reacted fraction contours at 100 seconds, 1000 seconds, and 2000 seconds, corresponding to 3.3%, 33.3%, and 66.7% respectively, are illustrated in fig. (4.6a), (4.6b), and (4.6c) respectively. Initially, as depicted in fig. (4.6a), absorption occurs uniformly throughout the entire bed until the temperature reaches approximately 335 K, as shown in fig. (4.7a). Subsequently, absorption stops due to the temperature's influence on the equilibrium pressure. At this point, the cooling fluid begins absorbing heat from the cooling boundaries, leading to the propagation of absorption contours from the heat transfer boundaries towards the interior of the bed. The distributions of the reacted fraction and temperature within the reactor bed are shown in fig. (4.6a), (4.6b), (4.6c) and fig. (4.7a), (4.7b), (4.7c) respectively.

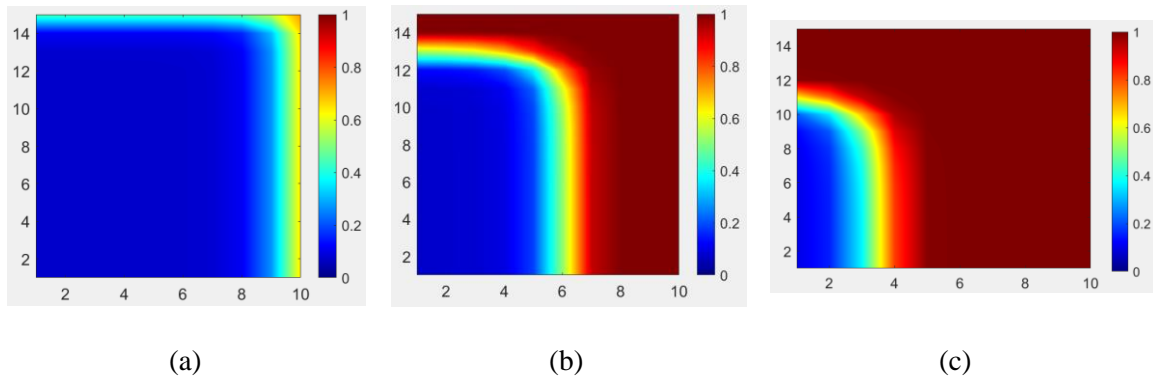


Figure 4.6: Comparison of reacted fraction contours for reactor 2 at (a) Time = 100 seconds (3.3% of the Charging Duration) (b) Time = 1000 seconds (33.3% of the Charging Duration) (c) Time = 2000 seconds (66.7% of the Charging Duration)

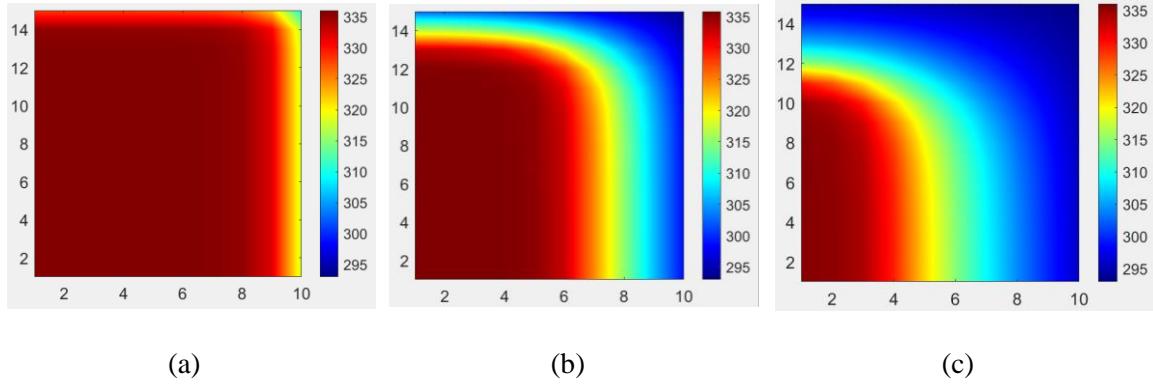


Figure 4.7: Comparison of temperature contours [in Kelvin] for reactor 2 at (a) Time = 100 seconds (3.3% of the Charging Duration) (b) Time = 1000 seconds (33.3% of the Charging Duration) (c) Time = 2000 seconds (66.7% of the Charging Duration)

#### 4.1.5. Shape Consideration for Reactor 2

Fig. (4.8a) presents a comparison of mean reacted fraction transients for two cross sections with equal volumes. The standard reactor, as considered in previous studies (Abdelmajid Jemni, Nasrallah, and Lamloumi 1999; Elkhatib and Louahlia 2023), has dimensions of 50 mm (diameter) and 60 mm (length), resulting in a volume of  $117.8 \text{ cm}^3$ . Given the saturation density of  $\rho_{\text{sat}} = 6.52 \text{ g/cm}^3$  and the empirical density of  $\rho_{\text{emp}} = 6.43 \text{ g/cm}^3$ , this is equivalent to a capacity of 10.6 grams. To illustrate the impact of altering the cylindrical reactor's dimensions while maintaining the same volume, another square cross-section with a diameter and length of 53.133 mm is considered, derived from the relation shown above.

The figure shows that changing the cross-section from rectangular to square increases the charging time from 2811 seconds to 3106.5 seconds. Charging time, in this case, is defined as the time when absorption reaches approximately 99.46% of total capacity. This change indicates that larger axial dimensions result in shorter charging times, as the cooling fluid surrounds both lateral sides, increasing heat exchange with the bed. Similarly, fig. (4.8b) shows the comparison of mean temperature profiles. As anticipated from fig. (4.8a), the square reactor takes longer to reach the fluid temperature due to the lower surface area exposed to the low-temperature fluid.



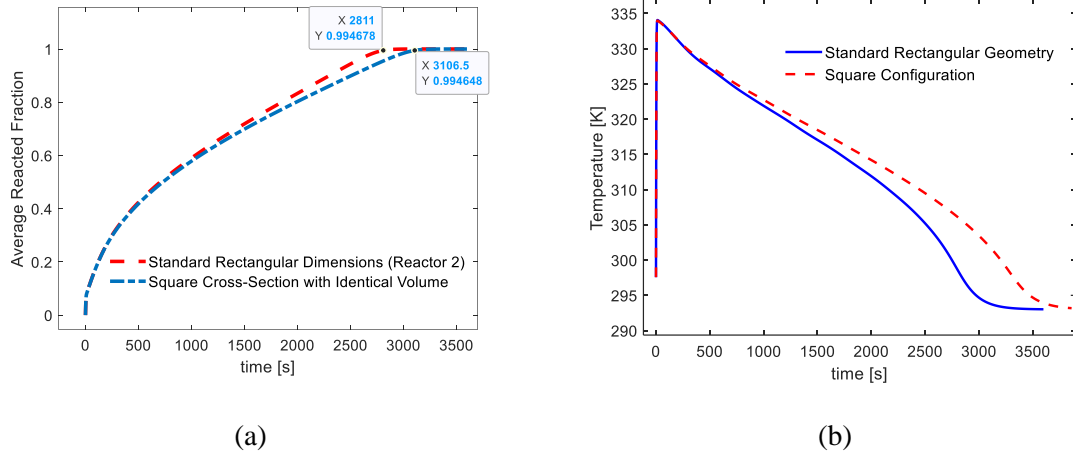


Figure 4.8: Comparison of (a) Reacted fraction and (b) Temperature evolution profiles

#### 4.1.6. Reactor Size Impact on Charging and Temperature Profiles

Fig. (4.9a) illustrates reacted fraction profiles for different reactor sizes, demonstrating that increased reactor dimensions lead to longer charging times. Fig. (4.10a) and (4.10b) depict the relationships between reactor dimensions and their respective charging durations. For the analyzed square cross-sections, length and charging time exhibit a second-order polynomial correlation, implying a linear relationship between area and charging time. In fig. (4.9b), the impact of reactor size on mean bed temperature is depicted. Larger reactors exhibit minimal differences in maximum temperature at the start of absorption. However, they take a longer duration to reach the cooling fluid's temperature as the cooling effect propagation through the entire domain is more time-consuming than in smaller reactors. The reactor sizes considered in fig. (4.9a) and (4.9b) have hydrogen mass capacities of about 1.11 g, 4.52 g, 8.84 g, 15.2 g, and 24.25 g respectively.

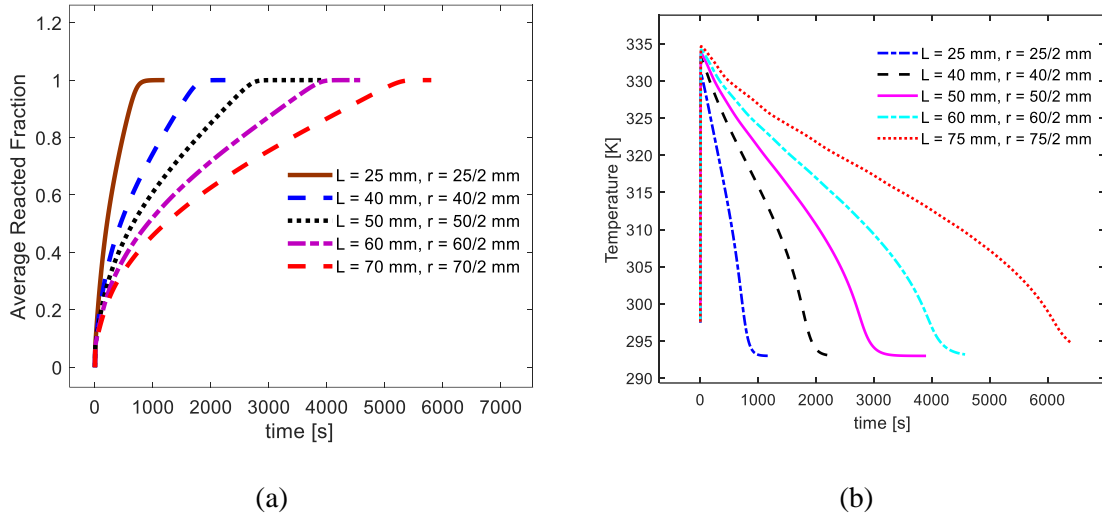
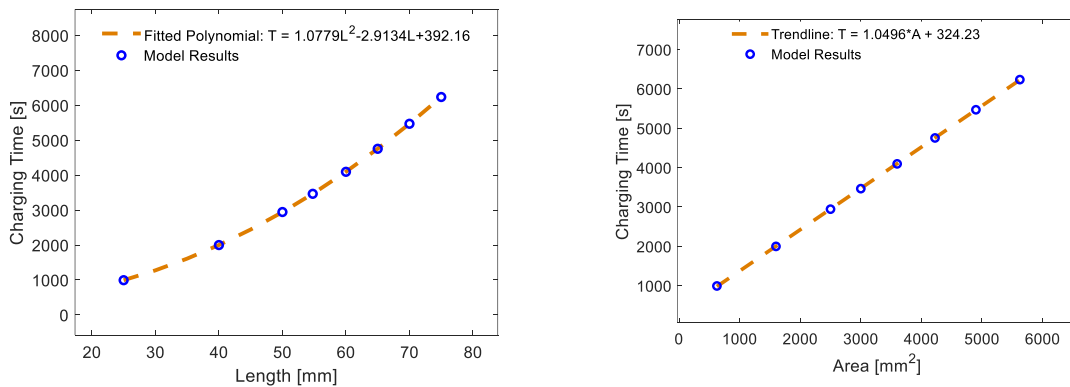


Figure 4.9: The effect of reactor size on (a) Mean reacted fraction profile and (b) Temperature evolution profile

#### 4.1.7. Pressure, Cooling Fluid Temperature and Boundary Conditions Analysis

The hydrogen feed pressure and cooling fluid temperature are two determining parameters for optimizing the storage system's performance. Fig. (4.11) compares reacted fraction profiles for charging pressures of 6, 8, and 10 bars. Higher hydrogen charging pressures result in shorter charging durations. Specifically, increasing the hydrogen supply pressure from 6 to 8 bars reduces the charging time by approximately 12.4 minutes, while further elevating it to 10 bars results in an additional 7-minute reduction in charging time. These findings underscore the importance of considering the required charging time when adjusting the hydrogen feed pressure in the reservoir.



(a)

(b)

Figure 4.10: Correlation of charging duration with (a) Length of the reactor, (b) Cross-sectional area of the reactor

Similarly, examining the temperature profiles presented in fig. (4.12a) and (4.12b), it becomes evident that pressure not only influences charging time and reaction kinetics but also significantly elevates the maximum temperature within the bed. Additionally, higher charging pressure leads to a more rapid convergence of bed temperature to the cooling fluid temperature. Two primary factors contribute to this behavior. Firstly, the accelerated reaction rates at higher pressures drive the system towards saturation more quickly, reducing heat generation near saturation. Secondly, the initially high reaction rates result in elevated bed temperatures, promoting increased heat exchange with the cooling fluid due to greater convection flux driven by the higher temperature gradient.

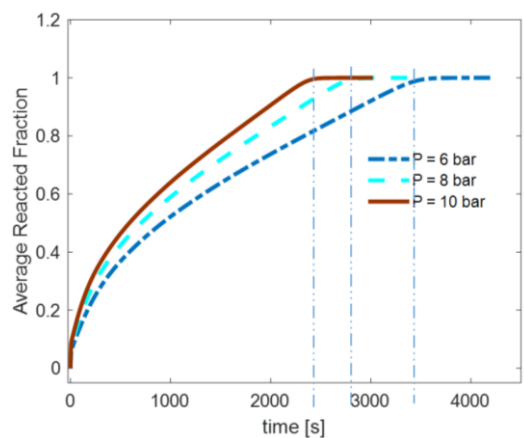


Figure 4.11: Comparison of the mean reacted fraction profiles for different charging pressures

Fig. (4.13a) demonstrates the comparison of reacted fraction profiles at different cooling fluid temperatures: 20°C, 30°C, and 40°C. Clearly, the temperature of the cooling fluid substantially influences reaction kinetics, consequently affecting the system's charging time. Increasing the cooling fluid temperature from 20°C to 30°C results in an additional 14 minutes of charging time, while further increasing it to 40°C extends the charging time by an additional 26

minutes. Lowering the cooling fluid temperature reduces the charging time, although this effect becomes less pronounced as temperatures decrease.

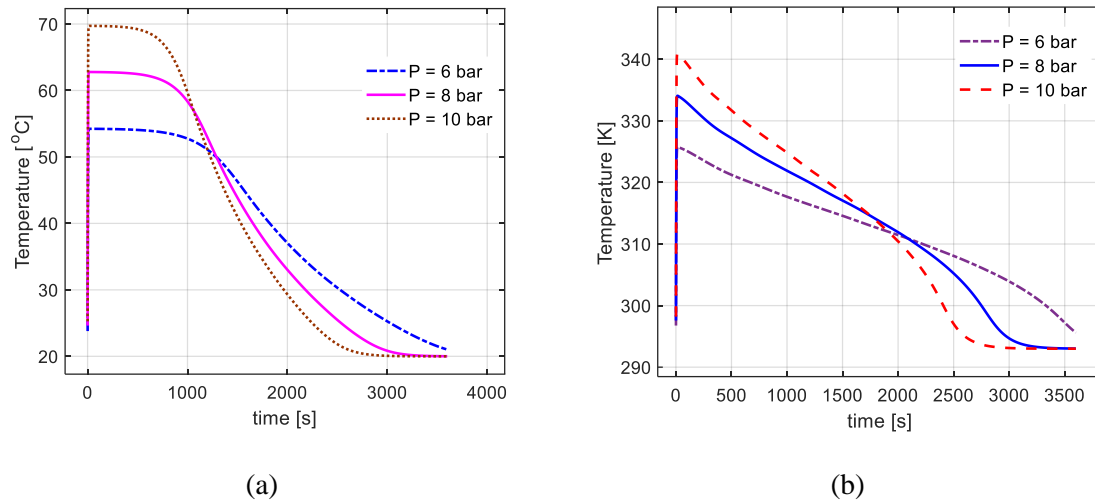


Figure 4.12: Comparison of the temperature profiles for different charging pressures (a) At (15, 45) mm, (b) Mean temperature

Fig. (4.13b) presents the reacted fraction profiles corresponding to three distinct boundary conditions. In the first case, a non-homogeneous flux boundary condition is considered with the cooling fluid at 293 K. The constant temperature cooling fluid (water) is considered to be moving with a steady velocity alongside the bed. Due to the varying temperature at the interface, a non-homogeneous heat flux occurs from the bed to the fluid. In the second case, a Dirichlet boundary condition with a temperature of 293 K is introduced, symbolizing the replacement of cooling fluid with a phase change material (having 293 K as its phase change temperature). This assumption is only valid when the absorbed heat by the material is less than the latent heat. Finally, the third boundary condition assumes a Dirichlet boundary condition at 273 K, signifying the utilization of water/ice as the phase change material (PCM). Transitioning from the first to the second boundary condition reduces the charging time from 2792 seconds to 2643.5 seconds, and further transitioning to the third boundary condition reduces it to 1849.5 seconds. This analysis emphasizes the

significant influence of boundary conditions, especially the incorporation of phase change materials, on the system's charging duration.

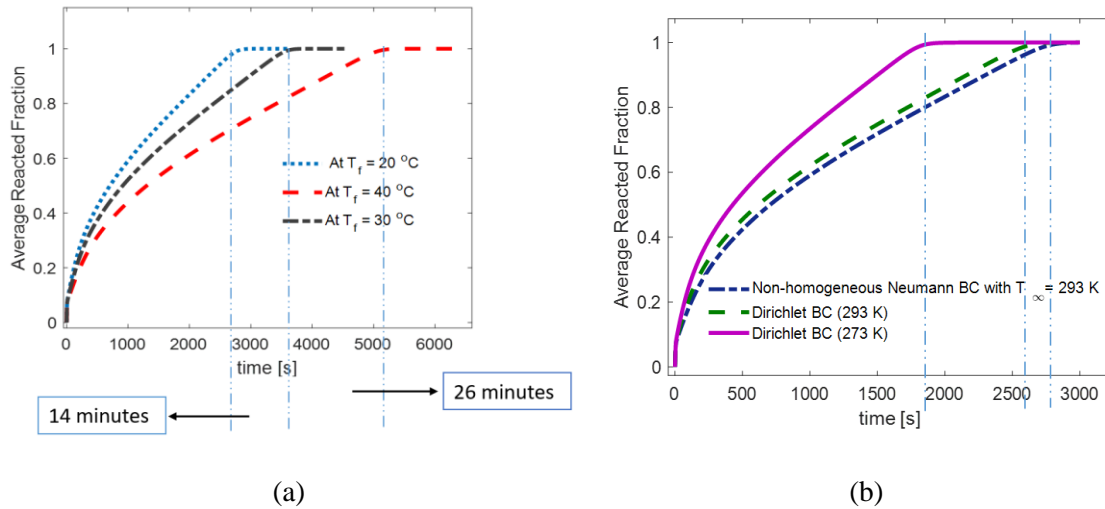


Figure 4.13: Comparison of mean reacted fraction profiles for different (a) Cooling fluid temperatures, (b) Boundary conditions

## 4.2. Results for Hydrogen Desorption Process in MH Reactors

### 4.2.1. Validation of the Developed Numerical Model for Desorption

#### 4.2.1.1. $P_{eq}$ as a Function of Temperature and H/M Atomic Ratio

To validate the hydrogen desorption model, initial numerical simulations were performed to predict and compare the equilibrium pressure profiles at different temperatures against the experimental data (Kyoung et al. 2015). Fig. 4.14 provides a comparison of experimental and model equilibrium pressure profiles at various temperatures, for  $\text{LaNi}_5\text{H}_6$  as the hydrogen desorption material. The equilibrium pressure is plotted against hydrogen-to-metal atomic ratio (H/M) at various temperatures. The predictions from the model are in good agreement with the experimental equilibrium pressure data. The results clearly show that equilibrium pressure is not only a function of temperature but also strongly depends on the H/M atomic ratio especially in the beginning and end of the desorption process.

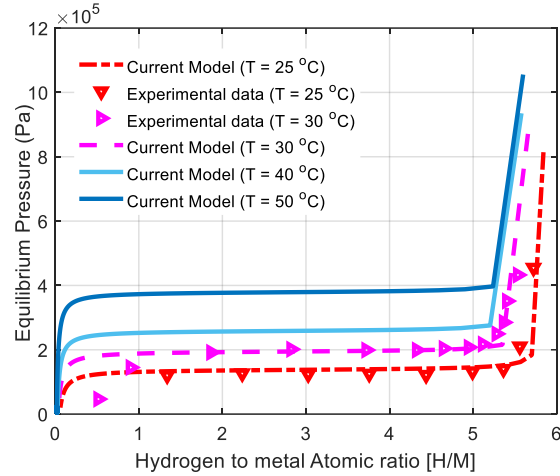


Figure 4.14: Equilibrium pressure as a function of H/M atomic ratio and temperature for hydrogen desorption (experimental data source: (Kyoung et al. 2015))

#### 4.2.1.2. Effect of Pressure Gradients on the Reacted Fraction Profile

Fig. (4.15) shows the reacted fraction profile during the desorption process for reactor 1. The current model neglects the effects of Darcy's velocity due to pressure gradients and assumes uniform pressure throughout the domain, implying instantaneous and uniform hydrogen availability at a constant pressure in the bed. The discharging curve from the current model is compared to the experimental data (taken from Yang et al. (Yang et al. 2010)) as well as Yang et al. model (Yang et al. 2010) that considers the effect of pressure gradients. It can be observed that the profile from the current model matches more closely to the experimental data demonstrating the negligible effect of considering Darcy's velocity due to the pressure gradients on the overall results. This concludes that even though including pressure gradients introduces significant numerical instability and stiffness to the modeling equations, its impact on the discharging curve is minimal.

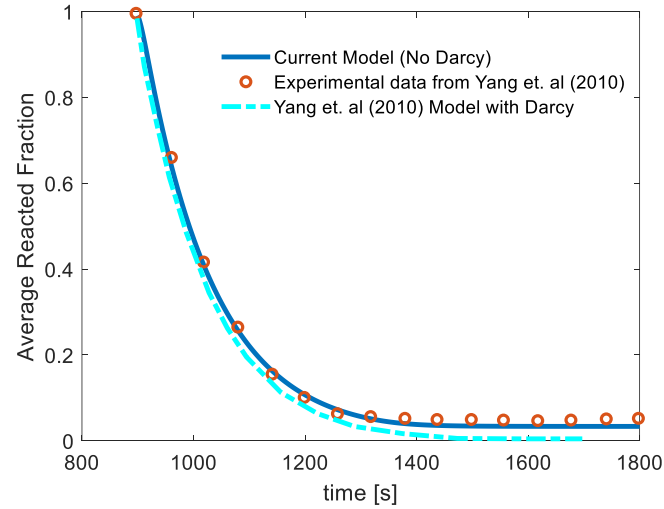


Figure 4.15: Experimental validation and verification of reacted fraction profile with Yang et al. (yang et al. 2010) for reactor 1

#### 4.2.1.3. Temperature Profile Validation

Fig. (4.16a) and (4.16b) present time histories of temperatures at points A and B, respectively, providing a comparison between experimental data and Kyoung et al. model (Kyoung et al. 2015). The locations of these points on the cross-section of reactor 2 are depicted in fig. (4.16c). The results obtained from the current model are for PCT parameters  $A = 14.045$  and  $B = 3704.6$  (Yang et al. 2010; Elkhatab and Louahlia 2023). Despite neglecting pressure gradients in the bed, the present numerical model exhibits strong agreement with experimental data, confirming the accuracy of the model. The comparison of both models clearly indicates that the inclusion of pressure gradients does not have significant impact on the temperature distribution in the MH bed.

Both the model and experimental results depict an initial rapid temperature drop, indicating a fast hydrogen desorption rate at the beginning. This is followed by a gradual rise in temperature, attributed to the influence of the heat transfer fluid and a decrease in equilibrium pressure.

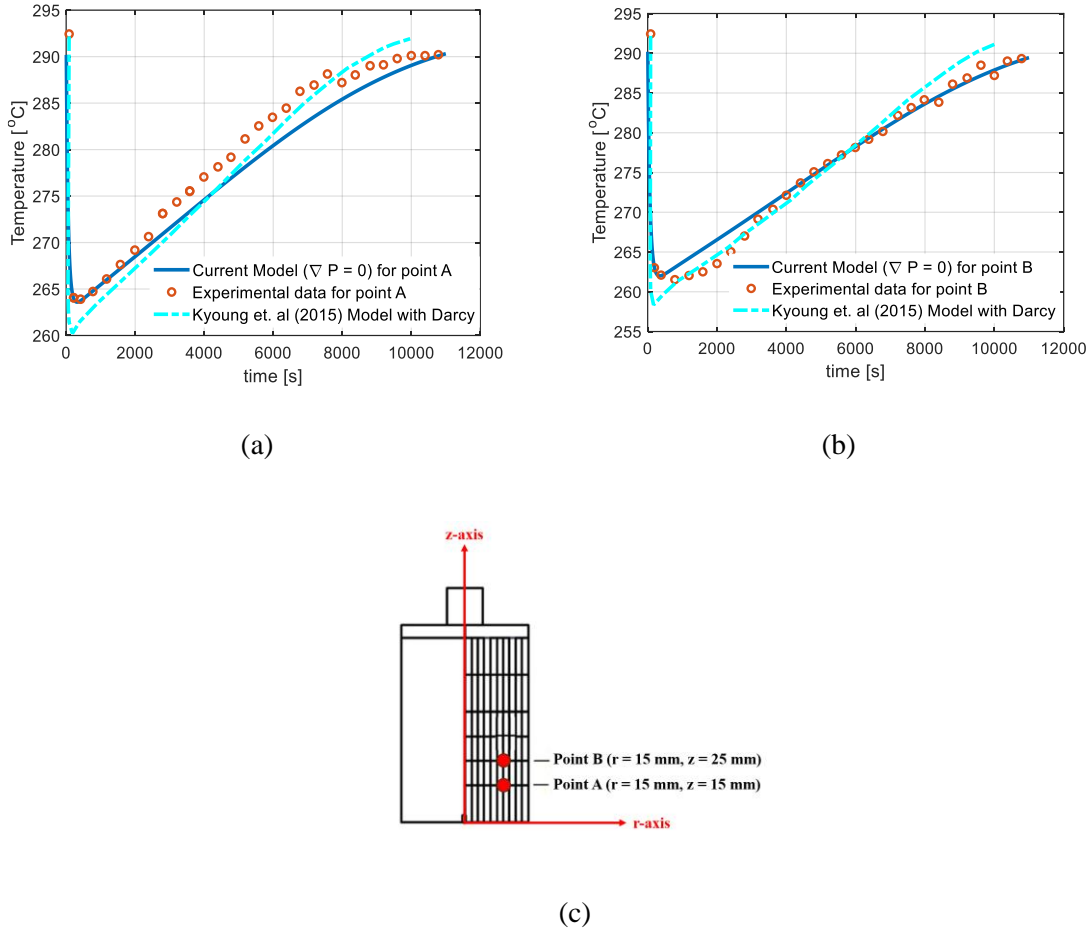


Figure 4.16: Experimental validation and verification of the temperature profiles with Kyoung et al. model (Kyoung et al. 2015) for reactor 2 (a) At point A, (b) At point B (c) locations of point A and point B in the reactor 2

#### 4.2.2. Parametric Analysis of Pressure, Heating Fluid Temperature, and Porosity for Reactor 2

The desorption pressure and heating fluid temperature are two important parameters for optimizing the reactor discharging duration. Fig. (4.17) compares reacted fraction profiles and mean temperature histories for discharging pressures of 100, 250, and 500 millibars at heating fluid temperature of 323 K. It can be observed from Fig. (4.17a) that lower hydrogen pressures result in faster desorption rates and ultimately shorter discharging durations. By reducing the pressure from



500 to 100 millibars, the discharging time decreases from approximately 10,000 seconds to about 8,000 seconds. These results demonstrate that, based on the reactor design and other constraints, the desired discharging duration can be achieved by adjusting the pressure inside the bed.

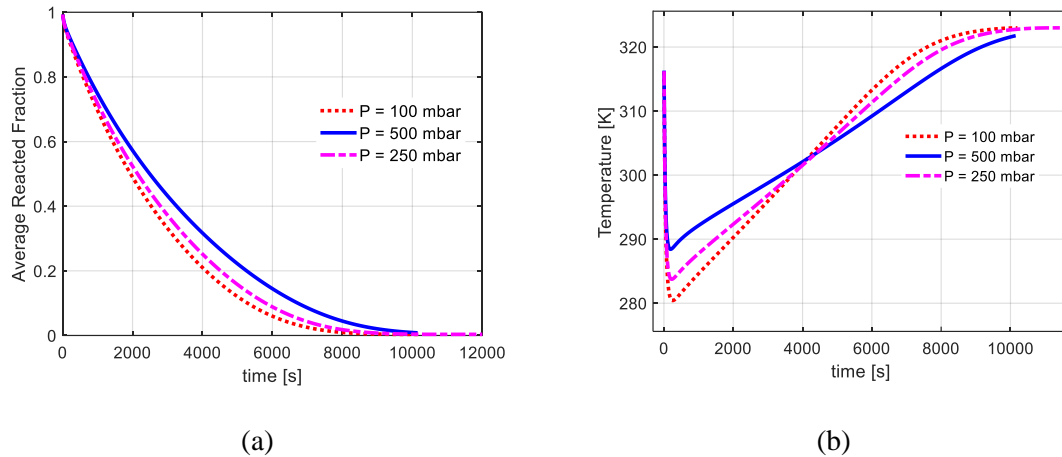


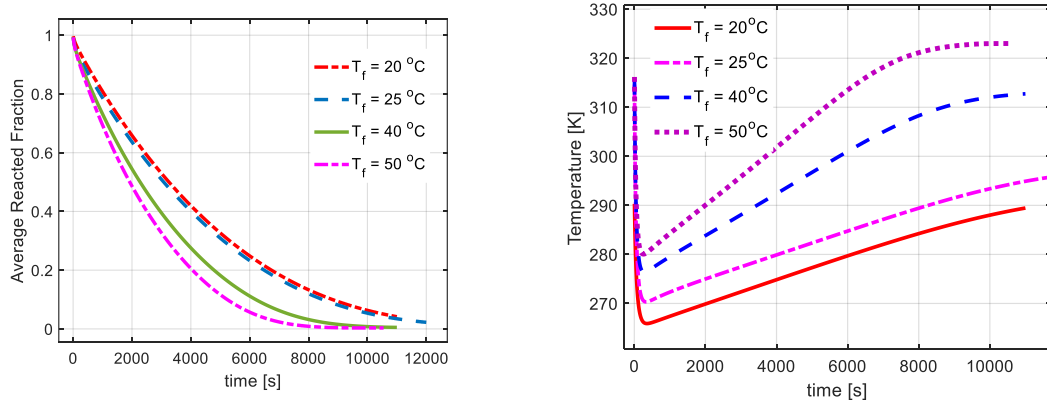
Figure 4.17: Comparison of the (a) Mean reacted fraction profiles (b) Time histories of mean temperature, at different discharging pressures

Likewise, upon analyzing the temperature histories depicted in fig. (4.17b) corresponding to varying pressures, it becomes evident that discharging pressure not only impacts the duration of the desorption process and reaction kinetics but also influences the minimum mean temperature attained inside the bed. By increasing the pressure from 100 to 500 millibars, the minimum mean temperature rises from 280 K to about 290 K. Note that at the beginning of the desorption process the sudden drop in temperature is attributed to the rapid desorption of hydrogen initially, which consumes a significant amount of heat since the reaction is endothermic.

Additionally, higher discharging pressure results in delaying the bed temperature to reach the heating fluid temperature. The first factor responsible for this behavior is the accelerated desorption at lower pressures that makes the reactor discharge quickly, reducing the amount of heat consumed at the later stages of the desorption. The initial high reaction rates due to lower pressure also results in lowering bed temperatures, promoting increased heat exchange with the heating fluid

due to greater convection flux driven by the higher temperature gradient. It is clear that higher discharging pressure prolongs the time taken for the bed temperature to reach the heating fluid temperature. This phenomenon is influenced by two primary factors. Firstly, higher pressures decelerate the desorption process, leading to relatively higher heat consumption in the later stages. Secondly, the initial low reaction rates at higher pressures result in higher bed temperatures, reducing the heat exchange rate with the heating fluid due to a lower convection flux resulting from low temperature gradient.

Figure (4.18a) demonstrates the impact of heating fluid temperature on the discharging profile for a desorption pressure of 85 millibars. In this study, the heating fluid is assumed to be flowing at a steady speed and constant temperature. The reacted fraction profiles are plotted for temperatures of 20°C, 25°C, 40°C, and 50°C, that cover the commonly adopted temperature range in the literature for the heating fluid. As the temperature of the heat transfer fluid increases, desorption accelerates because higher temperatures enhance the convective heat flux from the fluid to the bed due to greater temperature gradients. By increasing the heat transfer fluid temperature from 20°C to 50°C, the discharge time decreases from about 12,000 seconds to 7,000 seconds, representing a reduction in desorption duration of more than 40%. Evidently, the temperature of the heating fluid significantly influences reaction kinetics, thereby affecting the discharging time of the reactor.



(a)

(b)

Figure 4.18: Comparison of the (a) Mean reacted fraction profiles (b) Time histories of mean temperature, at different heating fluid temperatures

Similarly, in fig. (4.18b), the impact of heating fluid temperature on the time histories of mean bed temperatures is depicted. It is clear that higher fluid temperatures result in a reduction of the minimum mean temperature attained in the bed, consequently accelerating the rate of desorption reaction due to its endothermic nature. The minimum mean temperature, approximately 265 K at 20°C, increases to about 280 K as the heating fluid temperature rises to 50°C. Moreover, at higher fluid temperatures, the mean temperature converges to the fluid temperature more rapidly as the system discharges at a higher rate.

The porosity of MH bed is another material property that can influence the discharging kinetics and temperature distribution in the bed. Various values of porosities ranging from 0.5 to 0.63 are considered in literature. Fig. (4.19a) and (4.19b) respectively depict the effect of changing porosity on the reacted fraction profile and the time history of mean temperature in the bed for a heating fluid temperature of 323 K and a desorption pressure of 85 millibars. Observing fig. (4.19a), it is evident that as the porosity increases from 0.50 to 0.63, the discharging duration increases from around 6,000 to 8,000 seconds. This behavior can be attributed to the lower effective thermal conductivity of the bed and faster initial desorption due to high porosity, leading to a lower mean temperature attained as depicted in fig. (4.19b).

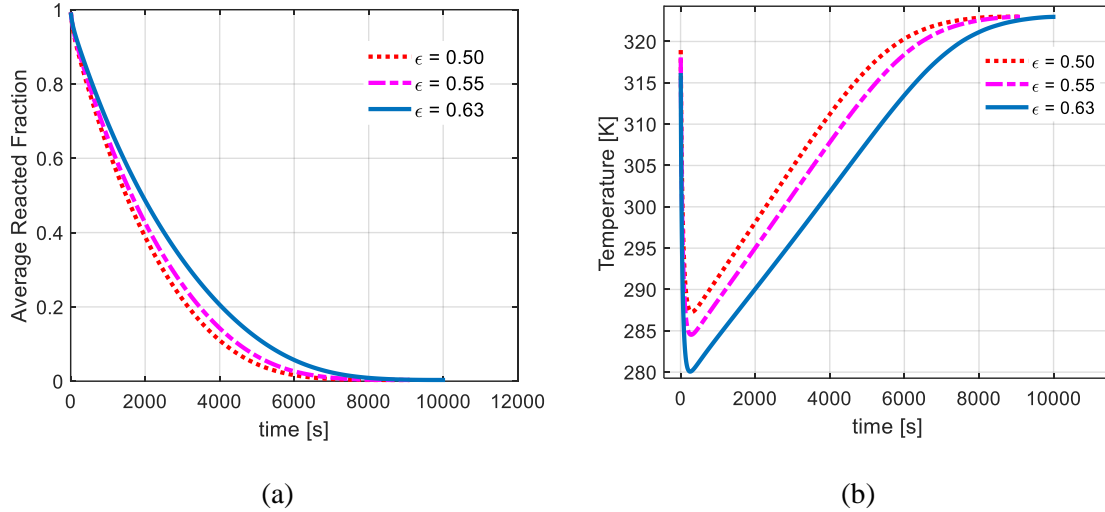


Figure 4.19: Comparison of the (a) Mean reacted fraction profiles (b) Time histories of mean temperature, at different porosities of the MH bed

#### 4.2.3. Reactor Size Impact on Discharging Profile and Temperature Histories

The size of the reactor is another important parameter that is considered in this work. It is important to assess how discharging times and temperature distribution in the reactor change when the reactor dimensions vary from the standard size to meet desired energy requirements. In this section, for comparison purposes, the reactor is assumed to have equal diameter and length. Both the length and diameter are modified by the same amount to preserve symmetric behavior and maintain the same effect of heating fluid configuration.

As illustrated in the reacted fraction profiles in fig. (4.20a), increased reactor dimensions result in longer discharging times. Fig. (4.20b) illustrates the relationships between reactor dimensions and their respective time histories of mean temperatures. It can be concluded that larger reactors achieve lower temperatures in the bed and require a longer duration to reach the temperature of the heating fluid. This is because the propagation of the heating effect through the entire domain is more time-consuming in larger reactors compared to smaller ones.

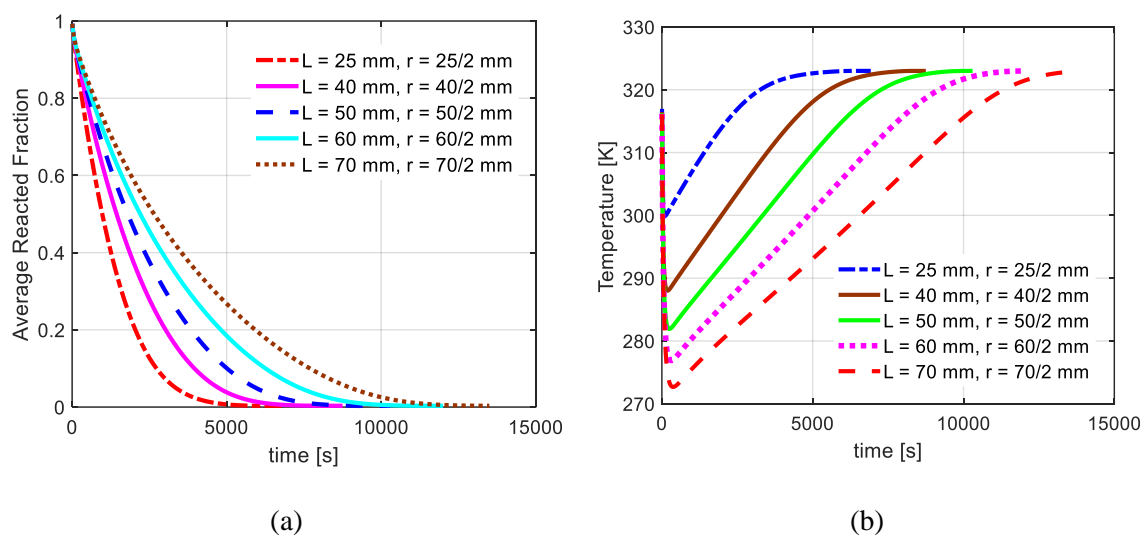


Figure 4.20: Effect of reactor size on the (a) Reacted fraction profiles (b) Time histories of mean temperatures

## CHAPTER 5

### CONCLUSION AND FUTURE SCOPE

#### 5.1. Conclusion

An in-house 2D numerical model is developed using the finite volume method and implicit Euler's time integration scheme to analyze the coupled heat and mass transfer within metal hydride (MH) reactors during the hydrogen absorption/desorption processes. The model incorporates a range of multi physics interactions, including chemical kinetics as well as mass and heat transfer by integrating the principles of conservation of mass and energy with hydrogen sorption kinetics in MH reactors. The model is validated for both absorption and desorption processes based on the experimental data available in the literature and can be implemented to applied to MH reactors involving different materials by updating the properties obtained from PCT curves like hysteresis term, plateau flatness factor, as well as PCT parameters.

Firstly, equilibrium pressure as a function of temperature and the hydrogen-to-metal atomic ratio (H/M) is plotted, and the equilibrium pressure profiles at varying temperatures are validated. Subsequently, two models, one with and one without incorporating pressure gradients, are compared. The results of both models show good agreement with experimental data available in the literature, successfully capturing the key experimental trends. The incorporation of Darcy's velocity in the modeling framework, despite introducing numerical instability, has a negligible overall impact on sorption kinetics and temperature histories in the bed. Despite this trade-off, the simplified model without pressure gradients aligns well with experimental data, offering a balance between precision and computational efficiency. That is why for further analysis in this work, the simplified model is chosen.

Through a rigorous examination of various factors, valuable insights are gained into the behavior of MH reactors. The detailed analysis of temperature profiles for absorption reaction

revealed an initial rapid increase in temperature followed by a gradual decline due to cooling fluid and equilibrium pressure effects. Lower cooling fluid temperatures were found to significantly reduce charging durations, emphasizing the importance of optimizing cooling strategies. The influence of reactor size and shape on both reacted fraction profiles and temperature evolution during charging was explored. Notably, alterations in reactor geometry demonstrated significant effects on the charging time, with larger axial dimensions resulting in shorter charging durations. This phenomenon arises from the increased exposure of surface area to the cooling fluid, facilitating more efficient heat exchange. The results indicated that the relationships between charging duration with reactor length and cross-sectional area followed second and first-order polynomial correlations, respectively.

For desorption, the analysis of temperature histories revealed an initial rapid temperature decrease followed by a gradual increase due to heat transfer from the heating fluid to the bed and the impact of  $[H/M]$  on equilibrium pressure. Additionally, the influence of various critical factors on the reaction rate in MH reactors was analyzed. Increasing heating fluid temperature for desorption significantly reduced discharging duration, highlighting the importance of optimizing heating strategies. Furthermore, porosity was identified as another pivotal property impacting desorption kinetics and temperature distribution, with increasing porosity leading to longer discharging durations and vice versa.

The transition from a flux boundary condition to a Dirichlet boundary condition at the same temperature significantly reduced the charging duration, highlighting the importance of considering phase change materials to customize metal hydride hydrogen storage systems for specific applications. Adjusting the charging/discharging pressure effectively modulated the absorption/desorption duration, with higher pressures resulting in shorter absorption times and higher temperature distribution within the bed and vice versa. In short, this work serves as a

valuable tool for optimizing MH-based hydrogen storage systems, offering both accuracy and computational efficiency.

This modeling work highlights the critical importance of further investigations into thermal management strategies and reactor configurations, serving as a roadmap for future studies aimed at enhancing the efficiency, safety, and practicality of metal hydride-based hydrogen storage systems. Integrating rigorous mathematical modeling with experimental validation will significantly contribute to the ongoing progress and widespread adoption of metal hydrides as sustainable and eco-friendly hydrogen storage solutions.

## **5.2. Future Scope**

Future research in this field may explore more complex reactor geometries and the interactions between various factors to deepen our understanding of metal hydride (MH) systems and their broader applications. Expanding the model to three dimensions (3D) will enable the incorporation of more intricate bed and flow field geometries. Additionally, parametric studies on microstructural properties using percolation theory offer a promising avenue for further investigation.

Further work should focus on identifying metal hydride materials with high gravimetric and volumetric capacities and conducting various experimental optimization studies and sensitivity analyses across different parameters. Sensitivity studies, coupled with the use of physics-informed neural networks, can help develop more robust modeling frameworks.

The integration of heat transfer fluids with finned heat exchangers into MH reactors and conducting parametric studies to optimize the number and size of fins relative to the reactor size is another unexplored area in the literature. Moreover, the mathematical modeling of MH reactors incorporating fluids and phase change materials (PCM) integrated with finned heat transfer presents another promising direction for future research.



## RESULTING PUBLICATIONS AND AWARDS

### Peer-Reviewed Publications:

- Muhammad Hasnain, Shehzad Khan, M.Amin Ezazi, Hayri Sezer, “Modeling heat and mass transfer in metal hydride-based hydrogen storage systems using the finite volume method”, Proceedings of the ASME 2023 International Mechanical Engineering Congress and Exposition October 29-November 2, 2023, New Orleans, Louisiana.  
<https://asmedigitalcollection.asme.org/IMECE/proceedings-abstract/IMECE2023/87677/1196202>
- Muhammad Hasnain, Hayri Sezer, Jerry Hunter Mason. 2024. “Modeling Heat and Mass Transfer in Metal Hydride Hydrogen Storage Systems: Impact of Operating Parameters and Reactor Geometry.” International Journal of Hydrogen Energy 71 (June):1045–1055.  
<https://doi.org/10.1016/J.IJHYDENE.2024.05.311>

### Awards in Paulson College of Engineering and Computing (PCEC) Research Symposiums:

- 2<sup>nd</sup> Place Innovation Award from Georgia Power Company, "Mathematical Modeling of Coupled Heat and Mass Transport in Metal-Hydrides for Safer and More Efficient Hydrogen Storage Systems", Student Research Symposium, Georgia Southern University, April-2024
- 3<sup>rd</sup> Place Computing Award from Southern Automation Logistics & Technology, "Modeling and Optimization of Metal Hydride Based Hydrogen Storage Systems", Student Research Symposium, Georgia Southern University, April-2023

## REFERENCES

- Abdalla, Abdalla M., Shahzad Hossain, Ozzan B. Nisfindy, Atia T. Azad, Mohamed Dawood, and Abul K. Azad. 2018. "Hydrogen Production, Storage, Transportation and Key Challenges with Applications: A Review." *Energy Conversion and Management* 165 (June):602–27. <https://doi.org/10.1016/J.ENCONMAN.2018.03.088>.
- Afzal, Mahvash, Rohit Mane, and Pratibha Sharma. 2017. "Heat Transfer Techniques in Metal Hydride Hydrogen Storage: A Review." *International Journal of Hydrogen Energy* 42 (52): 30661–82. <https://doi.org/10.1016/J.IJHYDENE.2017.10.166>.
- Akanji, Olaitan L., and Andrei V. Kolesnikov. 2012. "Modeling of Heat and Mass Transfer in LaNi<sub>5</sub> Matrix during Hydrogen Absorption-Desorption Cycle." *Polish Journal of Chemical Technology* 14 (3): 71–76. <https://doi.org/10.2478/V10026-012-0087-0>.
- Aldas, Kemal, Mahmut D. Mat, and Yuksel Kaplan. 2002. "A Three-Dimensional Mathematical Model for Absorption in a Metal Hydride Bed." *International Journal of Hydrogen Energy* 27 (10): 1049–56. [https://doi.org/10.1016/S0360-3199\(02\)00010-1](https://doi.org/10.1016/S0360-3199(02)00010-1).
- Andrews, John, and Bahman Shabani. 2012. "Where Does Hydrogen Fit in a Sustainable Energy Economy?" In *Procedia Engineering*, 49:15–25. Elsevier Ltd. <https://doi.org/10.1016/j.proeng.2012.10.107>.
- Askri, F., M. Ben Salah, A. Jemni, and S. Ben Nasrallah. 2009. "A New Algorithm for Solving Transient Heat and Mass Transfer in Metal–Hydrogen Reactor." *International Journal of Hydrogen Energy* 34 (19): 8315–21. <https://doi.org/10.1016/J.IJHYDENE.2009.07.072>.
- Askri, F., M. ben Salah, A. Jemni, and S. ben Nasrallah. 2009. "Optimization of Hydrogen Storage in Metal-Hydride Tanks." *International Journal of Hydrogen Energy* 34 (2): 897–905. <https://doi.org/10.1016/J.IJHYDENE.2008.11.021>.

- Azzaro-Pantel, C. 2018. *Hydrogen Supply Chain: Design, Deployment and Operation*.  
[https://books.google.com/books?hl=en&lr=&id=gyZqDwAAQBAJ&oi=fnd&pg=PP1&ots=69SI0wYImI&sig=-h9lv8LL56xXg\\_-iP8FTSGYYQOk](https://books.google.com/books?hl=en&lr=&id=gyZqDwAAQBAJ&oi=fnd&pg=PP1&ots=69SI0wYImI&sig=-h9lv8LL56xXg_-iP8FTSGYYQOk).
- Bao, Zewei, Zhen Wu, Serge Nyallang Nyamsi, Fusheng Yang, and Zaoxiao Zhang. 2013. “Three-Dimensional Modeling and Sensitivity Analysis of Multi-Tubular Metal Hydride Reactors.” *Applied Thermal Engineering* 52 (1): 97–108.  
<https://doi.org/10.1016/J.APPLTHERMALENG.2012.11.023>.
- Bao, Zewei, Fusheng Yang, Zhen Wu, Xinxin Cao, and Zaoxiao Zhang. 2013a. “Simulation Studies on Heat and Mass Transfer in High-Temperature Magnesium Hydride Reactors.” *Applied Energy* 112 (December):1181–89.  
<https://doi.org/10.1016/J.APENERGY.2013.04.053>.
- . 2013b. “Simulation Studies on Heat and Mass Transfer in High-Temperature Magnesium Hydride Reactors.” *Applied Energy* 112 (December):1181–89.  
<https://doi.org/10.1016/J.APENERGY.2013.04.053>.
- Bao, Zewei, Fusheng Yang, Zhen Wu, Serge Nyallang Nyamsi, and Zaoxiao Zhang. 2013. “Optimal Design of Metal Hydride Reactors Based on CFD–Taguchi Combined Method.” *Energy Conversion and Management* 65 (January):322–30.  
<https://doi.org/10.1016/J.ENCONMAN.2012.07.027>.
- Barreto, L., A. Makihira, and K. Riahi. 2003. “The Hydrogen Economy in the 21st Century: A Sustainable Development Scenario.” *International Journal of Hydrogen Energy* 28 (3): 267–84. [https://doi.org/10.1016/S0360-3199\(02\)00074-5](https://doi.org/10.1016/S0360-3199(02)00074-5).
- Beaudin, Marc, Hamidreza Zareipour, Anthony Schellenberglobe, and William Rosehart. 2010. “Energy Storage for Mitigating the Variability of Renewable Electricity Sources: An

- Updated Review.” *Energy for Sustainable Development*. Elsevier B.V.  
<https://doi.org/10.1016/j.esd.2010.09.007>.
- Broom, Darren P. 2011. “Potential Storage Materials.” In *Green Energy and Technology*, 27:19–59. Springer Verlag. [https://doi.org/10.1007/978-0-85729-221-6\\_2](https://doi.org/10.1007/978-0-85729-221-6_2).
- Brown, Tim M., Jacob Brouwer, G. Scott Samuelsen, Franklin H. Holcomb, and Joel King. 2008. “Accurate Simplified Dynamic Model of a Metal Hydride Tank.” *International Journal of Hydrogen Energy* 33 (20): 5596–5605. <https://doi.org/10.1016/J.IJHYDENE.2008.05.104>.
- Buschow, K. H.J., H. H. van Mal, and A. R. Miedema. 1975. “Hydrogen Absorption in Intermetallic Compounds of Thorium.” *Journal of The Less-Common Metals* 42 (2): 163–78. [https://doi.org/10.1016/0022-5088\(75\)90002-8](https://doi.org/10.1016/0022-5088(75)90002-8).
- Busqué, Raquel, Ricardo Torres, Joan Grau, Vicente Roda, and Attila Husar. 2017. “Effect of Metal Hydride Properties in Hydrogen Absorption through 2D-Axisymmetric Modeling and Experimental Testing in Storage Canisters.” *International Journal of Hydrogen Energy* 42 (30): 19114–25. <https://doi.org/10.1016/J.IJHYDENE.2017.06.125>.
- Chaise, A., P. Marty, P. de Rango, and D. Fruchart. 2009. “A Simple Criterion for Estimating the Effect of Pressure Gradients during Hydrogen Absorption in a Hydride Reactor.” *International Journal of Heat and Mass Transfer* 52 (19–20): 4564–72. <https://doi.org/10.1016/J.IJHEATMASSTRANSFER.2009.03.052>.
- Chaise, A, P de Rango, Ph Marty, and D Fruchart. 2010. “Experimental and Numerical Study of a Magnesium Hydride Tank.” *International Journal of Hydrogen Energy* 35:6311–22. <https://doi.org/10.1016/j.ijhydene.2010.03.057>.
- Chibani, Atef, Cherif Bougriou, and Slimane Merouani. 2018. “Simulation of Hydrogen Absorption/Desorption on Metal Hydride LaNi<sub>5</sub>-H<sub>2</sub>: Mass and Heat Transfer.” *Applied*

*Thermal Engineering* 142 (September):110–17.

<https://doi.org/10.1016/J.APPLTHERMALENG.2018.06.078>.

Chibani, Atef, Slimane Merouani, and Cherif Bougriou. 2022. “The Performance of Hydrogen Desorption from a Metal Hydride with Heat Supply by a Phase Change Material Incorporated in Porous Media (Metal Foam): Heat and Mass Transfer Assessment.” *Journal of Energy Storage* 51 (July):104449. <https://doi.org/10.1016/J.EST.2022.104449>.

Choy, Tuck C. 2016. *Effective Medium Theory : Principles and Applications*. 2nd edition. Vol. 165. Oxford University Press.

Chung, C. A., and Ci Jyun Ho. 2009. “Thermal–Fluid Behavior of the Hydriding and Dehydriding Processes in a Metal Hydride Hydrogen Storage Canister.” *International Journal of Hydrogen Energy* 34 (10): 4351–64. <https://doi.org/10.1016/J.IJHYDENE.2009.03.028>.

Chung, C. A., Su Wen Yang, Chien Yuh Yang, Che Weu Hsu, and Pai Yuh Chiu. 2013. “Experimental Study on the Hydrogen Charge and Discharge Rates of Metal Hydride Tanks Using Heat Pipes to Enhance Heat Transfer.” *Applied Energy* 103 (March):581–87. <https://doi.org/10.1016/J.APENERGY.2012.10.024>.

Demircan, A., M. Demiralp, Y. Kaplan, M. D. Mat, and T. N. Veziroglu. 2005. “Experimental and Theoretical Analysis of Hydrogen Absorption in LaNi<sub>5</sub>–H<sub>2</sub> Reactors.” *International Journal of Hydrogen Energy* 30 (13–14): 1437–46. <https://doi.org/10.1016/J.IJHYDENE.2005.02.002>.

Dhaou, H., F. Askri, M. Ben Salah, A. Jemni, S. Ben Nasrallah, and J. Lamloumi. 2007. “Measurement and Modelling of Kinetics of Hydrogen Sorption by LaNi<sub>5</sub> and Two Related Pseudobinary Compounds.” *International Journal of Hydrogen Energy* 32 (5): 576–87. <https://doi.org/10.1016/J.IJHYDENE.2006.07.001>.

- Dincer, Ibrahim, and Canan Acar. 2014. "Review and Evaluation of Hydrogen Production Methods for Better Sustainability." *International Journal of Hydrogen Energy* 40 (34): 11094–111. <https://doi.org/10.1016/j.ijhydene.2014.12.035>.
- Dunn, Seth. 2002. "Hydrogen Futures: Toward a Sustainable Energy System." *International Journal of Hydrogen Energy* 27 (3): 235–64. [https://doi.org/10.1016/S0360-3199\(01\)00131-8](https://doi.org/10.1016/S0360-3199(01)00131-8).
- Eftekhari, Ali Akbar, and Kai Schüller. 2015. "FVTool: A Finite Volume Toolbox for Matlab," October. <https://doi.org/10.5281/ZENODO.32745>.
- Eliaz, N., D. Eliezer, and D. L. Olson. 2000. "Hydrogen-Assisted Processing of Materials." *Materials Science and Engineering: A* 289 (1–2): 41–53. [https://doi.org/10.1016/S0921-5093\(00\)00906-0](https://doi.org/10.1016/S0921-5093(00)00906-0).
- Eliezer, D., N. Eliaz, O. N. Senkov, and F. H. Froes. 2000. "Positive Effects of Hydrogen in Metals." *Materials Science and Engineering: A* 280 (1): 220–24. [https://doi.org/10.1016/S0921-5093\(99\)00670-X](https://doi.org/10.1016/S0921-5093(99)00670-X).
- Elkhatib, Rafik, and Hasna Louahlia. 2023. "Metal Hydride Cylindrical Tank for Energy Hydrogen Storage: Experimental and Computational Modeling Investigations." *Applied Thermal Engineering* 230 (July):120756. <https://doi.org/10.1016/J.APPLTHERMALENG.2023.120756>.
- Eriksson, E. L.V., and E. Mac A. Gray. 2017. "Optimization and Integration of Hybrid Renewable Energy Hydrogen Fuel Cell Energy Systems – A Critical Review." *Applied Energy* 202 (September):348–64. <https://doi.org/10.1016/J.APENERGY.2017.03.132>.

- Freni, A., F. Cipiti, and G. Cacciola. 2009. "Finite Element-Based Simulation of a Metal Hydride-Based Hydrogen Storage Tank." *International Journal of Hydrogen Energy* 34 (20): 8574–82. <https://doi.org/10.1016/J.IJHYDENE.2009.07.118>.
- Gambini, M., M. Manno, and M. Vellini. 2008. "Numerical Analysis and Performance Assessment of Metal Hydride-Based Hydrogen Storage Systems." *International Journal of Hydrogen Energy* 33 (21): 6178–87. <https://doi.org/10.1016/J.IJHYDENE.2008.08.006>.
- Garrier, S., B. Delhomme, P. de Rango, P. Marty, D. Fruchart, and S. Miraglia. 2013. "A New MgH<sub>2</sub> Tank Concept Using a Phase-Change Material to Store the Heat of Reaction." *International Journal of Hydrogen Energy* 38 (23): 9766–71. <https://doi.org/10.1016/J.IJHYDENE.2013.05.026>.
- Gkanas, Evangelos I., Martin Khzouz, Grigorios Panagakos, Thomas Statheros, Giouli Mihalakakou, Gerasimos I. Siasos, Georgios Skodras, and Sofoklis S. Makridis. 2018. "Hydrogenation Behavior in Rectangular Metal Hydride Tanks under Effective Heat Management Processes for Green Building Applications." *Energy* 142 (January):518–30. <https://doi.org/10.1016/J.ENERGY.2017.10.040>.
- "Global Warming Update." n.d. Accessed May 9, 2024. <https://www.co2.earth/global-warming-update>.
- Gopal, M. Ram, and S. Srinivasa Murthy. 1995. "Studies on Heat and Mass Transfer in Metal Hydride Beds." *International Journal of Hydrogen Energy* 20 (11): 911–17. [https://doi.org/10.1016/0360-3199\(95\)00026-A](https://doi.org/10.1016/0360-3199(95)00026-A).
- Granovskii, Mikhail, Ibrahim Dincer, and Marc A. Rosen. 2006. "Environmental and Economic Aspects of Hydrogen Production and Utilization in Fuel Cell Vehicles." *Journal of Power Sources* 157 (1): 411–21. <https://doi.org/10.1016/J.JPOWSOUR.2005.07.044>.

- Hardy, Bruce J., and Donald L. Anton. 2009a. "Hierarchical Methodology for Modeling Hydrogen Storage Systems. Part I: Scoping Models." *International Journal of Hydrogen Energy* 34 (5): 2269–77. <https://doi.org/10.1016/J.IJHYDENE.2008.12.070>.
- . 2009b. "Hierarchical Methodology for Modeling Hydrogen Storage Systems. Part II: Detailed Models." *International Journal of Hydrogen Energy* 34 (7): 2992–3004. <https://doi.org/10.1016/J.IJHYDENE.2008.12.056>.
- Haseli, Y. 2018. "Maximum Conversion Efficiency of Hydrogen Fuel Cells." *International Journal of Hydrogen Energy* 43 (18): 9015–21. <https://doi.org/10.1016/J.IJHYDENE.2018.03.076>.
- Hasnain, Muhammad, Jairo Casa, Gregory E Gorbett, Hayri Sezer, Rylan Paye, Trevor Borth, and Shijin P Kozhumal. 2022. "3D Mathematical Model for Heat and Mass Transfer Mechanisms in Gypsum Board Exposed to Fire." In *13th U. S. National Combustion Meeting*. College Station, Texas. <https://www.researchgate.net/publication/373293420>.
- . n.d. "3D Mathematical Model for Heat and Mass Transfer Mechanisms in Gypsum Board Exposed to Fire." Accessed April 23, 2024. <https://www.researchgate.net/publication/373293420>.
- Hasnain, Muhammad, Shehzad Khan, M. Amin Ezazi, and Hayri Sezer. 2024. "Modeling Heat and Mass Transfer in Metal Hydride-Based Hydrogen Storage Systems Using the Finite Volume Method." *ASME International Mechanical Engineering Congress and Exposition, Proceedings (IMECE)* 10 (February). <https://doi.org/10.1115/IMECE2023-112874>.
- Hasnain, Muhammad, Rylan Paye, T Borth, G. E. Gorbett, S. P. Kozhumal, and Hayri Sezer. 2024. "Three-Dimensional Mathematical Modeling of Heat and Mass Transfer during Calcination of Gypsum Board Exposed to Fire." In *Spring Technical Meeting Eastern States*



*Section of the Combustion Institute*. Athens, Georgia.

<https://www.researchgate.net/publication/379034315>.

Hasnain, Muhammad, Hayri Sezer, and Jerry Hunter Mason. 2024. “Modeling Heat and Mass Transfer in Metal Hydride Hydrogen Storage Systems: Impact of Operating Parameters and Reactor Geometry.” *International Journal of Hydrogen Energy* 71 (June):1045–55.  
<https://doi.org/10.1016/j.ijhydene.2024.05.311>.

Helmolt, Rittmar von, and Ulrich Eberle. 2007. “Fuel Cell Vehicles: Status 2007.” *Journal of Power Sources* 165 (2): 833–43. <https://doi.org/10.1016/J.JPOWSOUR.2006.12.073>.

Hollmuller, Pierre, Jean Marc Joubert, Bernard Lachal, and Klaus Yvon. 2000. “Evaluation of a 5 KWp Photovoltaic Hydrogen Production and Storage Installation for a Residential Home in Switzerland.” *International Journal of Hydrogen Energy* 25 (2): 97–109.  
[https://doi.org/10.1016/S0360-3199\(99\)00015-4](https://doi.org/10.1016/S0360-3199(99)00015-4).

“Hydrogen Calculators - Stargate Hydrogen.” n.d. Accessed May 10, 2024.  
<https://stargatehydrogen.com/hydrogen-calculators/>.

“Hydrogen Tools | CMB.TECH.” n.d. Accessed May 10, 2024. <https://cmb.tech/hydrogen-tools>.

Ibrahim, H., A. Ilinca, and J. Perron. 2008. “Energy Storage Systems-Characteristics and Comparisons.” *Renewable and Sustainable Energy Reviews*.  
<https://doi.org/10.1016/j.rser.2007.01.023>.

Jain, I. P., Pragya Jain, and Ankur Jain. 2010. “Novel Hydrogen Storage Materials: A Review of Lightweight Complex Hydrides.” *Journal of Alloys and Compounds* 503 (2): 303–39.  
<https://doi.org/10.1016/J.JALLCOM.2010.04.250>.

- Jang, Dohyung, Hyun Seok Cho, and Sanggyu Kang. 2021. "Numerical Modeling and Analysis of the Effect of Pressure on the Performance of an Alkaline Water Electrolysis System." *Applied Energy* 287 (April). <https://doi.org/10.1016/j.apenergy.2021.116554>.
- Javaid, Rahat. 2021. "Catalytic Hydrogen Production, Storage and Application." *Catalysts* 2021, Vol. 11, Page 836 11 (7): 836. <https://doi.org/10.3390/CATAL11070836>.
- Jemni, A., and S. Ben Nasrallah. 1995a. "Study of Two-Dimensional Heat and Mass Transfer during Absorption in a Metal-Hydrogen Reactor." *International Journal of Hydrogen Energy* 20 (1): 43–52. [https://doi.org/10.1016/0360-3199\(93\)E0007-8](https://doi.org/10.1016/0360-3199(93)E0007-8).
- . 1995b. "Study of Two-Dimensional Heat and Mass Transfer during Absorption in a Metal-Hydrogen Reactor." *International Journal of Hydrogen Energy* 20 (1): 43–52. [https://doi.org/10.1016/0360-3199\(93\)E0007-8](https://doi.org/10.1016/0360-3199(93)E0007-8).
- . 1995c. "Study of Two-Dimensional Heat and Mass Transfer during Desorption in a Metal-Hydrogen Reactor." *International Journal of Hydrogen Energy* 20 (11): 881–91. [https://doi.org/10.1016/0360-3199\(94\)00115-G](https://doi.org/10.1016/0360-3199(94)00115-G).
- Jemni, Abdelmajid, Sassi Ben Nasrallah, and Jilani Lamloumi. 1999. "Experimental and Theoretical Study of A metal–Hydrogen Reactor." *International Journal of Hydrogen Energy* 24 (7): 631–44. [https://doi.org/10.1016/S0360-3199\(98\)00117-7](https://doi.org/10.1016/S0360-3199(98)00117-7).
- Khan, Muhammad Usman, Muhammad Hasnain, and Shehzad Khan. 2024. "Mathematical Model for Predicting Injuries and Temperature Distributions in Stem Exposed to Fire." In *Spring Technical Meeting Eastern States Section of the Combustion Institute*. Athens, Georgia. <https://www.researchgate.net/publication/379034461>.
- Khan, Shehzad, Sohail Anwar, Jairo Casa, Muhammad Hasnain, Hossain Ahmed, and Hayri Sezer. 2024. "Modeling Thermal Runaway in Prismatic Lithium-Ion Batteries." *ASME*

*International Mechanical Engineering Congress and Exposition, Proceedings (IMECE)* 10 (February). <https://doi.org/10.1115/IMECE2023-113787>.

Khan, Shehzad, Muhammad Hasnain, and Jairo Casa. 2024. "Mathematical Modeling of Heat-Induced Decomposition Kinetics Leading to Thermal Runaway in Lithium-Ion Batteries." In *Spring Technical Meeting Eastern States Section of the Combustion Institute*. Athens, Georgia. <https://doi.org/10.1149/1945-7111/ABA8B9>.

Khan, Shehzad, Muhammad Hasnain, Abdullah Liaqat, Vyacheslav Akkerman, Hossain Ahmed, Shijin P Kozhumal, and Hayri Sezer. 2022. "The Self-Heating Ignition of Lithium-Ion Batteries: A Comparative Study of COMSOL and GPYRO Models with Finite Volume Toolbox." In *13th U. S. National Combustion Meeting*. College Station, Texas. <https://www.researchgate.net/profile/Shehzad-Khan-13/publication/373013979>.

Khan, Shehzad, Muhammad Hasnain, and Hayri Sezer. 2024. "Numerical Modeling of Spontaneous Ignition in Large Coal Stockpiles Using Finite Volume Method." In *Spring Technical Meeting Eastern States Section of the Combustion Institute*. Athens, Georgia. [https://doi.org/10.1016/S0378-3820\(99\)00005-3](https://doi.org/10.1016/S0378-3820(99)00005-3).

Kharel, Subodh, and Bahman Shabani. 2018. "Hydrogen as a Long-Term Large-Scale Energy Storage Solution to Support Renewables." *Energies* 11 (10). <https://doi.org/10.3390/en11102825>.

Kumar Phate, Arvind, M. Prakash Maiya, and S. Srinivasa Murthy. 2007. "Simulation of Transient Heat and Mass Transfer during Hydrogen Sorption in Cylindrical Metal Hydride Beds." *International Journal of Hydrogen Energy* 32 (12): 1969–81. <https://doi.org/10.1016/J.IJHYDENE.2006.09.020>.

Kyoung, Sunghyun, Saad Ferekh, Geonhui Gwak, Ahrae Jo, and Hyunchul Ju. 2015. "Three-Dimensional Modeling and Simulation of Hydrogen Desorption in Metal Hydride Hydrogen

- Storage Vessels.” *International Journal of Hydrogen Energy* 40 (41): 14322–30.  
<https://doi.org/10.1016/J.IJHYDENE.2015.03.114>.
- Lai, Qiwen, Kondo-Francois Aguey-Zinsou, Qiwen Lai, and Kondo-Francois Aguey-Zinsou. 2018. “Borohydrides as Solid-State Hydrogen Storage Materials: Past, Current Approaches and Future Perspectives.” *General Chemistry* 4 (4): 180017.  
<https://doi.org/10.21127/YAOYIGC20180017>.
- Lototskyy, Mykhaylo V., Ivan Tolj, Lydia Pickering, Cordellia Sita, Frano Barbir, and Volodymyr Yartys. 2017. “The Use of Metal Hydrides in Fuel Cell Applications.” *Progress in Natural Science: Materials International*. Elsevier B.V. <https://doi.org/10.1016/j.pnsc.2017.01.008>.
- Lucas, G. G., and W. L. Richards. 1984. “Mathematical Modelling of Hydrogen Storage Systems.” *International Journal of Hydrogen Energy* 9 (3): 225–31.  
[https://doi.org/10.1016/0360-3199\(84\)90123-X](https://doi.org/10.1016/0360-3199(84)90123-X).
- Ma, Jincheng, Yuqi Wang, Shaofei Shi, Fusheng Yang, Zewei Bao, and Zaoxiao Zhang. 2014. “Optimization of Heat Transfer Device and Analysis of Heat & Mass Transfer on the Finned Multi-Tubular Metal Hydride Tank.” *International Journal of Hydrogen Energy* 39 (25): 13583–95. <https://doi.org/10.1016/J.IJHYDENE.2014.03.016>.
- Mâad, H. ben, F. Askri, and S. ben Nasrallah. 2016. “Heat and Mass Transfer in a Metal Hydrogen Reactor Equipped with a Phase-Change Heat-Exchanger.” *International Journal of Thermal Sciences* 99 (January):271–78. <https://doi.org/10.1016/J.IJTHERMALSCI.2015.09.003>.
- Mâad, Hatem ben, Faouzi Askri, Joseph Virgone, and Sassi ben Nasrallah. 2018. “Numerical Study of High Temperature Metal-Hydrogen Reactor (Mg<sub>2</sub>Ni-H<sub>2</sub>) with Heat Reaction Recovery Using Phase-Change Material during Desorption.” *Applied Thermal Engineering* 140 (July):225–34. <https://doi.org/10.1016/J.APPLTHERMALENG.2018.05.009>.

- Mâad, Hatem Ben, Amel Miled, Faouzi Askri, and Sassi Ben Nasrallah. 2016. "Numerical Simulation of Absorption-Desorption Cyclic Processes for Metal-Hydrogen Reactor with Heat Recovery Using Phase-Change Material." *Applied Thermal Engineering* 96 (March):267–76. <https://doi.org/10.1016/J.APPLTHERMALENG.2015.11.093>.
- MacDonald, Brendan D., and Andrew M. Rowe. 2006. "Impacts of External Heat Transfer Enhancements on Metal Hydride Storage Tanks." *International Journal of Hydrogen Energy* 31 (12): 1721–31. <https://doi.org/10.1016/J.IJHYDENE.2006.01.007>.
- Manai, Mohamed Sakreddine, Mikel Leturia, Carsten Pohlmann, Jorn Oubraham, Stéphane Mottelet, Michael Levy, and Khashayar Saleh. 2019. "Comparative Study of Different Storage Bed Designs of a Solid-State Hydrogen Tank." <https://doi.org/10.1016/j.est.2019.101024>.
- Maniatopoulos, Paul, John Andrews, and Bahman Shabani. 2015. "Towards a Sustainable Strategy for Road Transportation in Australia: The Potential Contribution of Hydrogen." *Renewable and Sustainable Energy Reviews*. Elsevier Ltd. <https://doi.org/10.1016/j.rser.2015.07.088>.
- Marty, Ph, P. de Rango, B. Delhomme, and S. Garrier. 2013. "Various Tools for Optimizing Large Scale Magnesium Hydride Storage." *Journal of Alloys and Compounds* 580 (SUPPL1): S324–28. <https://doi.org/10.1016/J.JALLCOM.2013.02.169>.
- Mat, Mahmut D., and Yüksel Kaplan. 2001. "Numerical Study of Hydrogen Absorption in an Lm–Ni<sub>5</sub> Hydride Reactor." *International Journal of Hydrogen Energy* 26 (9): 957–63. [https://doi.org/10.1016/S0360-3199\(01\)00030-1](https://doi.org/10.1016/S0360-3199(01)00030-1).
- Mayer, U., M. Groll, and W. Supper. 1987. "Heat and Mass Transfer in Metal Hydride Reaction Beds: Experimental and Theoretical Results." *Journal of the Less Common Metals* 131 (1–2): 235–44. [https://doi.org/10.1016/0022-5088\(87\)90523-6](https://doi.org/10.1016/0022-5088(87)90523-6).

- Mazloomi, Kaveh, and Chandima Gomes. 2012. "Hydrogen as an Energy Carrier: Prospects and Challenges." *Renewable and Sustainable Energy Reviews*.  
<https://doi.org/10.1016/j.rser.2012.02.028>.
- Mellouli, S., F. Askri, H. Dhaou, A. Jemni, and S. Ben Nasrallah. 2010. "Numerical Simulation of Heat and Mass Transfer in Metal Hydride Hydrogen Storage Tanks for Fuel Cell Vehicles." *International Journal of Hydrogen Energy* 35 (4): 1693–1705.  
<https://doi.org/10.1016/J.IJHYDENE.2009.12.052>.
- Modi, Poojan, and Kondo Francois Aguey-Zinsou. 2021. "Room Temperature Metal Hydrides for Stationary and Heat Storage Applications: A Review." *Frontiers in Energy Research* 9 (April):128. <https://doi.org/10.3389/FENRG.2021.616115/BIBTEX>.
- Mohammadshahi, S. S., E. Mac A. Gray, and C. J. Webb. 2016a. "A Review of Mathematical Modelling of Metal-Hydride Systems for Hydrogen Storage Applications." *International Journal of Hydrogen Energy*. Elsevier Ltd. <https://doi.org/10.1016/j.ijhydene.2015.12.079>.
- . 2016b. "A Review of Mathematical Modelling of Metal-Hydride Systems for Hydrogen Storage Applications." *International Journal of Hydrogen Energy* 41 (5): 3470–84.  
<https://doi.org/10.1016/J.IJHYDENE.2015.12.079>.
- Mohan, G., M. Prakash Maiya, and S. Srinivasa Murthy. 2007. "Performance Simulation of Metal Hydride Hydrogen Storage Device with Embedded Filters and Heat Exchanger Tubes." *International Journal of Hydrogen Energy* 32 (18): 4978–87.  
<https://doi.org/10.1016/J.IJHYDENE.2007.08.007>.
- Momirlan, M., and T. N. Veziroglu. 2002. "Current Status of Hydrogen Energy." *Renewable and Sustainable Energy Reviews* 6 (1–2): 141–79. [https://doi.org/10.1016/S1364-0321\(02\)00004-7](https://doi.org/10.1016/S1364-0321(02)00004-7).

- Moradi, Ramin, and Katrina M. Groth. 2019. "Hydrogen Storage and Delivery: Review of the State of the Art Technologies and Risk and Reliability Analysis." *International Journal of Hydrogen Energy* 44 (23): 12254–69. <https://doi.org/10.1016/J.IJHYDENE.2019.03.041>.
- Muhammad Hasnain, Shehzad Khan, M.Amin Ezazi, and Hayri Sezer. 2023. "Modeling Heat and Mass Transfer in Metal Hydride-Based Hydrogen Storage Systems Using the Finite Volume Method." In *Proceedings of the ASME 2023 International Mechanical Engineering Congress and Exposition (IMECE)*. New Orleans.
- Muthukumar, P., and M. Groll. 2010a. "Metal Hydride Based Heating and Cooling Systems: A Review." *International Journal of Hydrogen Energy* 35 (8): 3817–31. <https://doi.org/10.1016/J.IJHYDENE.2010.01.115>.
- . 2010b. "Metal Hydride Based Heating and Cooling Systems: A Review." *International Journal of Hydrogen Energy* 35 (8): 3817–31. <https://doi.org/10.1016/J.IJHYDENE.2010.01.115>.
- Muthukumar, P., U. Madhavakrishna, and Anupam Dewan. 2007. "Parametric Studies on a Metal Hydride Based Hydrogen Storage Device." *International Journal of Hydrogen Energy* 32 (18): 4988–97. <https://doi.org/10.1016/J.IJHYDENE.2007.08.010>.
- Muthukumar, P., A. Singhal, and G. K. Bansal. 2012. "Thermal Modeling and Performance Analysis of Industrial-Scale Metal Hydride Based Hydrogen Storage Container." *International Journal of Hydrogen Energy* 37 (19): 14351–64. <https://doi.org/10.1016/J.IJHYDENE.2012.07.010>.
- Nam, Jinmoo, Johan Ko, and Hyunchul Ju. 2012. "Three-Dimensional Modeling and Simulation of Hydrogen Absorption in Metal Hydride Hydrogen Storage Vessels." *Applied Energy* 89 (1): 164–75. <https://doi.org/10.1016/J.APENERGY.2011.06.015>.

- Nasrallah, S. Ben, and A. Jemni. 1997. "Heat and Mass Transfer Models in Metal-Hydrogen Reactor." *International Journal of Hydrogen Energy* 22 (1): 67–76.  
[https://doi.org/10.1016/S0360-3199\(96\)00039-0](https://doi.org/10.1016/S0360-3199(96)00039-0).
- Nguyen, Huy Quoc, and Bahman Shabani. 2020. "Proton Exchange Membrane Fuel Cells Heat Recovery Opportunities for Combined Heating/Cooling and Power Applications." *Energy Conversion and Management* 204 (January):112328.  
<https://doi.org/10.1016/J.ENCONMAN.2019.112328>.
- . 2021. "Review of Metal Hydride Hydrogen Storage Thermal Management for Use in the Fuel Cell Systems." *International Journal of Hydrogen Energy* 46 (62): 31699–726.  
<https://doi.org/10.1016/j.ijhydene.2021.07.057>.
- Niaz, Saba, Taniya Manzoor, and Altaf Hussain Pandith. 2015. "Hydrogen Storage: Materials, Methods and Perspectives." *Renewable & Sustainable Energy Reviews* 50 (May):457–69.  
<https://doi.org/10.1016/J.RSER.2015.05.011>.
- Nikolaïdis, Pavlos, and Andreas Poullikkas. 2017. "A Comparative Overview of Hydrogen Production Processes." *Renewable and Sustainable Energy Reviews* 67 (January):597–611.  
<https://doi.org/10.1016/J.RSER.2016.09.044>.
- Nishizaki, T., K. Miyamoto, and K. Yoshida. 1983. "Coefficients of Performance of Hydride Heat Pumps." *Journal of the Less Common Metals* 89 (2): 559–66. [https://doi.org/10.1016/0022-5088\(83\)90372-7](https://doi.org/10.1016/0022-5088(83)90372-7).
- Nyamsi, Serge Nyallang, Fusheng Yang, and Zaoxiao Zhang. 2012. "An Optimization Study on the Finned Tube Heat Exchanger Used in Hydride Hydrogen Storage System - Analytical Method and Numerical Simulation." *International Journal of Hydrogen Energy* 37 (21): 16078–92. <https://doi.org/10.1016/j.ijhydene.2012.08.074>.



- Onorati, A., R. Payri, B. M. Vaglieco, A. K. Agarwal, C. Bae, G. Bruneaux, M. Canakci, et al. 2022. "The Role of Hydrogen for Future Internal Combustion Engines." *International Journal of Engine Research* 23 (4): 529–40.  
[https://doi.org/10.1177/14680874221081947/ASSET/IMAGES/LARGE/10.1177\\_14680874221081947-FIG4.JPEG](https://doi.org/10.1177/14680874221081947/ASSET/IMAGES/LARGE/10.1177_14680874221081947-FIG4.JPEG).
- Osery, I. A. El. 1983. "Theory of the Computer Code RET 1 for the Calculation of Space-Time Dependent Temperature and Composition Properties of Metal Hydride Hydrogen Storage Beds." *International Journal of Hydrogen Energy* 8 (3): 191–98.  
[https://doi.org/10.1016/0360-3199\(83\)90064-2](https://doi.org/10.1016/0360-3199(83)90064-2).
- Pereira, C. A., P. M. Coelho, J. F. Fernandes, and M. H. Gomes. 2017. "Study of an Energy Mix for the Production of Hydrogen." *International Journal of Hydrogen Energy* 42 (2): 1375–82. <https://doi.org/10.1016/J.IJHYDENE.2016.07.182>.
- Qazi, Umair Yaqub. 2022. "Future of Hydrogen as an Alternative Fuel for Next-Generation Industrial Applications; Challenges and Expected Opportunities." *Energies* 15 (13). <https://doi.org/10.3390/en15134741>.
- Ram Gopal, M., and S. Srinivasa Murthy. 1992. "Prediction of Heat and Mass Transfer in Annular Cylindrical Metal Hydride Beds." *International Journal of Hydrogen Energy* 17 (10): 795–805. [https://doi.org/10.1016/0360-3199\(92\)90024-Q](https://doi.org/10.1016/0360-3199(92)90024-Q).
- Ramachandran, Ram, and Raghu K. Menon. 1998. "An Overview of Industrial Uses of Hydrogen." *International Journal of Hydrogen Energy* 23 (7): 593–98.  
[https://doi.org/10.1016/S0360-3199\(97\)00112-2](https://doi.org/10.1016/S0360-3199(97)00112-2).
- Rosen, M. A., and D. S. Scott. 1998. "Comparative Efficiency Assessments for a Range of Hydrogen Production Processes." *International Journal of Hydrogen Energy* 23 (8): 653–59.  
[https://doi.org/10.1016/S0360-3199\(97\)00080-3](https://doi.org/10.1016/S0360-3199(97)00080-3).

- Rowse, Jesse L.C., and Omar M. Yaghi. 2005. "Strategies for Hydrogen Storage in Metal-Organic Frameworks." *Angewandte Chemie - International Edition*.  
<https://doi.org/10.1002/anie.200462786>.
- Sánchez, J. M., M. M. Barreiro, and M. Maroño. 2014. "Bench-Scale Study of Separation of Hydrogen from Gasification Gases Using a Palladium-Based Membrane Reactor." *Fuel* 116 (January):894–903. <https://doi.org/10.1016/J.FUEL.2013.02.051>.
- Sandrock, Gary. 1999. "A Panoramic Overview of Hydrogen Storage Alloys from a Gas Reaction Point of View." *Journal of Alloys and Compounds* 293–295 (December):877–88.  
[https://doi.org/10.1016/S0925-8388\(99\)00384-9](https://doi.org/10.1016/S0925-8388(99)00384-9).
- Satheesh, A., P. Muthukumar, and Anupam Dewan. 2009. "Computational Study of Metal Hydride Cooling System." *International Journal of Hydrogen Energy* 34 (7): 3164–72.  
<https://doi.org/10.1016/J.IJHYDENE.2009.01.083>.
- Satya Sekhar, B., M. Lototskyy, A. Kolesnikov, M. L. Moropeng, B. P. Tarasov, and B. G. Pollet. 2015. "Performance Analysis of Cylindrical Metal Hydride Beds with Various Heat Exchange Options." *Journal of Alloys and Compounds* 645 (S1): S89–95.  
<https://doi.org/10.1016/J.JALLCOM.2014.12.272>.
- Shabani, Bahman, and John Andrews. 2015. "Hydrogen and Fuel Cells." *Green Energy and Technology* 201:453–91. [https://doi.org/10.1007/978-81-322-2337-5\\_17/COVER](https://doi.org/10.1007/978-81-322-2337-5_17/COVER).
- Shabani, Bahman, John Andrews, and Sukhvinder Badwal. 2010. "FUEL CELL HEAT RECOVERY, ELECTRICAL LOAD MANAGEMENT, AND THE ECONOMICS OF SOLAR-HYDROGEN SYSTEMS." *International Journal of Power and Energy Systems* 30 (4): 256–63. <https://doi.org/10.2316/JOURNAL.203.2010.4.203-4842>.

- Shafiee, Roxana. 2021. "Can Hydrogen Drive Scotland to Net-Zero? Part 1: What Is Hydrogen Energy? – SPICe Spotlight | Solas Air SPICe." *Environment & Energy, Transport*. 2021. <https://spice-spotlight.scot/2021/08/19/can-hydrogen-drive-scotland-to-net-zero-part-1-what-is-hydrogen-energy/>.
- Shamberger, Patrick J, and Nickolaus M Bruno. 2020. "Review of Metallic Phase Change Materials for High Heat Flux Transient Thermal Management Applications." *Applied Energy* 258:113955. <https://doi.org/10.1016/j.apenergy.2019.113955>.
- Sharma, Sunita, and Sib Krishna Ghoshal. 2015. "Hydrogen the Future Transportation Fuel: From Production to Applications." *Renewable and Sustainable Energy Reviews* 43 (March):1151–58. <https://doi.org/10.1016/J.RSER.2014.11.093>.
- Shin, Jungwoo, Won Sik Hwang, and Hyundo Choi. 2019. "Can Hydrogen Fuel Vehicles Be a Sustainable Alternative on Vehicle Market?: Comparison of Electric and Hydrogen Fuel Cell Vehicles." *Technological Forecasting and Social Change* 143 (June):239–48. <https://doi.org/10.1016/j.techfore.2019.02.001>.
- Singh, Anurag, M. P. Maiya, and S. Srinivasa Murthy. 2015. "Effects of Heat Exchanger Design on the Performance of a Solid State Hydrogen Storage Device." *International Journal of Hydrogen Energy* 40 (31): 9733–46. <https://doi.org/10.1016/j.ijhydene.2015.06.015>.
- Siyakatshana, Njabulo, Vladimír Kudrna, and Václav Machoň. 2005. "Incorporating Danckwerts' Boundary Conditions into the Solution of the Stochastic Differential Equation." *Chemical Engineering Science* 60 (7): 1987–94. <https://doi.org/10.1016/J.CES.2004.11.051>.
- Suda, S., N. Kobayashi, and K. Yoshida. 1980. "Reaction Kinetics of Metal Hydrides and Their Mixtures." *Journal of the Less Common Metals* 73 (1): 119–26. [https://doi.org/10.1016/0022-5088\(80\)90350-1](https://doi.org/10.1016/0022-5088(80)90350-1).

- Supper, W., M. Groll, and U. Mayer. 1984. "Reaction Kinetics in Metal Hydride Reaction Beds with Improved Heat and Mass Transfer." *Journal of the Less Common Metals* 104 (2): 279–86. [https://doi.org/10.1016/0022-5088\(84\)90412-0](https://doi.org/10.1016/0022-5088(84)90412-0).
- Tao, Y. B., and Y. L. He. 2015. "Effects of Natural Convection on Latent Heat Storage Performance of Salt in a Horizontal Concentric Tube." *Applied Energy* 143 (April):38–46. <https://doi.org/10.1016/J.APENERGY.2015.01.008>.
- Trommer, D., F. Noembrini, M. Fasciana, D. Rodriguez, A. Morales, M. Romero, and A. Steinfeld. 2005. "Hydrogen Production by Steam-Gasification of Petroleum Coke Using Concentrated Solar Power—I. Thermodynamic and Kinetic Analyses." *International Journal of Hydrogen Energy* 30 (6): 605–18. <https://doi.org/10.1016/J.IJHYDENE.2004.06.002>.
- Varkaraki, E., N. Lymberopoulos, and A. Zachariou. 2003. "Hydrogen Based Emergency Back-up System for Telecommunication Applications." *Journal of Power Sources* 118 (1–2): 14–22. [https://doi.org/10.1016/S0378-7753\(03\)00056-9](https://doi.org/10.1016/S0378-7753(03)00056-9).
- Verhelst, S. 2014. "Recent Progress in the Use of Hydrogen as a Fuel for Internal Combustion Engines." *International Journal of Hydrogen Energy* 39 (2): 1071–85. <https://doi.org/10.1016/J.IJHYDENE.2013.10.102>.
- Vucht, Van, J H.N., Kuijpers, A F, Bruning, and C.A.M. H. 1970. "REVERSIBLE ROOM-TEMPERATURE ABSORPTION OF LARGE QUANTITIES OF HYDROGEN BY INTERMETALLIC COMPOUNDS." *Philips Res. Rep.* 25:133–40. <https://www.osti.gov/biblio/4129528>.
- Walker, G. (Gavin), and Minerals Institute of Materials. 2008. *Solid State Hydrogen Storage : Materials and Chemistry*. Woodhead Pub.

- Wang, Di, Yuqi Wang, Zhuonan Huang, Fusheng Yang, Zhen Wu, Lan Zheng, Le Wu, and Zaoxiao Zhang. 2019. "Design Optimization and Sensitivity Analysis of the Radiation Mini-Channel Metal Hydride Reactor." *Energy* 173 (April):443–56.  
<https://doi.org/10.1016/J.ENERGY.2019.02.033>.
- Wang, Yun, Xavier Cordobes Adroher, Jixin Chen, Xiao Guang Yang, and Ted Miller. 2009. "Three-Dimensional Modeling of Hydrogen Sorption in Metal Hydride Hydrogen Storage Beds." *Journal of Power Sources* 194 (2): 997–1006.  
<https://doi.org/10.1016/J.JPOWSOUR.2009.06.060>.
- Wang, Yuqi, Fusheng Yang, Xiangyu Meng, Quanfa Guo, Zaoxiao Zhang, Il Seok Park, Sunwoo Kim, and Kwang J. Kim. 2010. "Simulation Study on the Reaction Process Based Single Stage Metal Hydride Thermal Compressor." *International Journal of Hydrogen Energy* 35 (1): 321–28. <https://doi.org/10.1016/J.IJHYDENE.2009.10.085>.
- Wijayanta, Agung Tri, Koichi Nakaso, Takuro Aoki, Yusuke Kitazato, and Jun Fukai. 2011. "Effect of Pressure, Composition and Temperature Characteristics on Thermal Response and Overall Reaction Rates in a Metal Hydride Tank." *International Journal of Hydrogen Energy* 36 (5): 3529–36. <https://doi.org/10.1016/J.IJHYDENE.2010.12.047>.
- Yang, F. S., G. X. Wang, Z. X. Zhang, and V. Rudolph. 2010. "Investigation on the Influences of Heat Transfer Enhancement Measures in a Thermally Driven Metal Hydride Heat Pump." *International Journal of Hydrogen Energy* 35 (18): 9725–35.  
<https://doi.org/10.1016/J.IJHYDENE.2010.06.110>.
- Yao, Jing, Pengfei Zhu, Chenhui Qian, Usamah Hamidullah, Sandra Kurko, Fusheng Yang, Zaoxiao Zhang, and Zhen Wu. 2020a. "Study of an Autothermal-Equilibrium Metal Hydride Reactor by Reaction Heat Recovery as Hydrogen Source for the Application of Fuel Cell

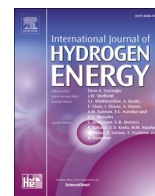
- Power System.” *Energy Conversion and Management* 213 (June):112864.  
<https://doi.org/10.1016/J.ENCONMAN.2020.112864>.
- . 2020b. “Study of an Autothermal-Equilibrium Metal Hydride Reactor by Reaction Heat Recovery as Hydrogen Source for the Application of Fuel Cell Power System.” *Energy Conversion and Management* 213 (June):112864.  
<https://doi.org/10.1016/J.ENCONMAN.2020.112864>.
- Ye, Yang, Jianfeng Lu, Jing Ding, Weilong Wang, and Jinyue Yan. 2022. “Performance Improvement of Metal Hydride Hydrogen Storage Tanks by Using Phase Change Materials.” *Applied Energy* 320 (August). <https://doi.org/10.1016/j.apenergy.2022.119290>.
- Young, David C., Greig A. Mill, and Rob Wall. 2007. “Feasibility of Renewable Energy Storage Using Hydrogen in Remote Communities in Bhutan.” *International Journal of Hydrogen Energy* 32 (8): 997–1009. <https://doi.org/10.1016/J.IJHYDENE.2006.07.002>.
- Zeng, Kai, and Dongke Zhang. 2010. “Recent Progress in Alkaline Water Electrolysis for Hydrogen Production and Applications.” *Progress in Energy and Combustion Science* 36 (3): 307–26. <https://doi.org/10.1016/J.PECS.2009.11.002>.
- Zhang, Jinsong, Timothy S. Fisher, P. Veeraraghavan Ramachandran, Jay P. Gore, and Issam Mudawar. 2005. “A Review of Heat Transfer Issues in Hydrogen Storage Technologies.” *Journal of Heat Transfer-Transactions of The Asme* 127 (12): 1391–99.  
<https://doi.org/10.1115/1.2098875>.
- Zhang, Yang, Pietro Elia Campana, Anders Lundblad, and Jinyue Yan. 2017. “Comparative Study of Hydrogen Storage and Battery Storage in Grid Connected Photovoltaic System: Storage Sizing and Rule-Based Operation.” *Applied Energy* 201 (September):397–411.  
<https://doi.org/10.1016/J.APENERGY.2017.03.123>.

Züttel, Andreas, Arndt Remhof, Andreas Borgschulte, and Oliver Friedrichs. 2010. "Hydrogen: The Future Energy Carrier." *Philosophical Transactions of the Royal Society A: Mathematical, Physical and Engineering Sciences* 368 (1923): 3329–42.

<https://doi.org/10.1098/RSTA.2010.0113>.







# Modeling heat and mass transfer in metal hydride hydrogen storage systems: Impact of operating parameters and reactor geometry

Muhammad Hasnain<sup>a</sup>, Hayri Sezer<sup>a,\*</sup>, Jerry Hunter Mason<sup>b</sup>

<sup>a</sup> Department of Mechanical Engineering, Georgia Southern University, Statesboro, GA 30458, USA

<sup>b</sup> Watt Fuel Cell, Mount Pleasant, PA, 15666, USA

## ARTICLE INFO

Handling Editor: Prof. A.B. Basile

### Keywords:

Hydrogen storage  
Metal hydrides  
Mathematical modeling  
Exothermic absorption  
Parametric analysis  
Reactive porous media

## ABSTRACT

This work introduces a transient 2D axis-symmetrical model for hydrogen absorption in a cylindrical LaNi<sub>5</sub> reactor employing finite volume method with a fully implicit Euler's time integration scheme, coupling equations for heat, mass, and momentum transport. The validated model is used to investigate the impacts of pressure, cooling fluid temperature, and variations in reactor geometry and size on temperature and reacted fraction profiles. The findings reveal that the charging pressure affects both peak temperature and reaction kinetics, whereas cooling fluid temperature predominantly impacts the absorption kinetics. A comparative analysis of two models, one incorporating Darcy's velocity and one without, demonstrates that while Darcy's law introduces numerical instability in the coupled equations, its impact on the model outcomes is negligible. The effect of changing the non-homogeneous Neumann to Dirichlet boundary condition is also demonstrated to anticipate the utilization of phase change materials (PCM) instead of the cooling fluid.

## 1. Introduction

Due to rapidly increasing global energy demands and concerns over non-renewable energy sources' environmental impacts, there is a growing need for reliable and sustainable alternatives. Renewable energy technologies, such as solar and wind power, play a crucial role in reducing greenhouse gas emissions and meeting energy demands. However, their intermittent nature can create imbalances in energy supply and demand [1]. Energy storage is a key solution to this challenge. While batteries are commonly used for energy storage, they have limitations such as high cost, uncertain lifespan, low energy density, self-discharge, safety concerns, and rapid degradation, making them unsuitable for long-term and high-capacity applications [2]. In this context, hydrogen (H<sub>2</sub>) emerges as a promising energy storage solution [3].

Hydrogen, a green energy source, can react with oxygen in fuel cells to produce water, heat, and electricity. Its major motivations as an energy source lies in its natural abundance, and high gravimetric energy density surpassing that of gasoline and diesel by up to three times [1,4]. The excess energy from the renewable sources can be used for water electrolysis to generate hydrogen gas which can then be stored and utilized in fuel cells to generate electric power when renewable energy

supply falls short of demand [3,5].

The storage of hydrogen presents a significant contemporary challenge, particularly in the context of integrated hydrogen-based systems, which necessitate efficient methods for storing and transporting H<sub>2</sub> for various applications [6,7]. Depending on the specific application, hydrogen can be stored either as a high-pressure gas or in liquid form, especially when space and weight considerations are critical. In its gaseous state, hydrogen exhibits a low volumetric energy density, approximately 27 kg H<sub>2</sub>/m<sup>3</sup> as shown in Table 1 [8]. Consequently, a substantially larger storage area is required relative to alternative energy storing solutions, posing technical challenges in storage, transportation, and portable applications [4,9].

To address this issue, two primary approaches have been explored: high-pressure gas compression at around 700 bars and liquefaction achieved by maintaining cryogenic temperatures near 20 K. However, both methods require additional costs associated with extreme temperature and pressure conditions [10–12]. Among these, high-pressure compression is the prevailing commercial method for hydrogen storage due to its simplicity and maturity [3]. Conversely, the liquefaction process consumes up to 30% of the output energy, rendering it less efficient [1,13]. Both of these solutions encounter notable limitations in large-scale applications, including safety and low storage efficiency due to high pressure and low volumetric density, respectively [14].

\* Corresponding author.

E-mail address: [hsezer@georgiasouthern.edu](mailto:hsezer@georgiasouthern.edu) (H. Sezer).

<https://doi.org/10.1016/j.ijhydene.2024.05.311>

Received 6 November 2023; Received in revised form 15 May 2024; Accepted 20 May 2024

Available online 24 May 2024

0360-3199/© 2024 Hydrogen Energy Publications LLC. Published by Elsevier Ltd. All rights are reserved, including those for text and data mining, AI training, and similar technologies.

Nomenclature		GREEK SYMBOLS	
A	parameter in P–C–T equation	$\beta$	hysteresis factor in P–C–T equation
B	parameter in P–C–T equation [K]	$\varepsilon$	porosity
$C_p$	specific heat capacity [J/(kg K)]	$\lambda$	thermal conductivity [W/m K]
E	activation energy [J/mol]	$\mu$	dynamic viscosity [Pa.s]
h	convective heat transfer coefficient [W/(m <sup>2</sup> K)]	$\rho$	density [kg/m <sup>3</sup> ]
$\Delta H$	reaction enthalpy [J/mol H <sub>2</sub> ]	$\varphi$	plateau flatness factor in P–C–T equation
[H/M]	hydrogen to metal mass ratio	$\varphi_0$	plateau flatness factor in P–C–T equation
k	reaction rate constant [s <sup>−1</sup> ]	SUBSCRIPTS	
K	permeability [m <sup>2</sup> ]	a	absorption
$\dot{m}$	mass source term of reaction [kg/(m <sup>3</sup> s)]	b	bulk
P	pressure [Pa]	d	desorption
P–C–T	pressure-composition-temperature	e, eq	equilibrium
q	mass flow rate [kg/s]	eff	effective
r	r-coordinate [m]	ex	exerted
$R_g$	general gas constant [J/(mol K)]	f	cooling fluid
t	time [s]	g	gaseous phase (hydrogen)
T	temperature [K]	in	inlet
U	gas velocity [m/s]	L	low
W	mass [kg]	MH	metal hydride
X	reacted fraction of adsorbed hydrogen	o	outer
z	z-coordinate [m]	sat	saturated

**Table 1**  
Hydrogen storage density comparison [8,20,24,25].

Hydrogen storage forms and conditions	Volumetric hydrogen density (kg H <sub>2</sub> /m <sup>3</sup> system)	Theoretical limit (kg H <sub>2</sub> /m <sup>3</sup> system)
Compressed hydrogen at 25 °C and 50 MPa	27	30.81
Liquefied hydrogen at −253 °C and 0.1 MPa	40	71
Metal hydride at 25 °C and 0.1 MPa	50	110

\*"Theoretical limit" is the storage density of the pure material under ideal conditions, and the "Volumetric hydrogen density" includes the reduction due to storage vessel and other practical limitations. The theoretical limit for compressed hydrogen is calculated by using online available tools like Stargate Hydrogen [25] and CMB Hydrogen Tools [24] since hydrogen does not behave as an ideal gas under 50 MPa.

Compared to gaseous and liquefied hydrogen storage approaches, utilizing solid-state metal hydrides (MH) as hydrogen storage materials offers competitive advantages, including high volumetric density, enhanced storage capacity, and reduced safety risks associated with high pressure [15–17]. MH-based hydrogen storage technology is currently developing in both research and industry. This is being driven primarily due to its relative safety and the absence of extremely high-pressure or low-temperature constraints needed for other forms of hydrogen storage. This approach involves hydrogen absorption as atoms onto the metal particles, but it comes with inherent weight due to the external MH storage medium, making it best suited for stationary and portable applications with no weight concern [16–18]. Other prominent benefits of this approach include its relatively high volumetric storage density, safety, and reversibility [19].

Hydrogen absorption in metals is an exothermic process. The heat produced during the absorption process elevates the temperature of the metal hydride (MH) bed, which, in turn, influences the equilibrium pressure of the reaction. As temperature rises, the equilibrium pressure increases, potentially slowing down the absorption reaction. Therefore, to speed up the reaction and reduce the charging time, the generated heat should be dissipated to maintain the temperature at a suitable level

[4,20]. The absorption of hydrogen requires substantial heat uptake; however, the poor thermal conductivity of metal hydride bed slows down the heat conduction inside the bed and extends charging duration. Therefore, when designing such systems, different thermal management measures including the use of fins, cooling fluid, or phase change materials (PCM) are considered [20,21]. Moreover, to operate the MH-based hydrogen storage systems at room temperature, the design optimization of the MH reactor tanks is a crucial challenge. This needs the consideration of many important physical parameters like the overall porosity of the hydride bed, the packing density, effective thermal conductivity, the material of the cylinder, and the compactness of bed [1,22,23].

Numerous computational models are developed in the literature to analyze one-dimensional [26–29], two-dimensional [20,30–42], and three-dimensional [43–47] metal hydride hydrogen storage systems. These models conventionally couple heat and mass balances alongside empirically derived reaction kinetic equations. The 3D models, while providing more promising results, are significantly more time consuming and require heavy computing resources for execution. Resultantly, they are mostly selectively utilized to investigate the effects that two-dimensional models are not able to capture [46].

Early studies by Jemni and Nasrallah [35] explored a two-dimensional metal hydride reactor model, examining key design and operational parameters during hydrogen absorption. Their work questioned the assumption of local thermal equilibrium between solid phase porous medium and hydrogen gas. However, Nasrallah and Jemni [36] later presented conflicting findings concerning this assumption and determined that disregarding the temperature difference between the two phases has a negligible impact on the mass evolution profile during both absorption and desorption processes. Subsequent modeling approaches often simplified their models by assuming local thermal equilibrium, aiming to reduce computational complexity. Additionally, many studies neglected pressure drop and advection heat transport due to the low hydrogen velocity in porous metal hydride vessels [36,42,48,49]. Some models also assumed that equilibrium pressure was solely a function of temperature, disregarding its dependency on the hydrogen-to-metal atomic ratio (H/M) [43,50–54]. Despite these efforts, there is a pressing need for a comprehensive investigation into factors such as considering the influence of Darcy's velocity due to

pressure gradients (Darcy's law), cooling strategy variations, reactor size impact on charging time, and a parametric analysis that is crucial for both enhancing fundamental understanding and optimizing the metal hydride hydrogen storage systems. While one or a few of these assumptions and phenomena are considered by previous studies, it is important to build a model framework which can handle all of these different possibilities.

As mentioned by Mohammadshahi [40], most MH models account for Darcy's velocity as a source term in the fluid transport equations. A simple form is applied in some studies, such as those by Jemni and Nasrallah [33,34], a simple form of Darcy's law was applied to solve for the gas phase transport of hydrogen. Others have opted to solve the conservation of momentum equations applying the Darcy velocity as part of the source term [30,32]. Regardless, it is often assumed that the heat transfer associated with hydrogen transport is negligible [40]. Chaise et al. [55] developed a set of criteria to use to evaluate the significance or negligibility of convective heat transfer and pressure variation, demonstrating that for a sample set of material and microstructural properties that both could be assumed to be negligible. On the other hand, results from Freni et al. [50] suggest that varying the permeability and thereby changing the pressure gradient induced by Darcy velocity can have a significant effect on the performance of MH reactors.

The objective of this work is to develop a numerical model using finite volume (FV) discretization with implicit Euler's time integration scheme [20,56–59] to optimize the absorption process in MH reactors. The resulting linear system of equations is solved using a sparse matrix solver available in MATLAB [20,58,60–63]. This paper focuses on the mathematical modeling of heat and mass transport mechanisms during the absorption of hydrogen in MH-based hydrogen storage systems.

The results obtained from the 2D axis-symmetrical model are found to be in good agreement with experimental data reported in the literature. Then the model is used to examine the effect of various critical parameters, including charging pressure, cooling fluid temperature, reactor geometry and size, and different boundary conditions on the thermal performance and reaction kinetics of the system. The influence of H/M atomic ratio on equilibrium pressure is also examined and validated with experimental data for varying temperatures. This framework allows us to systematically evaluate the sensitivity of these parameters by analyzing temperature and reaction fraction profiles aimed at optimizing the storage efficiency. Furthermore, we conducted a comparative analysis between two models: one incorporating Darcy's velocity and the other without, while maintaining constant pressure within the metal hydride bed. Interestingly, incorporating Darcy's law

introduces increased system complexity and numerical instability in the coupled equations, but it has minimal effect on the overall model outcomes. This study advances our comprehension of solid-state hydrogen storage and contributes to the development of efficient and dependable hydrogen storage technologies. Ultimately, this work plays a crucial role in advancing hydrogen as a green and sustainable future energy carrier.

## 2. Mathematical model

### 2.1. System description

In the present work, two distinct MH reactors are examined, each characterized by unique cooling fluid configurations and sizes. Experimental data for both reactors are available in the literature [36,48,64], allowing for the validation of our model for each reactor configuration and comparison with other models. In this context, the MH tank shown in Fig. 1a is referred to as 'Reactor 1,' while the MH tank depicted in Fig. 1b is denoted as 'Reactor 2'. The dimensions of both reactors and corresponding computational domains are shown in Fig. 2a and b respectively. Reactor 1 transfers heat only through its lateral side to the cooling fluid, whereas reactor 2 accomplishes this through both its lateral and base areas. Water is considered as the cooling fluid in this paper.

In the cross-sectional view of the system, as depicted in Fig. 1, the blue region at the base and lateral sides denotes the pathway for water flowing at a steady speed. The light blue color region represents the metal hydride (MH) powder bed, where the hydrogen absorption process occurs. During absorption, the hydrogen reacts and gets stored in the interstitial sites of the crystal structure. The third section is designated for pressurizing hydrogen gas before absorption as shown in figure. A thin stainless-steel [64] or brass [35] wall serves as a barrier, separating the heat transfer fluid from the MH bed. In this study, we utilize  $\text{LaNi}_5$  as the metal for hydrogen capture, which undergoes a transformation to  $\text{LaNi}_5\text{H}_6$  when it is fully saturated with hydrogen. The maximum mass of hydrogen that can be stored in reactor 1 and reactor 2 are, respectively, 0.2171 and 10.5975 g.

### 2.2. Formulation of mathematical model

The reactor is a discontinuous medium consisting of a solid porous phase (metal-hydride) and a gaseous phase (hydrogen). The mass and energy conservation equations that govern the heat and mass transport in reactive porous media are typically derived by transitioning from a microscopic to a macroscopic scale. We shift from a microscopic view-

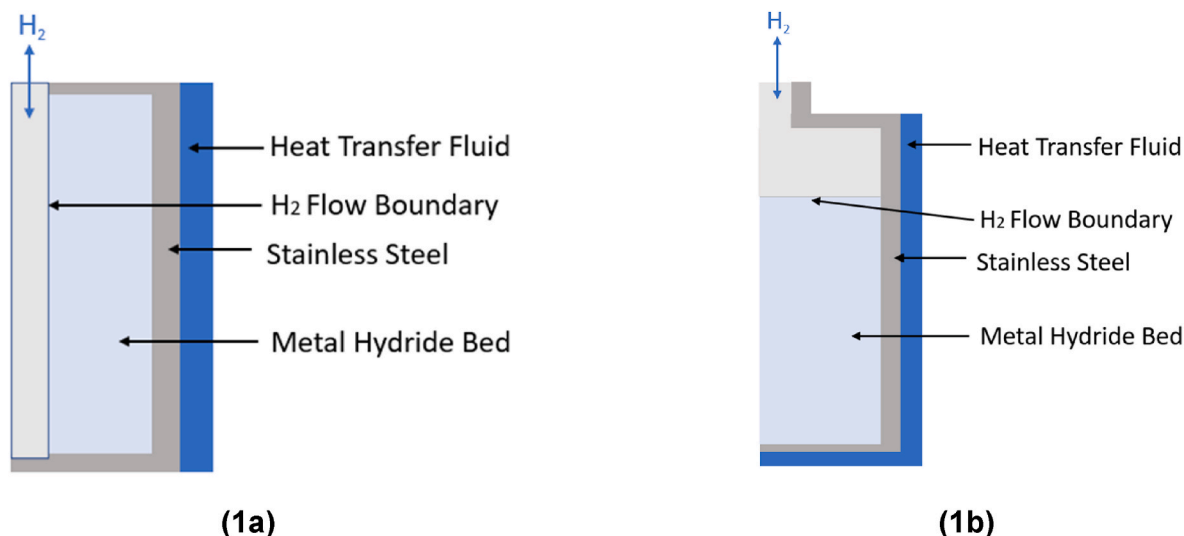


Fig. 1. Cross sectional schematic for (1a) MH reactor 1 [20], [35] (1b) MH reactor 2 [65].

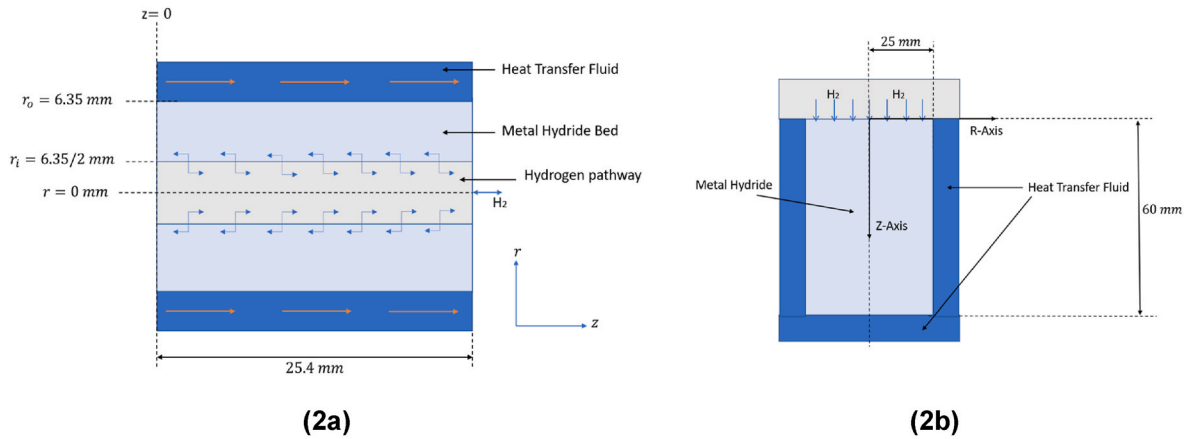


Fig. 2. 2D axis-symmetrical computational domain (2a) For reactor 1 (2b) For reactor 2

point, where the average volume ( $\omega$ ) is considerably smaller than the pores, to a macroscopic standpoint where the averaging volume is significantly larger in comparison to the pores. This change in scale enables us to consider the actual discontinuous medium into an equivalent hypothetical continuous medium [49,66]. Each macroscopic term is obtained through the process of averaging its respective microscopic counterpart. The average of a specific microscopic function ( $\bar{\varphi}$ ) is given by Eq. (1a). Similarly, the intrinsic average over a phase  $i$  is given by Eq. (1b).

$$\bar{\varphi} = \frac{1}{\omega} \int_{\omega} \varphi \, d\omega \quad (1a)$$

$$\bar{\varphi}_i = \frac{1}{\omega_i} \int_{\omega_i} \varphi_i \, d\omega \quad (1b)$$

where  $\omega_i$  is the volume occupied by phase  $i$  within the total averaging volume  $\omega$ .

The macroscopic differential equations are derived through the process of averaging microscopic equations across the averaging volume  $\omega$ , while incorporating closure assumptions. The microscopic equations encompass mass, energy, and momentum balance equations within each phase and at phase interfaces. These equations are established by applying the principles of thermodynamics and the mechanics of continuous media.

The mathematical formulation for modeling the multi physics absorption phenomenon in an MH reactor can be established based on the following simplifying assumptions.

- The gaseous phase within the metal hydride (MH) bed exhibits ideal gas characteristics, thus permitting the utilization of the ideal gas equation to relate the pressure and density.
- The medium is treated as continuous with both phases at the same temperature (local thermal equilibrium).
- The viscous dissipation and compression work are considered negligible.
- The radiation heat transfer mechanism is neglected because the system is operated in moderate temperature range.

Incorporating these assumptions, the macroscopic computational model for heat and mass transfer within a metal-hydrogen bed integrates the principles of mass conservation, energy conservation, and the application of Darcy's law within the reactive porous medium. These coupled principles are jointly employed to formulate the definitive modeling equations for metal hydride (MH)-based hydrogen storage systems [20,48,64,65]. The conservation of mass for the gas phase and solid phase are given by Eqs. (2a) and (2b) respectively [20,41,64].

$$\frac{\partial \epsilon_{MH} \rho_g}{\partial t} + \nabla \cdot (\rho_g \vec{U}) = -\dot{m} \quad (2a)$$

$$\frac{\partial (1 - \epsilon_{MH}) \rho_s}{\partial t} = \dot{m} \quad (2b)$$

In Eq. (2a),  $\epsilon_{MH}$  and  $\rho_g$  represents the porosity of the bed and density of the gaseous phase respectively, while  $\vec{U}$  is the Darcy's velocity of hydrogen inside MH bed that is shown by Eq. (4). The density of the gaseous phase  $\rho_g$  is described by ideal gas equation shown by Eq. (3b). On the right side  $\dot{m}$  is the source term, defining the consumption rate of hydrogen gas per unit volume during absorption, given by Eq. (3a) [41].

$$\dot{m} = k_a \cdot e^{\left(-\frac{E_a}{R T_b}\right)} \cdot \ln\left(\frac{P_g}{P_{eq}}\right) \cdot (\rho_{sat} - \rho_s) \quad (3a)$$

$$\rho_g = \frac{M_g P_g}{R T_b} \quad (3b)$$

$$\vec{U} = -\frac{K}{\mu} \nabla P_g \quad (4)$$

In Eq. (3a),  $\rho_{sat}$  and  $\rho_s$  represent the saturation density of the bed, and the instantaneous metal hydride density respectively. The absorption rate constant is denoted as  $k_a$ , while  $E_a$  represents the activation energy for the absorption reaction.

In Darcy's law Eq. (4) the quantities  $K$ , and  $\mu$  represent the permeability of the MH bed and dynamic viscosity of the gaseous phase respectively, while  $\nabla P_g$  shows the pressure gradient in the domain.

The equilibrium pressure for hydrogen absorption, denoted as  $P_{eq}$  in Eq. (3a), explicitly considers the effects of hysteresis and plateau slope [67] and exhibits a strong dependency on both the bed temperature and the H/M atomic ratio. The correlation between equilibrium pressure, bed temperature, and H/M ratio is described using by Eq. (5) [20,64,67].

$$P_{eq} = \exp\left(A - \frac{B}{T_b} + (\varphi + \varphi_0) \cdot \tan\left(\pi\left(X - \frac{1}{2}\right)\right) + \frac{\beta}{2}\right) \quad (5)$$

In Eq. (5), the variable  $X$  represents the reacted fraction of adsorbed hydrogen, providing a quantification of the H/M atomic ratio on a scale of 0–1. Following linear interpolation, considering a saturation density corresponding to a reacted fraction value of 1, and initializing the reacted fraction as 0 at the beginning of the absorption process when  $\rho_s = \rho_{emp}$ , the equation describing the reacted fraction  $X$  is presented in Eq. (6).

$$X = \frac{\rho_s - \rho_{\text{emp}}}{\rho_{\text{sat}} - \rho_{\text{emp}}} \quad (6)$$

The energy conservation equation for the MH reactors, assuming local thermal equilibrium, can be expressed in two ways. Eq. (7a) accounts for the impact of Darcy's velocity due to pressure gradients [20, 41,42,64], while Eq. (7b) neglects pressure gradients and incorporates an additional source term in the equation [48,68].

$$\frac{\partial(\rho_b C_{p,b})_{\text{eff}} T_b}{\partial t} + \nabla \cdot (\rho_g C_{p,g} \vec{U} T_b) = \nabla(\lambda_{\text{eff}} \nabla T_b) + \dot{m} \cdot \Delta H \quad (7a)$$

$$\frac{\partial(\rho_b C_{p,b})_{\text{eff}} T_b}{\partial t} = \nabla(\lambda_{\text{eff}} \nabla T_b) + \dot{m} \cdot \Delta H + \dot{m} \cdot T_b (C_{p,g} - C_{p,s}) \quad (7b)$$

The coefficients of the transient term, representing the effective heat capacity, and that of the diffusion term  $\lambda_{\text{eff}}$ , representing the effective thermal conductivity, are given by Eq. (8) and Eq. (9) respectively.

$$(\rho_b C_{p,b})_{\text{eff}} = \varepsilon_{\text{MH}} \rho_g C_{p,g} + (1 - \varepsilon_{\text{MH}}) \rho_s C_{p,s} \quad (8)$$

$$\lambda_{\text{eff}} = [\varepsilon_{\text{MH}} \lambda_g + (1 - \varepsilon_{\text{MH}}) \lambda_{\text{MH}}] \quad (9)$$

The coefficient of the transient term in the energy equation, representing the bulk heat capacity of the bed, is determined by the product of the MH bed density and specific heat. This value accounts for the sum of all constituent phases present in the system [64].

$$\rho_b C_{p,b} = \sum_{i=1} \varepsilon_i \rho_i C_{p,i} \quad (10)$$

The physical parameters like porosity, permeability, initial densities, and other pertinent values, considered in this work, are shown in Table 2. The constant reaction kinetic parameters are shown in Table 3.

### 2.3. Computational domain

The system can be modeled as an axis symmetrical two-dimensional domain in cylindrical coordinates. The dimensions of the MH tank cross section are shown in Fig. 2a and b for reactor 1 and reactor 2 respectively. These dimensions are considered for initial analysis and can be customized to optimize the performance of the system. It is assumed that the heat exchange between MH bed and heat transfer fluid takes place instantly and hence the tank material (stainless steel/brass) is not considered in the simplified model.

#### Reactor 1:

Axial coordinates:  $z = 0$ –25.4 mm.

Radial coordinates:  $r = r_i = 6.35/2$  mm to  $r_o = 6.35$  mm.

#### Reactor 2:

Axial coordinates:  $z = 0$ –60 mm.

Radial coordinates:  $r = r_i = 0$  to  $r_o = 25$  mm.

**Table 2**  
Thermo-physical properties and operating conditions [20,41,48,64].

Parameters	Value	Unit
Initial temperature, $T_0$	293	[K]
Cooling fluid temperature, $T_f$	293	[K]
Exerted hydrogen pressure, $P_{\text{ex}}$	6 and 8	[bars]
Specific heat of hydrogen, $C_{p,g}$	14890	[J/(kg.K)]
Specific heat of the metal, $C_{p,s}$	419	[J/(kg.K)]
Thermal conductivity of hydrogen, $k_g$	0.167	[W/(m.K)]
Thermal conductivity of the metal, $k_s$	3.18	[W/(m.K)]
Porosity of the metal, $\varepsilon_{\text{MH}}$	0.5	–
Permeability of the metal, $K$	$1.11 \times 10^{-11}$	[m <sup>2</sup> ]
Convective heat transfer coefficient, $h$	1500	[W/(m <sup>2</sup> .K)]
Dynamic viscosity of hydrogen, $\mu$	$8.9 \times 10^{-6}$	[Pa.s]
Molar mass of hydrogen, $M_g$	$2.0158 \times 10^{-3}$	[kg/mol]

**Table 3**

Reactions kinetics and P–C–T parameters in Eq. (8) and Eq. (9) [41,48,64].

Parameters	Values	Unit	Reference
Rate constant, $k_a$	59.187	[s <sup>-1</sup> ]	[48,64]
Activation energy, $E_a$	21179	[J/mol H <sub>2</sub> ]	[48,64]
P–C–T parameter, A	13.1	–	[48,64]
P–C–T parameter, B	3700	[K]	[64]
Plateau flatness factor, $\varphi$	0.038	–	[64]
Plateau flatness factor, $\varphi_0$	0	–	[64]
Hysteresis factor, $\beta$	0.137	–	[48,64]
Reaction enthalpy, $\Delta H$	30800	[J/mol]	[48,64]
Saturation density, $\rho_{\text{sat}}$	6520	[kg/m <sup>3</sup> ]	[48]
	6.52	[g/cm <sup>3</sup> ]	
Hydrogen-free metal density, $\rho_{\text{emp}}$	6430	[kg/m <sup>3</sup> ]	[48]
	6.43	[g/cm <sup>3</sup> ]	

### 2.4. Initial and boundary conditions

It is assumed that the MH bed is in thermodynamic equilibrium with hydrogen gas. This implies that the initial temperature of the hydride bed and hydrogen gas is the same.

$$T(r, z, t = 0) = T_0 = 293 \text{ K} \quad (11)$$

The insulated tank walls, in the case of reactor 1, are subject to homogeneous Neumann's boundary conditions due to zero slip velocity and no-flux. Likewise, because of the symmetry, the same boundary conditions are applied at the axis of reactor 2.

$$\nabla T_b = 0, \nabla P_g = 0 \quad (12)$$

The boundary conditions for the interfaces where the bed exchanges heat with the cooling fluid (heat transfer walls) are given by Eqs. (13) and (14), where  $T_f$  is the temperature of the fluid.

$$-\lambda_{\text{eff}} \nabla T_b = h(T_b - T_f) \quad (13)$$

$$\nabla P_g = 0 \quad (14)$$

At the mass transfer interface where hydrogen is adsorbed into the bed (mass exchange boundary), a Danckwerts' boundary condition [69] is considered as shown by Eq. (15a) to ensure the continuous flow rate of hydrogen across the wall for the model in the model that considers pressure gradients. In Eq. (15a),  $T_{\text{in}}$  represents the temperature of the wall in contact with the fluid and is obtained from the energy conservation equation. However, for the simplified model with  $\nabla P = 0$ , this boundary is treated under no flux condition given by Eq. (15b).

$$-\lambda_{\text{eff}} \nabla T_b = \rho_{g,\text{in}} \vec{U} C_{p,g} (T_{\text{in}} - T_b) \quad (15a)$$

$$\nabla T_b = 0 \quad (15b)$$

For the model considering Darcy's velocity, the gas pressure at the mass transfer boundary is assumed to be equal to the tank's internal pressure. The mass conservation equation for the gaseous phase, along with the ideal gas law, is utilized to determine the density and pressure within the bed. Conversely, for the model neglecting pressure gradients, a uniform pressure is assumed throughout the entire domain.

$$P_g|_{\text{@ mass transfer interface}} = P_{\text{ex}} \left( \begin{array}{c} \text{For} \\ \text{model considering } \vec{U} \end{array} \right) \quad (16a)$$

$$P_g = P_{\text{ex}} \left( \begin{array}{c} \text{For} \\ \text{model neglecting } \vec{U} \end{array} \right) \quad (16b)$$

### 2.5. Numerical approach: finite volume method

The finite volume method is a discretization approach used to solve complex differential equations by integrating the equations of mass, energy, and momentum conservation [20,60]. This technique divides



the domain into a finite number of adjacent control volumes, referred to as cells. Within each cell, the values of the variable parameters relevant to the differential equations are calculated at the cell's centroid. Surface values within the control volume are determined using mathematical interpolation methods, such as arithmetic or harmonic means, to accurately represent the distribution of variables. Fig. 3 illustrates a typical control volume for a two-dimensional model, with each cell having four faces labeled as East (E), West (W), North (N), and South (S) [20,57].

The finite volume method (FVM) utilizes control volumes rather than grid intersection points for discretization, which makes it highly adaptable and suitable for various grid types. In this study, we employ an open-source finite volume toolbox called Simulkade [20,56,57,59,60,63] to solve the partial differential equations (PDEs) resulting from the coupling of conservation equations and Darcy's law. To ensure the reliability of our numerical simulations, a mesh and time step independence study was conducted. The results of this study confirmed convergence, indicating that the chosen mesh resolution adequately captured the physics of the system. Specifically, simulations were performed using a mesh consisting of 15 cells in the axial direction and 10 cells in the radial direction with a time step of 0.5 s.

This toolbox allows for flexible and customized simulations to accurately model the system. FVM inherently satisfies the conservation equations for mass, heat, and momentum transfers across the cell boundaries therefore, along with more customization, this approach will be fast and will yield more accurate results [20,57–63].

### 3. Results and discussion

#### 3.1. Validation of the numerical model

##### 3.1.1. Equilibrium pressure as a function of temperature and H/M

To validate our hydrogen absorption model against experimental data, initial numerical simulations were performed. Fig. 4 provides a comprehensive comparison of experimental and theoretical equilibrium pressure profiles at various temperatures, for  $\text{LaNi}_5$  alloy as the hydrogen absorption material. The equilibrium pressure ( $P_{eq}$ ) is plotted against temperature and the hydrogen-to-metal atomic ratio (H/M) since it is not a function of the reactor size or computational domain. The H/M atomic ratio is derived by multiplying the reacted fraction 'X' in the model by 6, as it takes 6 hydrogen atoms to fully saturate  $\text{LaNi}_5$  and transform it into  $\text{LaNi}_5\text{H}_6$ . The model's predictions exhibit strong agreement with the experimental equilibrium pressure data [70], confirming its accuracy.

##### 3.1.2. Effect of pressure gradients on the reacted fraction profile

Fig. 5a presents the reacted fraction profile for reactor 1, where both models, one incorporating Darcy's law and the other without, closely match experimental data from Yang et al. [64]. The model neglecting Darcy's velocity assumes uniform pressure, implying instantaneous and uniform hydrogen availability at a constant pressure across the entire domain. Although it slightly overestimates the charging rate compared to experimental data, the overall agreement remains acceptable. In contrast, including pressure gradients improves results but introduces

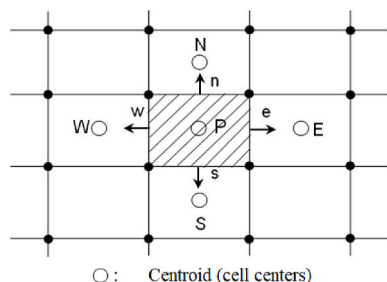


Fig. 3. Control volume for two-dimensional model [20].

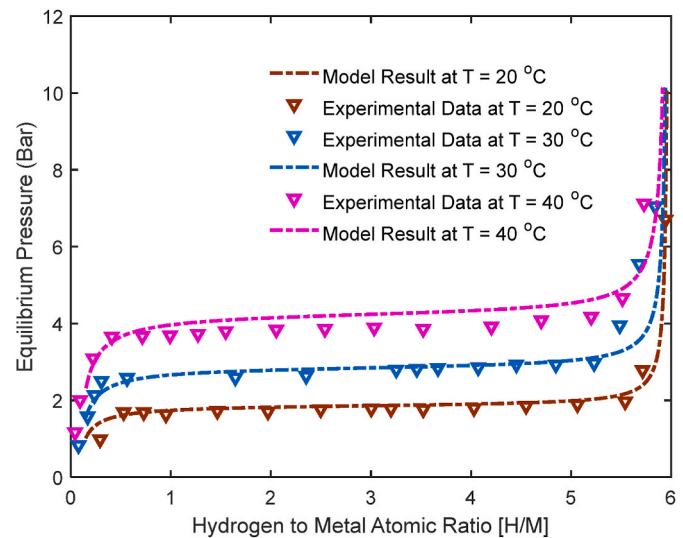


Fig. 4. Equilibrium pressure as a function of the H/M atomic ratio and temperature for hydrogen absorption (experimental data source: Dhaoui et al. [70])

significant numerical instability and stiffness. Given that the simplified model without pressure gradients aligns well with experimental data and requires less computational time, it is selected for further analysis.

During the initial absorption stages (first 50 s), both models produce similar results because pressurized hydrogen is readily available throughout the system. However, as the process continues, the model results diverge due to increasing pressure gradients, resulting from a concentration of hydrogen exceeding the advection supply. Near the end of the absorption process, the profiles reunite as the reaction rate slows down, and advection-driven hydrogen supply becomes sufficient to overcome the pressure gradients.

Different studies have reported varying values for PCT parameters A and B, with A ranging from 10.7 [41] to 14.045 [48,64], and B ranging from 3704.6 [41,48] to 3780 [64]. To validate the results of the developed simplified model without considering pressure gradients against the model considering them,  $A = 13.1$  and  $B = 3719.59$  were used based on the model developed by Nam et al. [41]. Fig. 5b illustrates a good agreement in the mean reacted fraction profiles for reactor 2 between both models.

##### 3.1.3. Temperature profile validation

Fig. 6a provides a comparison of temperature evolution profile for reactor 2, as predicted by the developed numerical model, and measurements conducted by Jemni and Nasrallah [35,68] inside the MH bed at  $r = 1.5$  cm and  $z = 4.5$  cm. Our numerical model demonstrates a strong agreement with experimental data, affirming the model's accuracy. Both simulations and experiments exhibit an initial rapid temperature increase, reflecting fast hydrogen absorption kinetics during the initial stage, followed by a gradual decline in temperature due to cooling fluid influence and diminishing absorption rates caused by an increase in equilibrium pressure.

In Fig. 6b, temperature profiles are compared at the point indicated in Fig. 6a (with PCT parameters  $A = 13.1$  and  $B = 3719.59$ ) between Nam et al.'s model [41], which accounts for Darcy velocity due to pressure gradients, and the developed model with a constant input pressure throughout the domain. The comparison reveals that the inclusion of Darcy effects has a negligible impact on the temperature variation at the selected point within the domain.

### 3.2. Shape and size considerations for the reactor

#### 3.2.1. Square VS rectangular cross-section for reactor 2

Fig. 7a presents a comparison of mean reacted fraction transients for

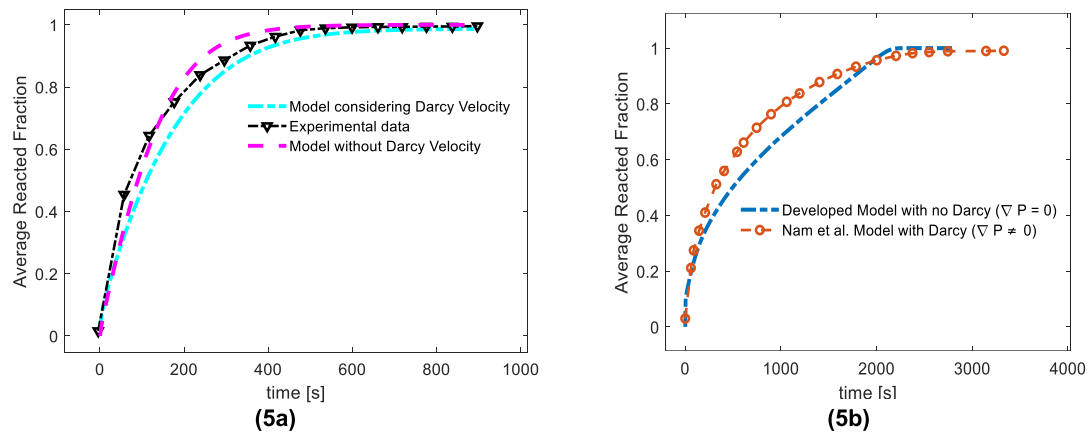


Fig. 5. Validation of reacted fraction profiles (5a) For reactor 1 with experimental data [64], (5b) Comparison between simplified model (no pressure gradients) and Nam et al. model (considering darcy's law) for reactor 2 [41].

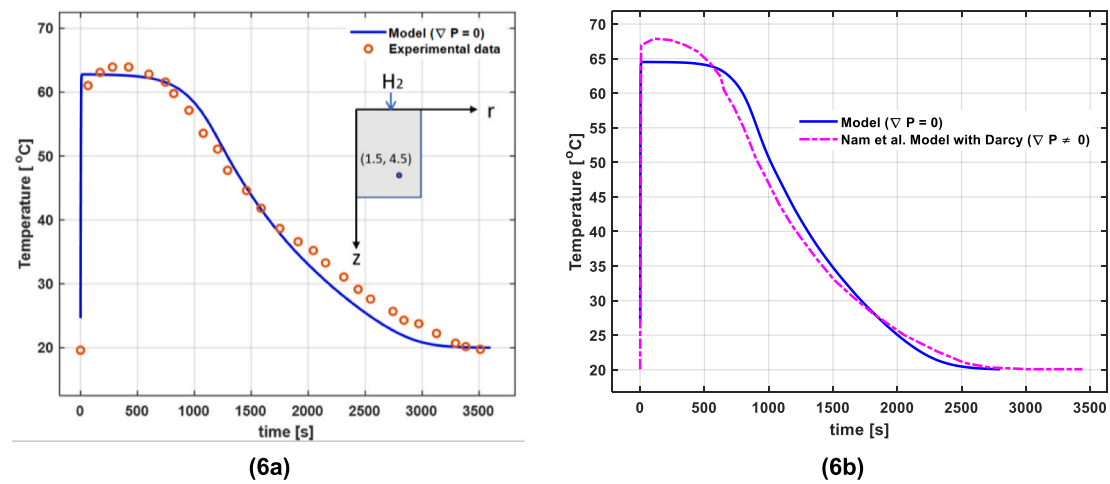


Fig. 6. Validation of the temperature profile at (1.5 cm, 4.5 cm) for reactor 2 with (6a) Experimental data [48,68], (6b) Comparison with Nam et al. model [41].

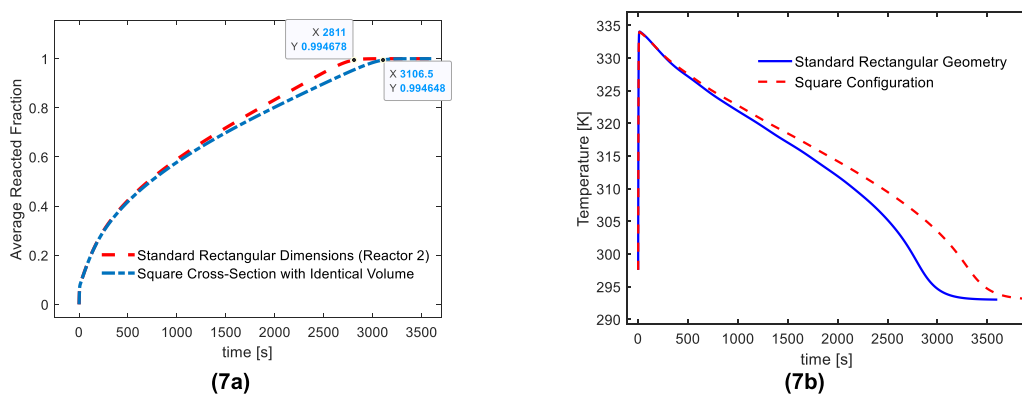


Fig. 7. Comparison of (7a) Reacted fraction and (7b) Temperature evolution profiles

two cross sections with equal volumes. The standard reactor, as considered in previous studies [48,68], has dimensions of 50 mm (diameter) and 60 mm (length), resulting in a volume of 117.8 cm<sup>3</sup>. Given the saturation density of  $\rho_{\text{sat}} = 6.52 \text{ g/cm}^3$  and the empirical density of  $\rho_{\text{emp}} = 6.43 \text{ g/cm}^3$ , this is equivalent to a capacity of 10.6 g. To illustrate the impact of altering the cylindrical reactor's dimensions

while maintaining the same volume, we consider another square cross-section with a diameter and length of 53.133 mm, derived from the relation shown above.

The figure shows that changing the cross-section from rectangular to square increases the charging time from 2811 s to 3106.5 s. Charging time, in this case, is defined as the time when absorption reaches

approximately 99.46% of total capacity. This change indicates that larger axial dimensions result in shorter charging times, as the cooling fluid surrounds both lateral sides, increasing heat exchange with the bed. Similarly, Fig. 7b shows the comparison of mean temperature profiles. As anticipated from Fig. 7a, the square reactor takes longer to reach the fluid temperature due to the lower surface area exposed to the low-temperature fluid.

### 3.2.2. Reactor size impact on charging and temperature profiles

Fig. 8a illustrates reacted fraction profiles for different reactor sizes, demonstrating that increased reactor dimensions lead to longer charging times. Fig. 9a and b depict the relationships between reactor dimensions and their respective charging durations. For the analyzed square cross-sections, length and charging time exhibit a second-order polynomial correlation, implying a linear relationship between area and charging time. In Fig. 8b, the impact of reactor size on mean bed temperature is depicted. Larger reactors exhibit minimal differences in maximum temperature at the start of absorption. However, they take a longer duration to reach the cooling fluid's temperature as the cooling effect propagation through the entire domain is more time-consuming than in smaller reactors. The reactor sizes considered in Fig. 8a and b have hydrogen mass capacities of about 1.11 g, 4.52 g, 8.84 g, 15.2 g, and 24.25 g respectively.

### 3.3. Pressure, cooling fluid temperature and boundary conditions analysis

The hydrogen feed pressure and cooling fluid temperature are critical parameters for optimizing the storage system's performance. Fig. 10 compares reacted fraction profiles for charging pressures of 6, 8, and 10 bars. Higher hydrogen charging pressures result in shorter charging durations. Specifically, increasing the hydrogen supply pressure from 6 to 8 bars reduces the charging time by approximately 12.4 min, while further elevating it to 10 bars results in an additional 7-min reduction in charging time. These findings underscore the importance of considering the required charging time when adjusting the hydrogen feed pressure in the reservoir.

Similarly, examining the temperature profiles presented in Fig. 11a and b, it becomes evident that pressure not only influences charging time and reaction kinetics but also significantly elevates the maximum temperature within the bed. Additionally, higher charging pressure leads to a more rapid convergence of bed temperature to the cooling fluid temperature. Two primary factors contribute to this behavior. Firstly, the accelerated reaction rates at higher pressures drive the system towards saturation more quickly, reducing heat generation near saturation. Secondly, the initially high reaction rates result in elevated bed temperatures, promoting increased heat exchange with the cooling fluid due to greater convection flux driven by the higher temperature

gradient.

Fig. 12a demonstrates the comparison of reacted fraction profiles at different cooling fluid temperatures: 20 °C, 30 °C, and 40 °C. Clearly, the temperature of the cooling fluid substantially influences reaction kinetics, consequently affecting the system's charging time. Increasing the cooling fluid temperature from 20 °C to 30 °C results in an additional 14 min of charging time, while further increasing it to 40 °C extends the charging time by an additional 26 min. Lowering the cooling fluid temperature reduces the charging time, although this effect becomes less pronounced as temperatures decrease.

Fig. 12b presents the reacted fraction profiles corresponding to three distinct boundary conditions. In the first case, a non-homogeneous flux boundary condition is considered with the cooling fluid at 293 K. The constant temperature cooling fluid (water) is considered to be moving with a steady velocity alongside the bed. Due to the varying temperature at the interface, a non-homogeneous heat flux occurs from the bed to the fluid. In the second case, a Dirichlet boundary condition with a temperature of 293 K is introduced, symbolizing the replacement of cooling fluid with a phase change material (having 293 K as its phase change temperature). This assumption is only valid when the absorbed heat by the material is less than the latent heat. Finally, the third boundary condition assumes a Dirichlet boundary condition at 273 K, signifying the utilization of water/ice as the phase change material (PCM). Transitioning from the first to the second boundary condition reduces the charging time from 2792 s to 2643.5 s, and further transitioning to the third boundary condition reduces it to 1849.5 s. This analysis emphasizes the significant influence of boundary conditions, especially the incorporation of phase change materials, on the system's charging duration.

## 4. Conclusion

A comprehensive computational model is developed to analyze the heat and mass transfer phenomena within MH based hydrogen storage systems. The model incorporates a range of multi physics interactions, including hydrogen absorption kinetics, thermal management, and fluid flow. Through a rigorous examination of various factors, we have gained valuable insights into the behavior of MH reactors. The investigation began by examining the equilibrium pressure as a function of temperature and the hydrogen-to-metal atomic ratio (H/M) followed by a comparative analysis of incorporating pressure gradients into the model. The results of the model agreed well with the experimental data available in the literature [64,68] and demonstrated that the model successfully captures key experimental trends observed in the data.

The incorporation of Darcy's velocity in the modeling framework, despite introducing numerical instability, had a negligible overall impact on the model outcomes. Despite this trade-off, the simplified

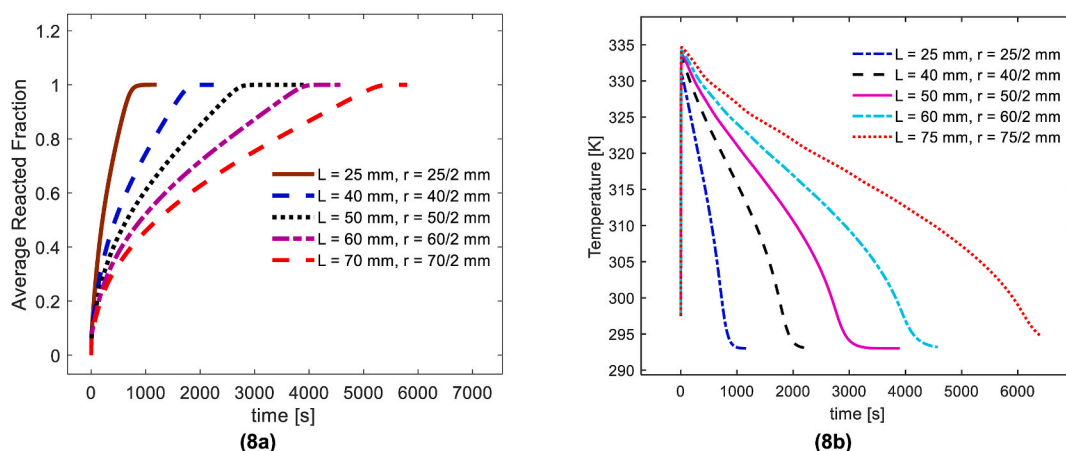


Fig. 8. The effect of reactor size on (8a) Mean reacted fraction profile and (8b) Temperature evolution profile



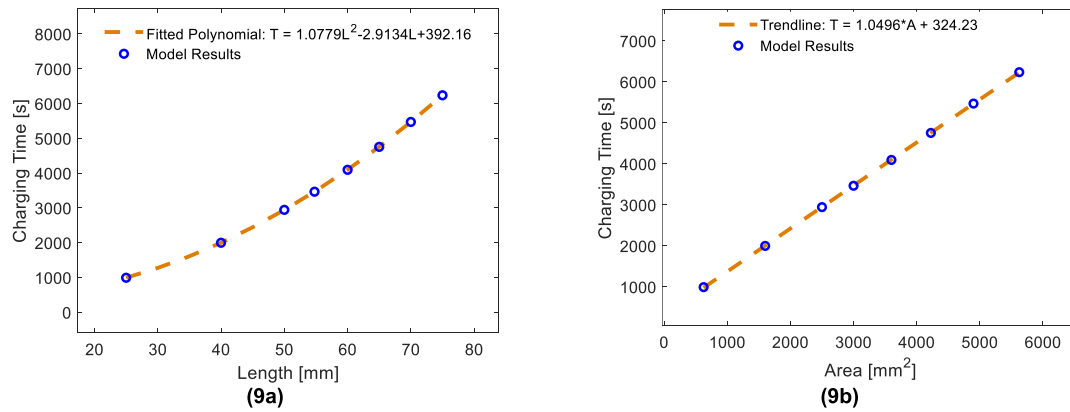


Fig. 9. Correlation of charging duration with (9a) Length of the reactor, (9b) Cross-sectional area of the reactor

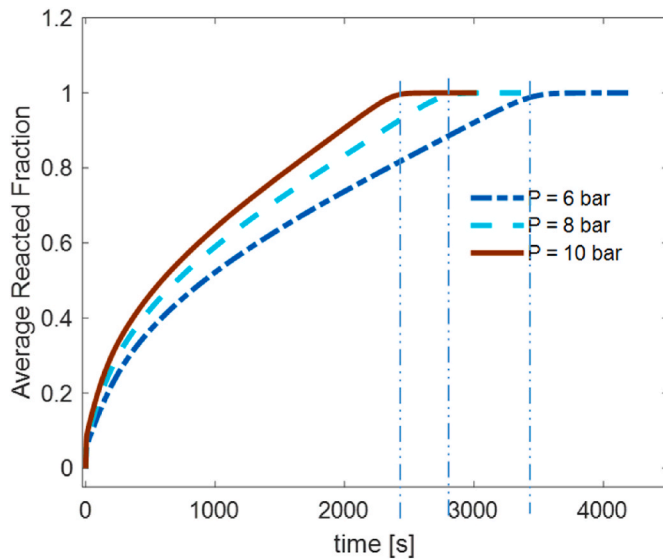


Fig. 10. Comparison of the mean reacted fraction profiles for different charging pressures

model without pressure gradients aligned well with experimental data, offering a balance between precision and computational efficiency. The detailed analysis of temperature profiles revealed an initial rapid increase in temperature followed by a gradual decline due to cooling fluid and equilibrium pressure effects. The influence of reactor size and shape on both reacted fraction profiles and temperature evolution was

explored. Notably, alterations in reactor geometry demonstrated significant effects on the charging time, with larger axial dimensions resulting in shorter charging durations. This phenomenon arises from the increased exposure of surface area to the cooling fluid, facilitating more efficient heat exchange. The results indicated that the relationships between charging duration with reactor length, and cross-sectional area, followed second and first-order polynomial correlations, respectively.

We also investigated the influence of other critical factors on the performance of the reactor. Adjusting the charging pressure effectively modulates charging duration, with higher pressures resulting in shorter times and elevated temperatures within the system. Lower cooling fluid temperatures were found to significantly reduce charging durations, emphasizing the importance of optimizing cooling strategies. The transition from a flux boundary condition to a Dirichlet boundary condition at the same temperature significantly reduced the charging duration, highlighting the importance of considering phase change materials to customize metal hydride hydrogen storage systems for specific applications.

This model serves as a valuable tool for optimizing MH-based hydrogen storage systems, offering both accuracy and computational efficiency. Future research may explore more complex reactor geometries and the interplay of these factors to advance our comprehension of MH systems and their broader applications. Additionally, expanding the model to 3D will allow for the incorporation of more complicated bed and flow field geometries. Parametric studies on microstructural properties using percolation theory present another promising avenue for further investigation. The model's applicability extends to the desorption phase and offers the potential to investigate the impact of incorporating Darcy's law in large-scale reactors.

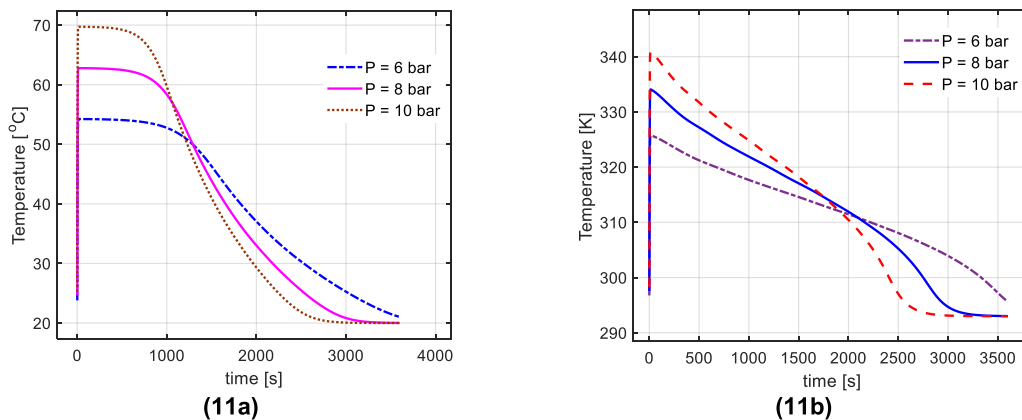


Fig. 11. Comparison of the temperature profiles for different charging pressures (11a) At (15, 45) mm, (11b) Mean temperature

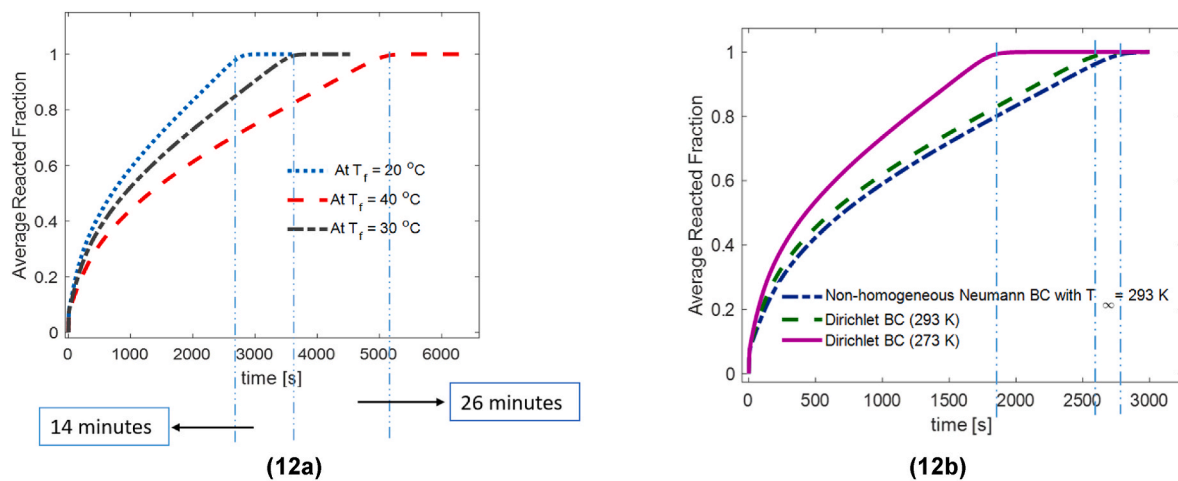


Fig. 12. Comparison of mean reacted fraction profiles for different (12a) Cooling fluid temperatures, (12b) Boundary conditions

### Declaration of ai-assisted technologies in the Writing process

During the preparation of this work, the authors used QuillBot and ChatGPT in order to enhance the language and readability of the manuscript. After utilizing these tools, the authors carefully reviewed and edited the content as necessary and take full responsibility for the content of the publication.

### CRediT authorship contribution statement

**Muhammad Hasnain:** Writing – original draft, Validation, Software, Methodology, Conceptualization. **Hayri Sezer:** Writing – review & editing, Supervision, Software, Methodology, Conceptualization. **Jerry Hunter Mason:** Writing – review & editing, Validation, Supervision, Conceptualization.

### Declaration of competing interest

The authors declare that they have no known competing financial interests or personal relationships that could have appeared to influence the work reported in this paper.

### Appendix A. Supplementary data

Supplementary data to this article can be found online at <https://doi.org/10.1016/j.ijhydene.2024.05.311>.

### References

- [1] Modi P, Aguey-Zinsou KF. Room temperature metal hydrides for stationary and heat storage applications: a review. *Front Energy Res Apr.* 2021;9:128. <https://doi.org/10.3389/FENRG.2021.616115/BIBTEX>.
- [2] Zhang Y, Campana PE, Lundblad A, Yan J. Comparative study of hydrogen storage and battery storage in grid connected photovoltaic system: storage sizing and rule-based operation. *Appl Energy Sep.* 2017;201:397–411. <https://doi.org/10.1016/J.APENERGY.2017.03.123>.
- [3] Jang D, Cho HS, Kang S. Numerical modeling and analysis of the effect of pressure on the performance of an alkaline water electrolysis system. *Appl Energy* 2021;287 (Apr). <https://doi.org/10.1016/j.apenergy.2021.116554>.
- [4] Nguyen HQ, Shabani B. Review of metal hydride hydrogen storage thermal management for use in the fuel cell systems. *Int J Hydrogen Energy Sep.* 2021;46 (62):31699–726. <https://doi.org/10.1016/j.ijhydene.2021.07.057>.
- [5] Kharel S, Shabani B. Hydrogen as a long-term large-scale energy storage solution to support renewables. *Energies* 2018;11(10). <https://doi.org/10.3390/en11102825>.
- [6] Jain IP, Jain P, Jain A. Novel hydrogen storage materials: a review of lightweight complex hydrides. *J Alloys Compd Aug.* 2010;503(2):303–39. <https://doi.org/10.1016/J.JALLCOM.2010.04.250>.
- [7] Shabani B, Andrews J, Badwal S. Fuel cell heat recovery, electrical load management, and the economics of solar-hydrogen systems. *Int J Power Energy Syst* 2010;30(4):256–63. <https://doi.org/10.2316/JOURNAL.203.2010.4.203-4842>.
- [8] Züttel A, Remhof A, Borgschulte A, Friedrichs O. Hydrogen: the future energy carrier. *Phil Trans Math Phys Eng Sci Jul.* 2010;368(1923):3329–42. <https://doi.org/10.1098/RSTA.2010.0113>.
- [9] Andrews J, Shabani B. Where does hydrogen fit in a sustainable energy economy? In: *Procedia engineering*. Elsevier Ltd; 2012. p. 15–25. <https://doi.org/10.1016/j.proeng.2012.10.107>.
- [10] Zhang J, Fisher TS, Ramachandran PV, Gore JP, Mudawar I. A review of heat transfer issues in hydrogen storage technologies. *Journal of Heat Transfer-transactions of The ASME Dec.* 2005;127(12):1391–9. <https://doi.org/10.1115/1.2098875>.
- [11] Azzaro-Pantel C. Hydrogen supply chain: design, deployment and operation. 2018 [Online]. Available: <https://books.google.com/books?hl=en&lr=&id=gyZqDwAAQBAJ&oi=fnd&pg=PP1&ots=69SI0wYlml&sig=h9lv8LL56xXg-ip8FTSGYYQOk>. [Accessed 10 October 2022].
- [12] Rowsell JLC, Yaghi OM. Strategies for hydrogen storage in metal-organic frameworks. *Angew Chem Int Ed Jul.* 2005;44(30):4670–9. <https://doi.org/10.1002/anie.200462786>.
- [13] von Helmolt R, Eberle U. Fuel cell vehicles: status 2007. *J Power Sources Mar.* 2007;165(2):833–43. <https://doi.org/10.1016/J.JPOWSOUR.2006.12.073>.
- [14] Abdalla AM, Hossain S, Nisfindy OB, Azad AT, Dawood M, Azad AK. Hydrogen production, storage, transportation and key challenges with applications: a review. *Energy Convers Manag Jun.* 2018;165:602–27. <https://doi.org/10.1016/J.ENCONMAN.2018.03.088>.
- [15] Niaz S, Manzoor T, Pandith AH. Hydrogen storage: materials, methods and perspectives. *Renewable Sustainable Energy Rev May* 2015;50:457–69. <https://doi.org/10.1016/J.RSER.2015.05.011>.
- [16] Bahhar S, Tahiri A, Jabar A, Louzazni M, Idiri M, Bioud H. Computational assessment of MgXH<sub>3</sub> (X = Al, Sc and Zr) hydrides materials for hydrogen storage applications. *Int J Hydrogen Energy Mar.* 2024;58:259–67. <https://doi.org/10.1016/J.IJHYDENE.2024.01.176>.
- [17] Bahhar S, Tahiri A, Jabar A, Louzazni M, Idiri M, Bioud H. DFT-based first-principles calculations of new NaXH<sub>3</sub> (X = Ti, Cu) hydride compounds for hydrogen storage applications. *Comput Mater Sci Apr.* 2024;238:112928. <https://doi.org/10.1016/J.COMMATSCI.2024.112928>.
- [18] Shabani B, Andrews J. Hydrogen and fuel cells, 201. *Green Energy and Technology*; 2015. p. 453–91. [https://doi.org/10.1007/978-81-322-2337-5\\_17/COVER](https://doi.org/10.1007/978-81-322-2337-5_17/COVER).
- [19] Lototsky MV, Tolj I, Pickering L, Sita C, Barbir F, Yartys V. The use of metal hydrides in fuel cell applications. *Prog Nat Sci: Mater Int Feb.* 01, 2017;27(1):3–20. <https://doi.org/10.1016/j.pnsc.2017.01.008>. Elsevier B.V.
- [20] Hasnain M, Khan S, Ezazi MA, Sezer H. Modeling heat and mass transfer in metal hydride-based hydrogen storage systems using the finite volume method. *ASME International Mechanical Engineering Congress and Exposition, Proceedings (IMECE)* 2024;10(Feb). <https://doi.org/10.1115/IMECE2023-112874>.
- [21] Afzal M, Mane R, Sharma P. Heat transfer techniques in metal hydride hydrogen storage: a review. *Int J Hydrogen Energy Dec.* 2017;42(52):30661–82. <https://doi.org/10.1016/J.IJHYDENE.2017.10.166>.
- [22] Singh A, Maiya MP, Murthy SS. Effects of heat exchanger design on the performance of a solid state hydrogen storage device. *Int J Hydrogen Energy Aug.* 2015;40(31):9733–46. <https://doi.org/10.1016/j.ijhydene.2015.06.015>.
- [23] Manai MS, et al. Comparative study of different storage bed designs of a solid-state hydrogen tank. 2019. <https://doi.org/10.1016/j.est.2019.101024>.
- [24] Hydrogen Tools | CMB.TECH." Accessed: May 10, 2024. [Online]. Available: <http://cmb.tech/hydrogen-tools>.
- [25] Hydrogen calculators - Stargate Hydrogen." Accessed: May 10, 2024. [Online]. Available: <https://stargatehydrogen.com/hydrogen-calculators/>.
- [26] El Oesry IA. Theory of the computer code RET 1 for the calculation of space-time dependent temperature and composition properties of metal hydride hydrogen storage beds. *Int J Hydrogen Energy Jan.* 1983;8(3):191–8. [https://doi.org/10.1016/0360-3199\(83\)90064-2](https://doi.org/10.1016/0360-3199(83)90064-2).

- [27] Lucas GG, Richards WL. Mathematical modelling of hydrogen storage systems. *Int J Hydrogen Energy* Jan. 1984;9(3):225–31. [https://doi.org/10.1016/0360-3199\(84\)90123-X](https://doi.org/10.1016/0360-3199(84)90123-X).
- [28] Ram Gopal M, Srinivasa Murthy S. Prediction of heat and mass transfer in annular cylindrical metal hydride beds. *Int J Hydrogen Energy* Oct. 1992;17(10):795–805. [https://doi.org/10.1016/0360-3199\(92\)90024-Q](https://doi.org/10.1016/0360-3199(92)90024-Q).
- [29] Mayer U, Groll M, Supper W. Heat and mass transfer in metal hydride reaction beds: experimental and theoretical results. *Journal of the Less Common Metals* Mar. 1987;131(1–2):235–44. [https://doi.org/10.1016/0022-5088\(87\)90523-6](https://doi.org/10.1016/0022-5088(87)90523-6).
- [30] Muthukumar P, Singhal A, Bansal GK. Thermal modeling and performance analysis of industrial-scale metal hydride based hydrogen storage container. *Int J Hydrogen Energy* Oct. 2012;37(19):14351–64. <https://doi.org/10.1016/J.IJHYDENE.2012.07.010>.
- [31] Akanji OL, Kolesnikov AV. Modeling of heat and mass transfer in LaNi<sub>5</sub> matrix during hydrogen absorption-desorption cycle. *Pol J Chem Technol* Oct. 2012;14(3):71–6. <https://doi.org/10.2478/V10026-012-0087-0>.
- [32] Demircan A, Demiralp M, Kaplan Y, Mat MD, Veziroglu TN. Experimental and theoretical analysis of hydrogen absorption in LaNi<sub>5</sub>-H<sub>2</sub> reactors. *Int J Hydrogen Energy* Oct. 2005;30(13–14):1437–46. <https://doi.org/10.1016/J.IJHYDENE.2005.02.002>.
- [33] Muthukumar P, Madhavakrishna U, Dewan A. Parametric studies on a metal hydride based hydrogen storage device. *Int J Hydrogen Energy* Dec. 2007;32(18):4988–97. <https://doi.org/10.1016/J.IJHYDENE.2007.08.010>.
- [34] Askri F, Ben Salah M, Jemni A, Ben Nasrallah S. A new algorithm for solving transient heat and mass transfer in metal-hydrogen reactor. *Int J Hydrogen Energy* Oct. 2009;34(19):8315–21. <https://doi.org/10.1016/J.IJHYDENE.2009.07.072>.
- [35] Jemni A, Ben Nasrallah S. Study of two-dimensional heat and mass transfer during absorption in a metal-hydrogen reactor. *Int J Hydrogen Energy* Jan. 1995;20(1):43–52. [https://doi.org/10.1016/0360-3199\(93\)E0007-8](https://doi.org/10.1016/0360-3199(93)E0007-8).
- [36] Ben Nasrallah S, Jemni A. Heat and mass transfer models in metal-hydrogen reactor. *Int J Hydrogen Energy* Jan. 1997;22(1):67–76. [https://doi.org/10.1016/S0360-3199\(96\)00039-0](https://doi.org/10.1016/S0360-3199(96)00039-0).
- [37] Gopal MR, Murthy SS. Studies on heat and mass transfer in metal hydride beds. *Int J Hydrogen Energy* Nov. 1995;20(11):911–7. [https://doi.org/10.1016/0360-3199\(95\)00026-A](https://doi.org/10.1016/0360-3199(95)00026-A).
- [38] Gambini M, Manno M, Vellini M. Numerical analysis and performance assessment of metal hydride-based hydrogen storage systems. *Int J Hydrogen Energy* Nov. 2008;33(21):6178–87. <https://doi.org/10.1016/J.IJHYDENE.2008.08.006>.
- [39] Brown TM, Brouwer J, Samuelsen GS, Holcomb FH, King J. Accurate simplified dynamic model of a metal hydride tank. *Int J Hydrogen Energy* Oct. 2008;33(20):5596–605. <https://doi.org/10.1016/J.IJHYDENE.2008.05.104>.
- [40] MacDonald BD, Rowe AM. Impacts of external heat transfer enhancements on metal hydride storage tanks. *Int J Hydrogen Energy* Sep. 2006;31(12):1721–31. <https://doi.org/10.1016/J.IJHYDENE.2006.01.007>.
- [41] Nam J, Ko J, Ju H. Three-dimensional modeling and simulation of hydrogen absorption in metal hydride hydrogen storage vessels. *Appl Energy* Jan. 2012;89(1):164–75. <https://doi.org/10.1016/J.APENERGY.2011.06.015>.
- [42] Mohammadshahi SS, Gray EMA, Webb CJ. A review of mathematical modelling of metal-hydride systems for hydrogen storage applications. *Int J Hydrogen Energy* Feb. 2016;41(5):3470–84. <https://doi.org/10.1016/J.IJHYDENE.2015.12.079>.
- [43] Aldas K, Mat MD, Kaplan Y. A three-dimensional mathematical model for absorption in a metal hydride bed. *Int J Hydrogen Energy* Oct. 2002;27(10):1049–56. [https://doi.org/10.1016/S0360-3199\(02\)00010-1](https://doi.org/10.1016/S0360-3199(02)00010-1).
- [44] Hardy BJ, Anton DL. Hierarchical methodology for modeling hydrogen storage systems. Part I: scoping models. *Int J Hydrogen Energy* Mar. 2009;34(5):2269–77. <https://doi.org/10.1016/J.IJHYDENE.2008.12.070>.
- [45] Bao Z, Yang F, Wu Z, Nyallang Nyamsi S, Zhang Z. Optimal design of metal hydride reactors based on CFD–Taguchi combined method. *Energy Convers Manag* Jan. 2013;65:322–30. <https://doi.org/10.1016/J.ENCONMAN.2012.07.027>.
- [46] Hardy BJ, Anton DL. Hierarchical methodology for modeling hydrogen storage systems. Part II: detailed models. *Int J Hydrogen Energy* Apr. 2009;34(7):2992–3004. <https://doi.org/10.1016/J.IJHYDENE.2008.12.056>.
- [47] Wang Y, Adroher XC, Chen J, Yang XG, Miller T. Three-dimensional modeling of hydrogen sorption in metal hydride hydrogen storage beds. *J Power Sources* Dec. 2009;194(2):997–1006. <https://doi.org/10.1016/J.JPOWSOUR.2009.06.060>.
- [48] Elkhatib R, Louahlia H. Metal hydride cylindrical tank for energy hydrogen storage: experimental and computational modeling investigations. *Appl Therm Eng* Jul. 2023;232:120756. <https://doi.org/10.1016/J.APPLTHERMALENG.2023.120756>.
- [49] Jemni A, Ben Nasrallah S. Study of two-dimensional heat and mass transfer during absorption in a metal-hydrogen reactor. *Int J Hydrogen Energy* Jan. 1995;20(1):43–52. [https://doi.org/10.1016/0360-3199\(93\)E0007-8](https://doi.org/10.1016/0360-3199(93)E0007-8).
- [50] Freni A, Cipiti F, Cacciola G. Finite element-based simulation of a metal hydride-based hydrogen storage tank. *Int J Hydrogen Energy* Oct. 2009;34(20):8574–82. <https://doi.org/10.1016/J.IJHYDENE.2009.07.118>.
- [51] MacDonald BD, Rowe AM. Impacts of external heat transfer enhancements on metal hydride storage tanks. *Int J Hydrogen Energy* Sep. 2006;31(12):1721–31. <https://doi.org/10.1016/J.IJHYDENE.2006.01.007>.
- [52] Kumar Phate A, Prakash Maiya M, Murthy SS. Simulation of transient heat and mass transfer during hydrogen sorption in cylindrical metal hydride beds. *Int J Hydrogen Energy* Aug. 2007;32(12):1969–81. <https://doi.org/10.1016/J.IJHYDENE.2006.09.020>.
- [53] Chung CA, Ho CJ. Thermal–fluid behavior of the hydriding and dehydriding processes in a metal hydride hydrogen storage canister. *Int J Hydrogen Energy* May 2009;34(10):4351–64. <https://doi.org/10.1016/J.IJHYDENE.2009.03.028>.
- [54] Mohan G, Prakash Maiya M, Srinivasa Murthy S. Performance simulation of metal hydride hydrogen storage device with embedded filters and heat exchanger tubes. *Int J Hydrogen Energy* Dec. 2007;32(18):4978–87. <https://doi.org/10.1016/J.IJHYDENE.2007.08.007>.
- [55] Chaise A, De Rango P, Marty P, Fruchart D. Experimental and numerical study of a magnesium hydride tank. *Int J Hydrogen Energy* Jun. 2010;35(12):6311–22. <https://doi.org/10.1016/J.IJHYDENE.2010.03.057>.
- [56] Eftekhari AA, Schüller K. FVTool: a finite volume toolbox for Matlab. Oct. 2015. <https://doi.org/10.5281/ZENODO.32745>.
- [57] Khan S, et al. The self-heating ignition of lithium-ion batteries: a comparative study of COMSOL and GPYRO models with finite volume toolbox. College Station, Texas: 13th U. S. National Combustion Meeting; 2022 [Online], <https://www.researchgate.net/profile/Shehzad-Khan-13/publication/373013979>. [Accessed 29 April 2024].
- [58] Khan S, Anwar S, Casa J, Hasnain M, Ahmed H, Sezer H. Modeling thermal runaway in prismatic lithium-ion batteries. ASME International Mechanical Engineering Congress and Exposition, Proceedings (IMECE) 2024;10(Feb). <https://doi.org/10.1115/IMECE2023-113787>.
- [59] Hasnain M, et al. 3D mathematical model for heat and mass transfer mechanisms in gypsum board exposed to fire [Online], <https://www.researchgate.net/publication/373293420>. [Accessed 23 April 2024].
- [60] Khan S, Hasnain M, Sezer H. Numerical modeling of spontaneous ignition in large coal stockpiles using finite volume method. In: Spring technical meeting eastern states section of. Athens, Georgia: the Combustion Institute; Mar. 2024. [https://doi.org/10.1016/S0378-3820\(99\)00005-3](https://doi.org/10.1016/S0378-3820(99)00005-3).
- [61] Khan S, Hasnain M, Casa J. Mathematical modeling of heat-induced decomposition kinetics leading to thermal runaway in lithium-ion batteries. In: Spring technical meeting eastern states section of. Athens, Georgia: the Combustion Institute; Mar. 2024. <https://doi.org/10.1149/1945-7111/ABA8B9>.
- [62] Khan MU, Hasnain M, Khan S. Mathematical model for predicting injuries and temperature distributions in stem exposed to fire. In: Spring technical meeting eastern states section of. Athens, Georgia: the Combustion Institute; Mar. 2024 [Online], <https://www.researchgate.net/publication/379034461>. [Accessed 2 April 2024].
- [63] Hasnain M, Paye R, Borth T, Gorbett GE, Kozhumal SP, Sezer H. Three-dimensional mathematical modeling of heat and mass transfer during calcination of gypsum board exposed to fire. In: Spring technical meeting eastern states section of. Athens, Georgia: the Combustion Institute; Mar. 2024 [Online], <https://www.researchgate.net/publication/379034315>. [Accessed 12 April 2024].
- [64] Yang FS, Wang GX, Zhang ZX, Rudolph V. Investigation on the influences of heat transfer enhancement measures in a thermally driven metal hydride heat pump. *Int J Hydrogen Energy* Sep. 2010;35(18):9725–35. <https://doi.org/10.1016/J.IJHYDENE.2010.06.110>.
- [65] Satheesh A, Muthukumar P, Dewan A. Computational study of metal hydride cooling system. *Int J Hydrogen Energy* Apr. 2009;34(7):3164–72. <https://doi.org/10.1016/J.IJHYDENE.2009.01.083>.
- [66] Choy TC. *Effective medium theory : principles and applications*. second ed., vol. 165. Oxford University Press; 2016.
- [67] Nishizaki T, Miyamoto K, Yoshida K. Coefficients of performance of hydride heat pumps. *Journal of the Less Common Metals* Feb. 1983;89(2):559–66. [https://doi.org/10.1016/0022-5088\(83\)90372-7](https://doi.org/10.1016/0022-5088(83)90372-7).
- [68] Jemni A, Ben Nasrallah S, Lamoumi J. Experimental and theoretical study of ametal–hydrogen reactor. *Int J Hydrogen Energy* Jul. 1999;24(7):631–44. [https://doi.org/10.1016/S0360-3199\(98\)00117-7](https://doi.org/10.1016/S0360-3199(98)00117-7).
- [69] Siyakatshana N, Kudrna V, Machon V. Incorporating Danckwerts' boundary conditions into the solution of the stochastic differential equation. *Chem Eng Sci* Apr. 2005;60(7):1987–94. <https://doi.org/10.1016/J.CES.2004.11.051>.
- [70] Dhaou H, Askri F, Ben Salah M, Jemni A, Ben Nasrallah S, Lamoumi J. Measurement and modelling of kinetics of hydrogen sorption by LaNi<sub>5</sub> and two related pseudobinary compounds. *Int J Hydrogen Energy* Apr. 2007;32(5):576–87. <https://doi.org/10.1016/J.IJHYDENE.2006.07.001>.

**IMECE2023-112874**

## MODELING HEAT AND MASS TRANSFER IN METAL HYDRIDE-BASED HYDROGEN STORAGE SYSTEMS USING THE FINITE VOLUME METHOD

**Muhammad Hasnain**  
 Department of  
 Mechanical Engineering,  
 Georgia Southern  
 University  
 Statesboro, GA

**Shehzad Khan**  
 Department of  
 Mechanical Engineering,  
 Georgia Southern  
 University  
 Statesboro, GA

**M.Amin Ezazi**  
 Department of Mechanical  
 Engineering,  
 Georgia Southern  
 University  
 Statesboro, GA

**Hayri Sezer**  
 Department of  
 Mechanical Engineering,  
 Georgia Southern  
 University  
 Statesboro, GA

### ABSTRACT

*Integrated hydrogen systems need technology to store hydrogen ( $H_2$ ) for many applications. Conventionally, hydrogen can be kept either in the gaseous state (under 500-700 bars) or as a liquid at cryogenic temperature (almost 20 K). Alternatively, metal hydrides (MH)-based storage of hydrogen is currently the state-of-the-art approach to storing hydrogen that offers both safety and higher storage efficiency. However, the main challenge in the MH is the low thermal conductivity that limits the heat transfer during the exothermic adsorption and endothermic desorption processes. This ultimately leads to slow reaction rates and ultimately to higher charging and discharging durations. To improve the performance of MH-based hydrogen storage systems, it is crucial to optimize the heat and mass transfer mechanisms within the MH bed. This work is an attempt to model the heat and mass transfer phenomena during the adsorption process of hydrogen. The governing equations are discretized based on Finite Volume Method and Euler's implicit method is used for time integration. This method offers a robust and customizable numerical approach that can examine the performance of a broad range of metal hydrides and system configurations for varying environmental conditions. This will enable the modeling and optimization of heat and mass transfers, aimed at reducing the charging and discharging times of these systems. The analyzed parameters include temperature, equilibrium pressure, and average reacted fraction of hydrogen during the adsorption process. The reacted fraction profile from the inhouse developed 2D axis symmetrical model is validated with the experimental data reported in the literature.*

**Keywords:** Hydrogen storage, Metal hydrides, Mathematical modeling, Exothermic adsorption, Finite volume method

### NOMENCLATURE

A	parameter in P-C-T equation
B	parameter in P-C-T equation [K]
$C_p$	specific heat capacity [J/(kg K)]
E	activation energy [J/mol]
h	convective heat transfer coefficient [W/(m <sup>2</sup> K)]
$\Delta H$	reaction enthalpy [J/mol $H_2$ ]
[H/M]	hydrogen to metal ratio
k	reaction rate constant [s <sup>-1</sup> ]
K	permeability [m <sup>2</sup> ]
m	mass source term of reaction [kg/(m <sup>3</sup> s)]
P	pressure [Pa]
P-C-T	pressure-composition-temperature
q	mass flow rate [kg/s]
r	r-coordinate [m]
$R_g$	general gas constant [J/(mol K)]
t	time [s]
T	temperature [K]
U	gas velocity [m/s]
W	mass [kg]
X	reacted fraction of hydrogen
z	z-coordinate [m]

### GREEK SYMBOLS

$\alpha$	ratio of thermal mass
$\beta$	hysteresis factor in P-C-T equation
$\varepsilon$	porosity
$\lambda$	thermal conductivity [W/m K]
$\mu$	dynamic viscosity [Pa.s]
$\rho$	density [kg/m <sup>3</sup> ]
$\phi$	plateau flatness factor in P-C-T equation
$\phi_0$	plateau flatness factor in P-C-T equation

## SUBSCRIPTS

a	adsorption
b	bulk
d	desorption
e	equilibrium
eff	effective
ex	exerted
f	heat transfer fluid
g	hydrogen gas
H	high
i	inner
in	inlet
L	low
MH	metal hydride
o	outer
sat	saturated

## 1. INTRODUCTION

Due to the rapidly increasing global energy demand and the contribution of non-renewable energy sources towards global warming and air pollution, it has become inevitable to find reliable and sustainable energy sources. To reduce greenhouse emissions and meet the energy demand, the world is shifting towards renewable energy technology. Power generation from renewable energy sources (like solar and wind energy) is contributing to mitigate these issues. However, due to the dependence of these sources on many natural factors, its availability at a given location and time cannot be predicted [1]. It can result in an imbalance between energy demand and supply. Storing surplus energy is one solution to this issue. Batteries provide a typical way to store energy, however, due to their high cost, uncertain lifetime, low energy density, self-discharge, and rapid degradation, they are unsuitable for long-term and high-capacity energy storage applications [2]. In this regard, one of the promising ideas is to use hydrogen ( $H_2$ ) as the energy storage solution [3].

A green energy source, hydrogen reacts with oxygen to produce water ( $H_2O$ ), heat, and electricity in fuel cells. The major motivations behind using hydrogen as an energy source are its natural abundance, and high energy density per unit mass (up to 3 times that of gasoline and diesel). The excess energy from the renewable sources can be used for electrolysis of water to produce hydrogen gas [3]. Then it can be stored and used in fuel cells to generate electric power when the supply of energy from renewable sources does not meet the demand [4].

The storage of hydrogen is currently a major challenge. Hydrogen systems (such as fuel cells) need technology to store and transport  $H_2$  for many applications [5], [6]. Hydrogen can be kept either in gaseous state under high pressure or as a liquid, depending on the application where space and weight constraints are crucial. In its gaseous state, hydrogen has a low energy density per unit volume of approximately  $27 \text{ kg } H_2/m^3$  [7]. Consequently, if held at ambient temperature and pressure, a substantial area of storage space will be needed that gives rise to a technical challenge in storage, transportation, and portable applications [8], [9]. The high-pressure compression of gas at

about 700 bar or its conversion to liquid by maintaining a cryogenic temperature of almost 20 K are two solutions to address this issue, however both require additional costs to achieve these extreme conditions for temperature and pressures [10]–[12]. The former is the most popular commercial way for storing and transporting hydrogen to demand locations due to its simplicity and maturity [3]. The latter approach consumes—up to 30%—of energy during the liquefaction process, thus, making it ever more inefficient [1], [13]. For large-scale applications, however, these both technologies have significant obstacles, including efficiency and safety due to low volumetric density and high pressure respectively [14].

In comparison to the gaseous and liquified hydrogen storage methods, using solid state MH as hydrogen storage materials has the competitive potential to provide high volumetric density, high storage capacity as well as minimize the safety risk associated with high pressure [15]. The popularity of MH based hydrogen storage systems, both in research and industry, is mainly attributed to its safety and no high pressure or low temperature requirements. Unlike the former approaches, this method involves the adsorption of hydrogen as atoms rather than molecules to the metal hydride material. However, due to the involvement of external metal hydride material (MH) as the storage medium, this method for hydrogen storage is intrinsically heavy, and is therefore, best suited for stationary applications where bulk is not a major concern [16]. Other compelling advantages of using this technology include its relatively high volumetric storage density, safety and compactness, and reversibility (leading to fast hydrogen absorption and desorption processes), all of which enhance the viability of this solution [17].

The adsorption of hydrogen in metals is an endothermic process. The heat produced during adsorption process elevates the temperature of MH bed and lead to a decrease in hydrogen adsorption rate and storage capacity. Therefore, to maximize the storage efficiency and reduce the charging time, the generated heat should be expelled to maintain the temperature at a suitable level [9]. The desorption and adsorption of hydrogen requires substantial heat uptake and release; however, the poor thermal conductivity of metal hydride bed slows down the heat conduction inside the bed and extends charging and discharging times. Therefore, when designing such systems, the thermal management measures should be considered [18].

The objective of this work is to use the finite volume (FV) based discretization approach and model the MH-based hydrogen storage process involving a heat transfer fluid (HTF). This paper focuses on the mathematical modeling of heat and mass transfer mechanisms during the adsorption of hydrogen in MH-based hydrogen storage systems. The FV method is employed to discretize the governing equations of mass and energy conservation for the adsorption process, and Euler's implicit method is used for time integration. The resulting linear system of equations is solved using a sparse matrix solver available in MATLAB. The model is used to analyze the effects of various parameters, such as temperature, pressure, and average reacted fraction of hydrogen, on the adsorption process.



The results obtained from the 2D axis-symmetrical model are found to be in good agreement with experimental data reported in the literature. This model can be used to optimize the performance of MH-based hydrogen storage systems by reducing the charging time and increasing the hydrogen storage efficiency.

## 2. MATHEMATICAL MODEL

### 2.1. SYSTEM DESCRIPTION

The schematic of the cross section of the MH based hydrogen storage system is given in figure 1. The tank can be divided into three sections as shown. The blue region at the outer side represents the pathway for HTF that is mostly considered to be water. The middle region is metal hydride bed where the hydrogen absorption and desorption processes take place. The third section in the center of the cylinder represents the pathway for hydrogen gas. During absorption process hydrogen is pressurized in the central region where it is absorbed into the MH bed. The heat transfer fluid is separated from the MH bed with a thin wall of stainless steel.

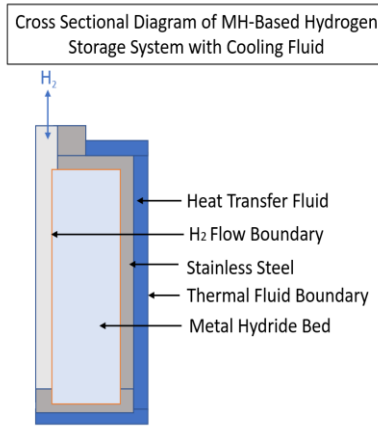


**FIGURE 1: MH TANK SCHEMATIC WITH HEAT TRANSFER FLUID [19]**

The metal used for capturing hydrogen in this work is  $\text{LaNi}_5$ , that transforms to  $\text{LaNi}_5\text{H}_6$  when hydrogen is fully adsorbed. Initially the MH bed is considered to be at room temperature (298 K) while the heat transfer fluid (water) is at 273 K to maximize the rate of heat transfer.

### 2.2. FORMULATION OF MATHEMATICAL MODEL

The mathematical formulation for modeling the multi physics phenomena in MH storage system can be established based on assumptions given as follows:

- Thermodynamically the gas phase inside the MH bed exhibits ideal gas characteristics and therefore, ideal gas equation can be applied.
- There is local thermal equilibrium between hydrogen gas and MH bed boundary. In other words, there is a

common temperature on the interface between solid and gas phases and no temperature slip is involved.

- The heat transfer through radiation mechanism is negligible and therefore, it is not considered. This assumption is valid since only moderate temperatures are involved in the system.

The computational model is based on the conservation of mass, the application of Darcy's law and heat transfer in porous media. All these principles are coupled and applied in porous medium to derive the final modeling equations for MH based hydrogen storage system [19], [20]. The conservation of mass for gas phase can be written as:

$$\frac{\partial \varepsilon_g \rho_g}{\partial t} + \nabla(\rho_g \vec{U}) = -\dot{m} M_{\text{MH}} \quad (1)$$

In eq. (1),  $\varepsilon_g$  and  $\rho_g$  represents the porosity and density of the gaseous phase while  $\vec{U}$  is the Darcy's velocity of hydrogen inside MH bed that is shown by eq. (3). On the right side  $\dot{m}$  is the source term that is given by eq. (2):

$$\dot{m} = \frac{\varepsilon_{\text{MH}} \rho_{\text{MH}}}{M_{\text{MH}}} \cdot \left[ \frac{H}{M} \right]_{\text{sat}} \cdot \frac{dX}{dt} \quad (2)$$

Similarly, in this equation  $\varepsilon_{\text{MH}}$ ,  $\rho_{\text{MH}}$ , and  $M_{\text{MH}}$  represent the porosity of MH bed, density of the bed, and molar mass of metal hydride material respectively. The other parameter  $\left[ \frac{H}{M} \right]_{\text{sat}}$  quantifies the maximum value of the ratio of absorbed hydrogen mass to metal mass in metal hydride bed that occurs at saturation point. The last factor in eq. (2)  $\frac{dX}{dt}$  shows the rate of change of the reacted fraction of hydrogen inside MH bed at any given time.

$$\vec{U} = \frac{K}{\mu} \nabla P \quad (3)$$

In Darcy's law eq. (3) the quantities  $K$ , and  $\mu$  represent the effective permeability and dynamic viscosity of the gaseous phase respectively, while  $\nabla P$  shows the pressure gradient along the axial coordinate.

Based on the local thermal equilibrium assumption, the law of conservation of energy for the system is shown by eq. (4).

$$\frac{\partial(\rho_b C_{p,b})_{\text{eff}} T_b}{\partial t} + \nabla \cdot (\rho_g C_{p,g} \vec{U} T_b) = \nabla(\lambda_{\text{eff}} \nabla T_b) + \frac{\dot{m}}{M_g} \cdot \Delta H \quad (4)$$

where the coefficients of the transient term (that represents the effective heat capacity) and that of the diffusion term  $\lambda_{\text{eff}}$  (effective thermal conductivity) are given by eq. (5) and eq. (6).

$$(\rho_b C_{p,b})_{eff} = \varepsilon_{MH} \rho_g C_{p,g} + (1 - \varepsilon_{MH}) \rho_{MH} C_{p,b} \quad (5)$$

$$\lambda_{eff} = [\varepsilon_{MH} \lambda_g + (1 - \varepsilon_{MH}) \lambda_{MH}] \quad (6)$$

The product of MH bed density and specific heat in the coefficient of convective term (bulk heat capacity of the bed) is the sum of all constituent phases involved in the system [20].

$$\rho_b C_{p,b} = \sum_{i=1} \varepsilon_i \rho_i C_{pi} \quad (7)$$

The equations for reaction kinetics used for absorption process (eq. (8)) are recommended by [21] while that of desorption (eq. (9)) are suggested by [22].

$$\frac{dX}{dt} = k_a \cdot \exp\left(-\frac{E_a}{R_g T_b}\right) \cdot \ln\left(\frac{P}{P_{e,a}}\right) \cdot (1 - X) \quad (8)$$

The effective pressures for absorption and desorption processes explicitly consider the effects of hysteresis and plateau slope [23]. The equation to represent the equilibrium pressure during adsorption is given by eq. (9). The constant parameters in kinetics eq. (8) and eq. (9) are shown in table 1. The physical parameters like porosity, permeability, initial densities of the bed and the gas are taken from [20].

$$P_{e,a} = \exp\left(\frac{A - \frac{B}{T_b} + (\phi + \phi_0) \cdot \tan\left(\pi\left(X - \frac{1}{2}\right)\right) + \frac{\beta}{2}}{\right)} \quad (9)$$

**TABLE 1: REACTIONS KINETICS AND P-C-T PARAMETERS IN EQ. (8) AND EQ. (9) [20]**

Parameters	Adsorption	Unit
Rate constant, k	59.187	[s <sup>-1</sup> ]
Activation energy, E	21179	[J/mol H <sub>2</sub> ]
P-C-T parameter, A	13.44	---
P-C-T parameter, B	3780	[K]
Plateau flatness factor, $\phi$	0.038	---
Plateau flatness factor, $\phi_0$	0	---
Hysteresis factor, $\beta$	0.137	---

## 2.3. COMPUTATIONAL DOMAIN

The system can be modeled as an axis symmetrical two-dimensional domain in cylindrical coordinates. The approximate dimensions of the MH tank are shown in fig. 2. It can be noticed

that the values of axial and radial coordinates for a typical MH system are from 0 mm to 500 mm and -12.5 mm to +12.5 mm respectively. These dimensions are considered for initial analysis and can be customized to optimize the performance of the system. It is assumed that the heat exchange between MH bed and heat transfer fluid takes place instantly and hence stainless steel is not considered in the simplified model.

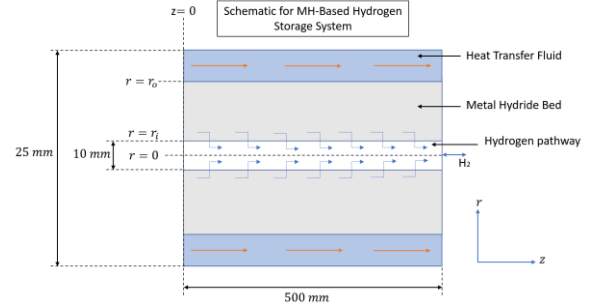


**FIGURE 2: TWO-DIMENSIONAL COMPUTATIONAL DOMAIN FOR THE MATHEMATICAL MODEL**

## 2.4. INITIAL AND BOUNDARY CONDITIONS

Hydrogen is axially entered into MH bed in the center of the tank. Initially it is assumed that initially the MH bed is in thermodynamic equilibrium with hydrogen. This implies that the initial temperature of the hydride bed, and hydrogen gas is the same.

$$T(r, z, t = 0) = T_{initial} \quad (10)$$

The left and right walls where hydrogen is entered and exited from the tank can be treated under Neumann's boundary conditions. Therefore, the derivatives of bed temperature and gas pressure with respect to the axial coordinate at  $z=0$  and  $z=L$  are given by eq. (11a) and (11b) respectively:

$$\left. \frac{\partial T_b}{\partial z} \right|_{z=0} = 0, \quad \left. \frac{\partial P_g}{\partial z} \right|_{z=0} = 0 \quad (11a)$$

$$\left. \frac{\partial T_b}{\partial z} \right|_{z=L} = 0, \quad \left. \frac{\partial P_g}{\partial z} \right|_{z=L} = 0 \quad (11b)$$

At HTF-MH bed interface (heat transfer wall), the boundary conditions are given as follows:

$$-\lambda_{eff} \left. \frac{\partial T_b}{\partial r} \right|_{r=r_o} = h(T_b - T_f) \quad (12a)$$

$$\left. \frac{\partial P_g}{\partial r} \right|_{r=r_o} = 0 \quad (12b)$$

Here  $T_f$  varies along the axial direction, and the differential equation for  $T_f$  along the heat transfer boundary in the longitudinal direction is given by eq. (13).

$$h(T_b - T_f) = q_f C_{p,f} \frac{\partial T_f}{\partial z} \quad (13)$$

At the mass transfer boundary where the adsorption of hydrogen into MH bed takes place, a Danckwerts' boundary condition [24] is considered to ensure the continuous flow rate of hydrogen across the wall.

$$-\lambda_{\text{eff}} \frac{\partial T_b}{\partial r} \Big|_{r=r_i} = \rho_{g,\text{in}} \vec{U} C_{p,g} (T_{\text{in}} - T_b) \quad (14)$$

Finally, the pressure of the gas at the mass transfer boundary can be taken to be equal to the exerted pressure in the tank.

$$P_g \Big|_{r=r_i} = P_{\text{ex}} \quad (15)$$

## 2.5. NUMERICAL APPROACH: FINITE VOLUME METHOD

The finite volume method is a discretization approach for solving complex differential equations by inherently incorporating the integral form of the equations of mass, energy, and momentum conservations. This technique involves the splitting of the domain into a finite number of adjacent control volumes known as cells. The values of the variable parameters included in the differential equations are computed at the cell center (centroid) of each control volume. To calculate the values on the surface of control volume, arithmetic or harmonic means or other mathematical interpolation methods can be used. A typical control volume for a two-dimensional model is shown in fig. 3.

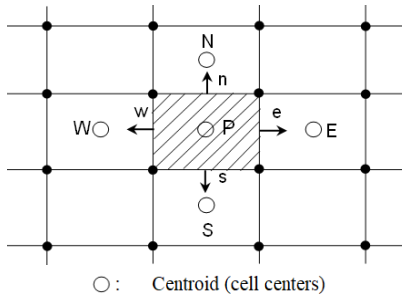


**FIGURE 3: CONTROL VOLUME FOR TWO-DIMENSIONAL MODEL (EACH CELL HAS FOUR FACES LABELED WITH EAST (E), WEST (W), NORTH (N), AND SOUTH (S))**

The discretization in FVM is based on the control volumes instead of grid intersection points, therefore FVM has the tendency to be customized and accommodate any type of grid. This work utilizes an open-source finite volume toolbox (Simulkade) to solve the PDEs model resulting from coupling of conservation equations and Darcy's law [25]. FVM inherently satisfies the conservation equations for mass, heat, and

momentum transfers across the cell boundaries therefore, along with more customization, this approach will be fast and will yield more accurate results [26], [27].

## 3. RESULTS AND DISCUSSION

The model can be applied to any MH based system involving heat transfer fluid. Initially hydrogen is compressed in the central pathway of the tank at a pressure of 6 bars. The curve showing the variation profile of the average reacted fraction of hydrogen inside MH bed with respect to time is shown in fig. 4. It can be noticed that the simulations results are in good agreement with the experimental results [20]. For the storage system considered, it can be seen from the graph that the average reacted fraction reaches from 0% to about 99.3% in about 600 seconds during adsorption process. The initial steep curve implies a high adsorption rate of hydrogen at the start of the process that is gradually reduced as the concentration of hydrogen reaches saturation. The adsorption time for the current simulation is reduced from 800 seconds to about 600 seconds as the initial temperature of the cooling fluid is decreased from 298 K to 273 K [20], [28].

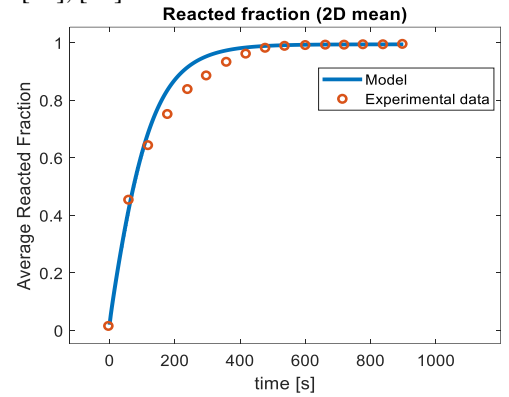


**FIGURE 4: EXPERIMENTAL VALIDATION OF THE AVERAGE REACTED FRACTION PROFILE DURING ADSORPTION PROCESS [20]**

The distribution of the reacted fraction of hydrogen in the metal hydride (MH) bed and temperature in the domain during the adsorption process at three different times were analyzed. The three different times considered for retrieving the results are 10, 100 and 600 seconds, corresponding to the start, middle, and end of the adsorption process, respectively.

The results showed that at 10 seconds, the reacted fraction of hydrogen in the domain varied from 9.5% at the heat transfer boundary (outer boundary) to 12.5% at the mass transfer boundary (inner boundary) as shown in fig. 5A. This indicates that the adsorption rate was higher at the inner boundary due to direct contact with hydrogen. Additionally, the temperature distribution at the beginning of the adsorption process (as shown in Figure 5B) revealed a maximum temperature of approximately 301 K at the inner boundary and a minimum temperature of about 295 K at the outer boundary, where it was in contact with the low-temperature cooling fluid.



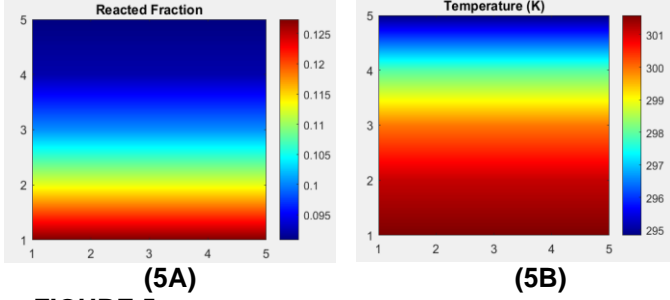


**FIGURE 5: REACTION FRACTION AND TEMPERATURE DISTRIBUTION IN THE DOMAIN AT TIME = 10 SECONDS (11% CHARGED SYSTEM: START OF THE ADSORPTION)**

As the adsorption process progressed, the reacted fraction of hydrogen in the MH bed increased and spread towards the outer boundary. At 100 seconds, as can be noticed from fig. 6A, the reacted fraction ranged from 59% at the outer boundary to 67% at the inner boundary, indicating that the system was charged to more than 50% of its full capacity within the first 100 seconds. The high rate of adsorption was facilitated by the significant temperature difference between the cooling fluid and the MH bed. Interestingly, the temperature distribution revealed a reduction in temperature in the MH bed, despite the exothermic nature of the adsorption process, as the cooling fluid absorbed the heat from the computational domain. The temperature profile in Figure 6B indicated that the temperature of the MH bed decreased from 298 K to 285 K at the heat transfer boundary and to 288 K at the mass transfer boundary, suggesting that the rate of heat release due to adsorption was less than the rate of heat absorption by the cooling fluid.

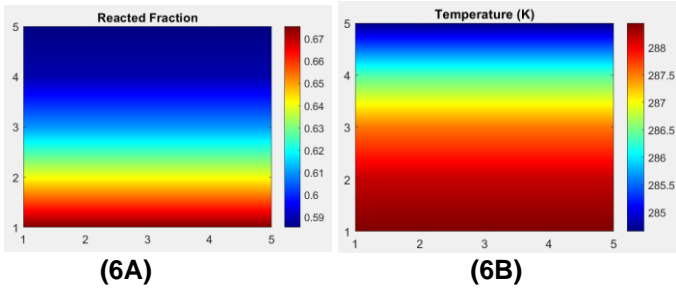


**FIGURE 6: REACTION FRACTION AND TEMPERATURE DISTRIBUTION IN THE DOMAIN AT TIME = 100 SECONDS (63% CHARGED SYSTEM: MIDDLE OF THE ADSORPTION)**

The final stage of the adsorption process was analyzed by studying the distribution of the reacted fraction of hydrogen in the MH bed at 600 seconds. The results from fig. 7A indicate that the reacted fraction increased to a maximum of 99.31% at the inner boundary and 99.27% at the outer boundary. This suggests that most of the metal molecules  $\text{LaNi}_5$  are now attached with hydrogen and are present as  $\text{LaNi}_5\text{H}_6$ , indicating that the adsorption process has almost reached the saturation point.

As the adsorption progresses to saturation, its rate becomes negligible, and the rate of heat production also decreases.

Therefore, the cooling fluid absorbs heat from the MH bed, and it can be observed from fig. 7B that the whole domain is almost at the same temperature as the initial temperature of the cooling fluid.

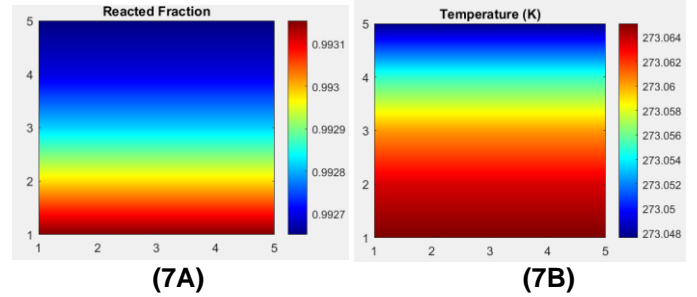


**FIGURE 7: REACTION FRACTION AND TEMPERATURE DISTRIBUTION IN THE DOMAIN AT TIME = 600 SECONDS (99.3% CHARGED SYSTEM: END OF THE ADSORPTION)**

To gain insights into the temperature variation for MH bed during the adsorption process of hydrogen, the mean temperature of the two-dimensional domain was plotted as a function of time. As shown in fig. 8, the average temperature initially rose due to the high hydrogen adsorption at the inner mass transfer boundary. However, as the high temperature propagated towards the outer heat transfer boundary, the cooling fluid started to absorb more heat from the MH bed, resulting in a decrease in the mean temperature curve. This cooling effect caused the mean temperature to fall until it reached 273 K at the end of the adsorption process after approximately 600 seconds.

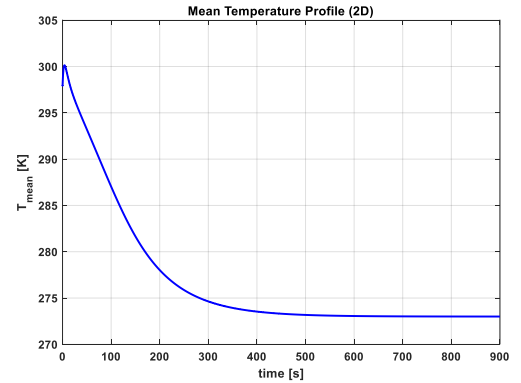


**FIGURE 8: MEAN TEMPERATURE PROFILE DURING ADSORPTION PROCESS (CHARGING)**

Equilibrium pressure refers to the pressure at which the rate of adsorption of hydrogen onto the metal hydride (MH) bed is equivalent to the rate of desorption, resulting in no net change in the amount of adsorption. The equilibrium pressure curve during the adsorption process is depicted in fig. 9. Initially, the adsorption of hydrogen on the surface of the MH particles causes an increase in the equilibrium pressure. However, as the MH particles reach their saturation point at the inner boundary, the rate of adsorption decreases, leading to a decline in the equilibrium pressure.

As the hydrogen concentration propagates from the inner boundary and temperature from the outer boundary throughout the domain, the equilibrium pressure gradually rises again. Once the MH bed becomes fully saturated, the pressure curve reaches a plateau, indicating the maximum capacity of the adsorption process, and the rate of adsorption becomes negligible as almost all the available adsorption sites are already occupied by the adsorbate molecules.

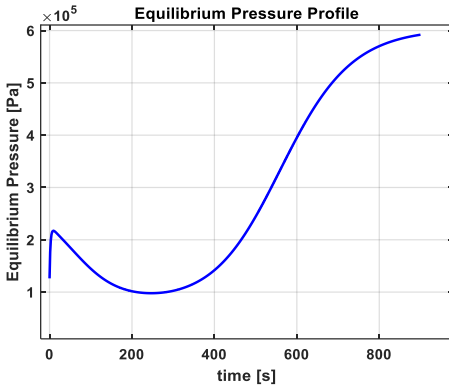


**FIGURE 9: EQUILIBRIUM PRESSURE PROFILE DURING ADSORPTION PROCESS (CHARGING)**

#### 4. CONCLUSION

A computational model based on finite volume method (FVM) is developed for the analysis of hydrogen storage systems using metal hydrides. The FVM discretization approach employs control volumes in the computational domain, allowing for customization to accommodate any type of grid for a wide range of MH-based storage applications. The accuracy of the model is enhanced by FVM's inherent ability to satisfy governing laws of conservation of mass, energy, and momentum. The developed model is implemented for a simplified MH-based hydrogen storage system, involving only the heat transfer fluid, and is used to plot temperature and average reacted fraction profiles for the system during the adsorption process. The results demonstrate good agreement with experimental data for the reacted fraction profile.

The model can be extended to the desorption process as well as applied to a system involving both HTF and annular fins by modifying the boundary condition and system configurations. It can be utilized to develop an optimization tool that can lead to higher hydrogen storage efficiency and rapid system charging and discharging. By analyzing the concentration and temperature distributions inside the system, the optimal dimensions can be determined. These results suggest that the adsorption process is influenced by both mass and heat transfer mechanisms. Overall, this study presents a comprehensive computational tool that can be conveniently customized for a wide range of metal hydrides and environmental conditions.

#### REFERENCES

- [1] P. Modi and K. F. Aguey-Zinsou, "Room Temperature Metal Hydrides for Stationary and Heat Storage Applications: A Review," *Front Energy Res*, vol. 9, p. 128, Apr. 2021, doi: 10.3389/FENRG.2021.616115/BIBTEX.
- [2] Y. Zhang, P. E. Campana, A. Lundblad, and J. Yan, "Comparative study of hydrogen storage and battery storage in grid connected photovoltaic system: Storage sizing and rule-based operation," *Appl Energy*, vol. 201, pp. 397–411, Sep. 2017, doi: 10.1016/J.APENERGY.2017.03.123.
- [3] D. Jang, H. S. Cho, and S. Kang, "Numerical modeling and analysis of the effect of pressure on the performance of an alkaline water electrolysis system," *Appl Energy*, vol. 287, Apr. 2021, doi: 10.1016/j.apenergy.2021.116554.
- [4] S. Kharel and B. Shabani, "Hydrogen as a long-term large-scale energy storage solution to support renewables," *Energies (Basel)*, vol. 11, no. 10, 2018, doi: 10.3390/en11102825.
- [5] I. P. Jain, P. Jain, and A. Jain, "Novel hydrogen storage materials: A review of lightweight complex hydrides," *J Alloys Compd*, vol. 503, no. 2, pp. 303–339, Aug. 2010, doi: 10.1016/J.JALLCOM.2010.04.250.
- [6] B. Shabani, J. Andrews, and S. Badwal, "FUEL CELL HEAT RECOVERY, ELECTRICAL LOAD MANAGEMENT, AND THE ECONOMICS OF SOLAR-HYDROGEN SYSTEMS," *International Journal of Power and Energy Systems*, vol. 30, no. 4, pp. 256–263, 2010, doi: 10.2316/JOURNAL.203.2010.4.203-4842.
- [7] A. Züttel, A. Remhof, A. Borgschulte, and O. Friedrichs, "Hydrogen: the future energy carrier," *Philosophical Transactions of the Royal Society A: Mathematical, Physical and Engineering Sciences*, vol. 368, no. 1923, pp. 3329–3342, Jul. 2010, doi: 10.1098/RSTA.2010.0113.
- [8] J. Andrews and B. Shabani, "Where does hydrogen fit in a sustainable energy economy?," in *Procedia Engineering*, Elsevier Ltd, 2012, pp. 15–25. doi: 10.1016/j.proeng.2012.10.107.
- [9] H. Q. Nguyen and B. Shabani, "Review of metal hydride hydrogen storage thermal management for use in the fuel cell systems," *Int J Hydrogen Energy*, vol. 46, no. 62, pp. 31699–31726, Sep. 2021, doi: 10.1016/j.ijhydene.2021.07.057.
- [10] J. Zhang, T. S. Fisher, P. V. Ramachandran, J. P. Gore, and I. Mudawar, "A Review of Heat Transfer Issues in Hydrogen Storage Technologies," *Journal of Heat Transfer-transactions of The Asme*, vol. 127, no. 12, pp. 1391–1399, Dec. 2005, doi: 10.1115/1.2098875.
- [11] C. Azzaro-Pantel, *Hydrogen supply chain: design, deployment and operation*. 2018. Accessed: Oct. 10, 2022. [Online]. Available:

- [https://books.google.com/books?hl=en&lr=&id=gyZqDwAAQBAJ&oi=fnd&pg=PP1&ots=69Sl0wYlml&sig=-h9lv8LL56xXg\\_-iP8FTSGYYQOk](https://books.google.com/books?hl=en&lr=&id=gyZqDwAAQBAJ&oi=fnd&pg=PP1&ots=69Sl0wYlml&sig=-h9lv8LL56xXg_-iP8FTSGYYQOk)
- [12] J. L. C. Rowsell and O. M. Yaghi, "Strategies for hydrogen storage in metal-organic frameworks," *Angewandte Chemie - International Edition*, vol. 44, no. 30, pp. 4670–4679, Jul. 25, 2005. doi: 10.1002/anie.200462786.
- [13] R. von Helmolt and U. Eberle, "Fuel cell vehicles: Status 2007," *J Power Sources*, vol. 165, no. 2, pp. 833–843, Mar. 2007, doi: 10.1016/J.JPOWSOUR.2006.12.073.
- [14] A. M. Abdalla, S. Hossain, O. B. Nisfindy, A. T. Azad, M. Dawood, and A. K. Azad, "Hydrogen production, storage, transportation and key challenges with applications: A review," *Energy Convers Manag*, vol. 165, pp. 602–627, Jun. 2018, doi: 10.1016/J.ENCONMAN.2018.03.088.
- [15] S. Niaz, T. Manzoor, and A. H. Pandith, "Hydrogen storage: Materials, methods and perspectives," *Renewable & Sustainable Energy Reviews*, vol. 50, pp. 457–469, May 2015, doi: 10.1016/J.RSER.2015.05.011.
- [16] B. Shabani and J. Andrews, "Hydrogen and fuel cells," *Green Energy and Technology*, vol. 201, pp. 453–491, 2015, doi: 10.1007/978-81-322-2337-5\_17/COVER.
- [17] M. v. Lototskyy, I. Tolj, L. Pickering, C. Sita, F. Barbir, and V. Yartys, "The use of metal hydrides in fuel cell applications," *Progress in Natural Science: Materials International*, vol. 27, no. 1. Elsevier B.V., pp. 3–20, Feb. 01, 2017. doi: 10.1016/j.pnsc.2017.01.008.
- [18] M. Afzal, R. Mane, and P. Sharma, "Heat transfer techniques in metal hydride hydrogen storage: A review," *Int J Hydrogen Energy*, vol. 42, no. 52, pp. 30661–30682, Dec. 2017, doi: 10.1016/J.IJHYDENE.2017.10.166.
- [19] A. Satheesh, P. Muthukumar, and A. Dewan, "Computational study of metal hydride cooling system," *Int J Hydrogen Energy*, vol. 34, no. 7, pp. 3164–3172, Apr. 2009, doi: 10.1016/J.IJHYDENE.2009.01.083.
- [20] F. S. Yang, G. X. Wang, Z. X. Zhang, and V. Rudolph, "Investigation on the influences of heat transfer enhancement measures in a thermally driven metal hydride heat pump," *Int J Hydrogen Energy*, vol. 35, no. 18, pp. 9725–9735, Sep. 2010, doi: 10.1016/J.IJHYDENE.2010.06.110.
- [21] A. Jemni and S. ben Nasrallah, "Study of two-dimensional heat and mass transfer during absorption in a metal-hydrogen reactor," *Int J Hydrogen Energy*, vol. 20, no. 1, pp. 43–52, Jan. 1995, doi: 10.1016/0360-3199(93)E0007-8.
- [22] A. Jemni and S. ben Nasrallah, "Study of two-dimensional heat and mass transfer during desorption in a metal-hydrogen reactor," *Int J Hydrogen Energy*, vol. 20, no. 11, pp. 881–891, Nov. 1995, doi: 10.1016/0360-3199(94)00115-G.
- [23] T. Nishizaki, K. Miyamoto, and K. Yoshida, "Coefficients of performance of hydride heat pumps," *Journal of the Less Common Metals*, vol. 89, no. 2, pp. 559–566, Feb. 1983, doi: 10.1016/0022-5088(83)90372-7.
- [24] N. Siyakatshana, V. Kudrna, and V. Machoň, "Incorporating Danckwerts' boundary conditions into the solution of the stochastic differential equation," *Chem Eng Sci*, vol. 60, no. 7, pp. 1987–1994, Apr. 2005, doi: 10.1016/J.CES.2004.11.051.
- [25] A. A. Eftekhari and K. Schüller, "FVTool: a finite volume toolbox for Matlab," Oct. 2015, doi: 10.5281/ZENODO.32745.
- [26] M. Hasnain *et al.*, "3D Mathematical Model for Heat and Mass Transfer Mechanisms in Gypsum Board Exposed to Fire."
- [27] S. Khan *et al.*, "The self-heating ignition of lithium-ion batteries: a comparative study of COMSOL and GPYRO models with finite volume toolbox."
- [28] C. A. Chung, S. W. Yang, C. Y. Yang, C. W. Hsu, and P. Y. Chiu, "Experimental study on the hydrogen charge and discharge rates of metal hydride tanks using heat pipes to enhance heat transfer," *Appl Energy*, vol. 103, pp. 581–587, Mar. 2013, doi: 10.1016/J.APENERGY.2012.10.024.